NASA Technical Memorandum 100812

NASA-TM-100812 19880014610

Parameter Identification Methods for Improving Structural Dynamic Models

Charles Lawrence
Lewis Research Center
Cleveland, Ohio

June 1988

NASA

PARAMETER IDENTIFICATION METHODS FOR IMPROVING STRUCTURAL DYNAMIC MODELS

Charles Lawrence
National Aeronautics and Space Administration
Lewis Research Center
Cleveland, Ohio 44135

SUMMARY

Recently, there has been an increased need to develop Parameter Identification methods for improving structural dynamic models. This need has arisen out of the inability of engineers to produce mathematical models which correlate with experimental data. The present research explores the efficiency of combining Component Mode Synthesis (substructuring) methods with Parameter Identification procedures in order to improve analytical modeling of structural components and their connections. Improvements are computed in terms of physical stiffness and damping parameters in order that the physical characteristics of the model can be better understood. Connections involving both viscous and friction damping are investigated.

Substructuring methods are utilized to reduce the complexity of the identification problem. Component and inter-component structural connection properties are evaluated and identified independently, thus simplifying the identification problem. In the present research it was shown that modal test data is effective for identifying modeling problems associated with structural components, and for determining the stiffness and

damping properties of inter-component connections. In general, Parameter Identification is improved when greater quantities of experimental data are available. The results of the present research demonstrate the relative ease of generating models which duplicate the experimental data. However, it is difficult to generate physically accurate models.

ACKNOWLEDGEMENTS

I would like to give a very warm and special "thank-you" to Art Huckelbridge, my advisor, for his guidance, support, thought-provoking questions, and most of all his friendship.

I also give my thanks to Fred Moses, Bob Mullen, and Dwight Davy. I respect their comments and suggestions, and feel privileged to have them on my committee.

TABLE OF CONTENTS

APPENDIX A. EVALUATION OF SHEPARD'S METHOD FOR IDENTIFYING MODELING ERRORS

CHAPTER I

Introduction

Recently, there has been an increased need to develop Parameter Identification methods for improving structural dynamic models. This need has arisen out of the inability of engineers to produce mathematical models which correlate with experimental data. While great strides in computer technology and analysis methods have enabled engineers to solve relatively large and complex structural problems, the results often do not compare well with test data due to limitations in the quality of the mathematical model.

The field which addresses mathematical modeling is termed System Identification (1,2,3,4,5). In general, System Identification involves the utilization of input and output relations in order to determine differential equations. Once the relevant differential equations are determined, the unknown parameters within the equations are resolved and the equations can be used to represent the actual system. When the differential equation is known a priori (e.g., a vibrating beam), the identification problem is reduced to the more specific area of Parameter Identification.

Parameter Identification methods can be separated into modal and physical model identification. In modal Parameter Identification experimental data is used to derive modal parameters such as characteristic frequencies and mode shapes. These parameters then

are used to create a frequency domain, modal model. Physical Parameter Identification also involves the use of experimental data, except that a physical, time domain based model, is generated.

The present research is unique and contributes to the field of parameter identification in a number of ways. It provides critical evaluations of existing methods for "component" parameter identification. Research in the past has utilized overly simplified structures, making their applicability to general identification problems uncertain. The present research assesses the extent of applicability of a number of methods by applying them to a range of systems. The present research also contributes to the field of parameter identification in the development of methods for identifying inter-component (connection) structural properties. In this facet of the research an original concept involving the coupling of substructuring methods with parameter identification procedures is introduced. As a result of the application of this concept the proportions of the identification problem are reduced, thus permitting larger, more complex problems to be solved.

The present dissertation consists of three "complete" studies related to physical domain Parameter Identification methods for structural dynamic systems. The groundwork for a fourth study is in Appendix A. In Chapter II, a procedure for identifying differences between Finite Element component models and modal test data is expanded to include structural components with viscous damping. This procedure

is advantageous in that differences are identified in terms of physical mass, damping, and stiffness parameters as opposed to frequencies and mode shapes. Since the differences are computed in terms of physical parameters, locations of modeling problems can be directly identified in the finite element model.

The study presented in Chapter III explores the identification of structural connection properties using Component Mode Synthesis. Connection properties are computed in terms of physical stiffness parameters in order that the physical characteristics of the connections can be better understood, and so that improved input to the system physical model is provided. Two sample problems, one utilizing simulated data, the other using experimental data from a rotor dynamic test rig, are presented in this study.

Chapter IV extends the research presented in Chapter III. In this study connection damping is included as a part of the Parameter Identification. The effects of friction damping on an assumed viscously damped model also are investigated.

Appendix A briefly examines a method which utilizes discrepancies between predicted and measured frequencies to identify mass and stiffness differences in the model. This method, which is applicable to either connections or components, is in contrast to the previous methods which require both experimental frequency and mode shape data.

References To Chapter I

1. Hart, G.C.; and Yao, J.T.: System Identification in Structural Dynamics. ASCE J. Eng. Mech. Div., vol. 103, no. 6, Dec. 1977, pp. 1089-1104.

2. Ibanez, P.: Review of Analytical and Experimental Techniques for Improving Structural Dynamic Models. Weld. Res. Counc. Bull., no. 249, June 1979.

3. Collins, J.D.; Young, J.P.; and Kiefling, L.: Methods and Application of System Identification in Shock and Vibration. System Identification Of Vibrating Structures: Mathematical Models From Test Data, W.D. Pilkey and R. Cohen, eds., ASME, 1972, pp. 45-71.

4. Ibraham, S.R.; and Saafan, A.A.: Correlation of Analysis and Test in Modeling of Structures, Assessment and Review. Proceedings of the 5th International Modal Analysis Conference, Union College, Schenectady, NY, 1987, pp. 1651-1660.

5. Sage, A.P.: System Identification History, Methodology, Future Prospects. System Identification of Vibrating Structures: Mathematical Models From Test Data, W.D. Pilkey and R. Cohen, eds., ASME, 1972, pp. 1-22.

CHAPTER II

IDENTIFICATION OF DIFFERENCES BETWEEN FINITE ELEMENT ANALYSIS AND EXPERIMENTAL VIBRATION

Introduction

The dynamic characteristics of structural components are often predicted using Finite Element (F.E.) analysis and then later verified experimentally with dynamic analysis testing systems. Increased demands for reliability, minimal vibrations, optimum performance, and low cost design, among other criteria, have increased designers needs for sophisticated dynamic analysis testing techniques. Since the 1960's F.E. computer programs have become the preference of designers for analytical dynamic analysis. The use of F.E. computer codes has become especially widespread in the automotive and aerospace industries due to the requirement to analyze very large and complex structures. Commercial F.E. computer programs such as NASTRAN, ANSYS, and SAP (1) are available to anyone having access to a computer terminal.

In many situations experimental verification is required to insure the validity of the results predicted by the F.E. analysis. Aerospace structures, which are very expensive and have rigorous safety and reliability requirements normally require experimental verification (2). Automobile prototypes are also experimentally verified to insure that vibration and noise problems will not exist in production models. Hundreds of other applications of F.E. analysis and experimental validation can be found.

Digital signal analyzers are the most commonly used systems for experimental verification. Digital signal analyzers, which utilize the Fast Fourier Transform (FFT) developed in the 1960's (3), allow rapid and relatively accurate determination of structural transfer functions, resonant frequencies, and characteristic mode shapes. Modern digital analysis equipment has both automated the modal extraction process and decreased the required data acquisition and post-processing time. These systems have replaced traditional analog devices because of their high speed and their ability to measure many modes simultaneously.

An important problem that has emerged from these combined analytical/experimental investigations is the task of identifying and quantifying the differences between results predicted by F.E. analysis and results obtained from the experiment. Although both the F.E. and experimental methods can be accurate from a theoretical standpoint, inaccuracies do exist in their applications to real structural problems. In the case of F.E. modeling there is considerable uncertainty in the modeling of items such as boundary conditions, joint flexibilities, and damping. Because of this, the F.E. results are not exact since the input data itself is approximated. Also, it is not possible to completely eliminate experimental error. F.E. analysts take the responsibility for producing theoretically correct computer codes but sometimes do not place enough emphasis on predicting the

behavior of real world structures. The experimentalist, through testing, often show the limitations of the F.E. analysis, but do not always present clear cut procedures for quantifying the differences in a useful manner.

A communication gap can exist between the experimentalist and the F.E. analyst when the experimentalist can not provide the quantitative data required by the analyst to identify the differences between the experimental data and the F.E. model. The gap exists because the experimentalist normally measures frequencies and mode shapes in a vibration test, while the analyst requires a mass, damping, and stiffness matrix for describing the F.E. model.

It would be useful if the differences between the experimental data and F.E. model could be found in terms of discrete mass, stiffness, and damping. If this could be done, and the experimental data was reliable, a more accurate F.E. model with improved mass, damping, and stiffness descriptions could be created. This model could then be used for not only subsequent dynamic analysis, but also for static analysis, for studying the effects of structural modifications, or for any analysis requiring the use of a mass, damping, or stiffness matrix. It would be ideal if the discrete parameters could be measured experimentally but this is not practical. For example, to measure the values for

a row or column in the stiffness matrix, a displacement would have to be applied to the real structure while every other degree of freedom was constrained, and then the forces at all the other degrees of freedom would need to be measured. This would be both time consuming and require elaborate fixtures and instrumentation. Experimental measurement of the mass and damping matrix would be at least equally complex, if not impossible.

One possible way to compare the experimental results to the F.E. model is to compute analytical frequencies and mode shapes from the F.E. equation of motion and then compare them to the frequencies and mode shapes obtained from the experiment. The limitation of making a comparison at this level is that even though disagreements can be identified, the cause of the disagreements namely differences in the mass, damping, and stiffness matrices, can not be identified of quantified.

A more useful comparison between F.E. and experiment can be made through the equations of motion. By using the original F.E. equations and the equations of motion derived from the experimental data, differences between experiment and F.E. coefficients can be identified and corrected. Unfortunately, the procedure of deriving an equation of motion from the experimental frequencies and mode shapes is not straight forward. To derive the equation of motion from experimental data requires that the

same number of modes as degrees of freedom in the F.E. model be experimentally measured and that the experimental data not contain any measurement error or noise. If both of these requirements are not met the experimental data can not be used to construct a correct equation of motion. Since the coefficients for the equations of motion are computed by inverting matrices containing the experimental mode shapes, these matrices must be square. In a typical experiment, the number of measured modes will not be equal to the number of degrees of freedom so the modal matrices will be rectangular instead of square. Another difficulty is that the experimental data will always contain some amount of experimental error and noise which makes the outcome of a matrix inversion questionable. Also, if the highest modes in the structure are not included in the experimental data the stiffness matrix computed from a modal matrix inversion will be incorrect (4). Finally, it is difficult to measure the values of the mode shapes corresponding to every degree of freedom used in the F.E. model. This causes the order of the experimental matrices to be less than those in the F.E. equations.

Previous research in this area has focused on using experimental data to improve F.E. models rather than on identifying the differences. Most of the techniques have been based on some form of a least squares fit. In the work by Berman and Flannelly (4), the analytical matrices are assumed to be close to the actual

solution and then the smallest change in the analytical model that makes the experimental and analytical frequencies and mode shapes identical is found. This assumption will not necessarily lead to an analytical model that is physically representative of the actual structure. The only assurance is that the revised model will correctly predict the modes that were measured. The problems arising from using "incomplete" data (data containing fewer modes than there are in the F.E. model) are also discussed in this work. In Ref. 5, Fuh, Chen, and Berman use similar approaches for correcting structures with viscous damping.

Chen, Peretti, and Garba (6) refined a F.E. model of the Galileo spacecraft by first performing static tests to improve the stiffness matrix, and then dynamic tests for correcting the mass matrix. The mass matrix correction was based on a minimum change criteria. The limitations of this approach are that two independent sets of tests must be run, and again, there is no guarantee that actual physical characteristics will result from the least squares approach.

Hart and Yao (7) discuss the advantages of using weighted least squares and Bayesian estimation. By using these extended forms of least squares methods, uncertainties in both the experimental data and analytical model can be included in the updating procedure. It can be very important to define the uncertainty in the

experimental data since this data often contains more error than the F.E. description. It does not make much sense to attempt to improve a F.E. model with experimental data that is less certain than the F.E. model. By including relative uncertainties in the procedure, changes to the analytical model will not be applied indiscriminately and the possibility exists for retaining the physical meaning of the structure in the updated model.

Dobb, Blakely, and Gundey (8), and Blakely and Walton (9) applied the Bayesian estimation procedure to a F.E. model of an offshore platform and a dam. In their study the effects of change in the uncertainties in both the experimental data and the F.E. parameters were investigated. Unfortunately, well defined procedures do not exist for quantifying uncertainties so they had to be estimated using engineering judgement.

Sidhu (10) developed a procedure for approximating the difference between experimentally measured frequencies and mode shapes and F.E. parameters in terms of differences in mass, damping, and stiffness matrices. This approach has the potential for providing a direction to correct a F.E. model while retaining the physical characteristics of the real structure. The objective of the work presented in this chapter is to extend the procedure developed by Sidhu for correlation of linear finite element and modal test data to include structures with viscous damping. In this study, the

derivation of the extended procedure and several case studies which use simulated experimental data are presented. The purpose of developing this procedure is to formalize a process for identifying the differences between experimentally measured frequencies and mode shapes and F.E. models in terms of differences in mass, damping, and stiffness.

Formulation of Equations

The free vibration equation of motion for a damped, linear system can be written as:

$$[M]\{\ddot{u}\} + [C]\{\dot{u}\} + [K]\{u\} = \{0\} \qquad (1)$$

where $[M]$ is the mass matrix, $[C]$ is the viscous damping matrix, $[K]$ is the stiffness matrix, and $\{\ddot{u}\}$, $\{\dot{u}\}$, and $\{u\}$ are the acceleration, velocity, and displacement vectors, respectively. The size of $[M]$, $[C]$, and $[K]$ are nxn and $\{\ddot{u}\}$, $\{\dot{u}\}$, and $\{u\}$ are of size n, where n is the number of degrees of freedom in the equations of motion.

In only special cases can Eq. (1) be decoupled using normal modes (11). In general, when damping is present, the solution of this equation results in complex eigenvalues and eigenvectors appearing in conjugate pairs. Since there are pairs of roots there will be twice as many roots as there are displacement degrees of freedom and the modal matrix will be of the order $nx2n$ instead of nxn.

This rectangular modal matrix can not be used to decouple Eq. (1). Equation (1) can be rewritten in state vector form as:

$$[A]\{\dot{y}\} + [B]\{y\} = \{0\} \tag{2}$$

where $\{y\} = \begin{Bmatrix}\{\dot{u}\}\\ \{u\}\end{Bmatrix}$ $[A] = \begin{bmatrix}[0] & [M]\\ [M] & [C]\end{bmatrix}$ $[B] = \begin{bmatrix}-[M] & [0]\\ [0] & [K]\end{bmatrix}$

([A] and [B] are of order 2n x 2n and {y} is of order 2n.)

The advantage of writing the equation of motion in state vector form is that the modal matrix can now be used to decouple the equation. Assuming a solution $\{y\} = \{\Phi\}e^{st}$ and substituting into Eq. (2) leads to the eigenvalue problem:

$$\{[A]s + [B]\}\{\Phi\} = \{0\} \tag{3}$$

For less than critical damping, the solution of this equation yields 2n complex eigenvalues s_r, where $s_r = -w_r \zeta_r +/- iw_{Dr}$. w_r is the natural frequency, W_{Dr} is the damped natural frequency, and ζ_r is the damping ratio for mode r. An equal number of complex eigenvectors are also obtained.

Substituting the modal matrix $[\Phi]$ into Eq. (3) and premultiplying by $[\Phi]^T$ leads to:

$$[\Phi]^T[A][\Phi][\diagdown s \diagup] + [\Phi]^T[B][\Phi] = \{0\} \tag{4}$$

from orthogonality

$$[\Phi]^T[A][\Phi] = [\diagdown a \diagup] \quad \text{and} \quad [\Phi]^T[B][\Phi] = [\diagdown b \diagup]$$

where $[\backslash a \backslash]$ and $[\backslash b \backslash]$ are diagonal matrices.

If the eigenvectors are normalized with respect to the [A] matrix then:

$$[\Phi]^T[A][\Phi] = [I] \tag{5}$$

and

$$[\Phi]^T[B][\Phi] = -[\backslash s \backslash] \tag{6}$$

Since the objective is to determine the differences between the experimental model and the analytical model we need to find a common ground that will allow the comparison of the structural matrices computed from the F.E. analysis to the experimental frequencies and mode shapes. The differences between the F.E. "[B]" matrix and the [B] matrix computed from the experimental data (assuming that a [B] matrix can be created from the experimental data) is written as:

$$[D]_B = [B]_{exp} - [B]_{F.E.} \tag{7}$$

rearranging

$$[B]_{exp} = [B]_{F.E.} + [D]_B$$

then inverting both sides

$$[B]_{exp}^{-1} = \{[B]_{F.E.} + [D]_B\}^{-1}$$

and factoring out $[B]_{F.E.}$

$$[B]_{exp}^{-1} = \{[B]_{F.E.}^{-1}\{[I] + [B]_{F.E.}^{-1}[D]_B\}\}^{-1}$$

and

$$[B]^{-1}_{exp} = \{[I] + [B]^{-1}_{F.E.}\,[D]_B\}\,[B]^{-1}_{F.E.} \qquad (8)$$

If the bracketed expression in Eq. (8) is expanded using a Taylor series (12,13) and terms past the first derivative are dropped, Eq. (8) can be approximated by:

$$[B]^{-1}_{exp} \approx \{[I] - [B]^{-1}_{F.E.}\,[D]_B\}[B]^{-1}_{F.E.}$$

multiplying out $[B]^{-1}_{F.E.}$

$$[B]^{-1}_{exp} \approx [B]^{-1}_{F.E.} - [B]^{-1}_{F.E.}\,[D]_B\,[B]^{-1}_{F.E.}$$

and then rearranging

$$-[B]^{-1}_{exp} + [B]^{-1}_{F.E.} \approx [B]^{-1}_{F.E.}\,[D]_B\,[B]^{-1}_{F.E.}$$

and solving for $[D]_B$

$$[D]_B \approx [B]_{F.E.} \{[B]_{F.E.}^{-1} - [B]_{exp}^{-1}\}[B]_{F.E.} \tag{10}$$

Using Eq. (6) to obtain $[B]^{-1}$ and substituting into Eq. (10) the final expression for the difference matrix $[D]_B$ is obtained:

$$[D]_B \approx [B]_{F.E.} \{[\Phi]_{F.E.} [\lambda]_{F.E.}^{-1} [\Phi]_{F.E.}^T - [\Phi]_{exp} [\lambda]_{exp}^{-1} [\Phi]_{exp}^T\}[B]_{F.E.} \tag{11}$$

The same approach can be used for deriving the difference in the [A] matrix. In this case:

$$[D]_A \approx [A]_{F.E.} \{[D]_{F.E.} [D]_{F.E.}^T - [D]_{exp} [D]_{exp}^T\}[A]_{F.E.} \tag{12}$$

The format of Eqs. (11) and (12) are well suited for computing the differences between the F.E. model and experimental data. Since these equations do not require any inversion of the modal matrices, the fact that all the modes are not measured does not cause a problem. As discussed previously, the modal matrix will not be completely known since fewer modes than degrees of freedom are typically measured. An inversion of the frequency matrices are required, but this does not present any problems since these matrices are diagonal and their inverses are just the reciprocal of the diagonal terms.

Once $[D]_A$ and $[D]_B$ are computed, the disagreement between the F.E. and experimental descriptions of the component can be found. Since there is a direct relationship between the elements of the mass, damping, and stiffness matrices and the elements of the [A] and [B] matrices, the discrepancies in mass, damping, and stiffness at any degree of freedom in the structure can be found by merely picking out values from the $[D]_A$ and $[D]_B$ matrices. For example, the disagreement in damping at the first degree of freedom would be obtained from the $[D]_A$ matrix at location $[D(n + 1, n + 1)]_A$, the mass disagreement at $[D(1, n + 1)]_A$, and the stiffness disagreement at $[D(n + 1, n + 1)]_B$. Note that the mass discrepancy can be found from either one of two partitions in the $[D]_A$ matrix or the $[D]_B$ matrix.

It was mentioned previously that in practive experimental mode shape data will normally not be available at all of the degrees of freedom used in the F.E. model. When this situation exists, either the mode shape data must be interpolarted (7) or the F.E. model reduced (16). In this work it will be assumed that one of these procedures has already been applied, thus rendering the number of degrees of freedom equal to the number of experimental measurement points where mode shape data is taken. It will also be assumed that the experimental mode shapes are measured at the F.E. node locations.

Sample Problem One: Cantilever Beam

Sample problem one consists of a planar cantilever beam. Two finite element models were used in the analysis. This first model, referred to as the analytical model, is used for computing the frequencies and mode shapes that would normally be generated by an analytical analysis. The second model, referred to as the "experimental" model, is used for simulating frequencies and mode shapes that would be obtained by performing an actual experimental modal analysis on a real beam. It is advantageous to use simulated data in place of real data because the property matrices corresponding to the simulated data are known, whereas the property matrices for any real structure are unknown. Since the mass, damping, and stiffness matrix are known for the simulated experimental data, the exact error matrices can be compared to the error matrices generated by the equations derived in this study and the procedures can be evaluated.

The analytical model is made up of nine, equally spaced node points and eight connecting beam elements (Fig. 1). All of the degrees of freedom are constrained at node 1 and every degree of freedom except for the z-displacement and y-rotation are constrained at the other node points. This leaves sixteen active degrees of freedom for the structure. The section properties for the beam elements are 2.6×10^{-3} for the moment of inertia, 10×10^{6}

for Young's modulus, and 2.6×10^{-4} for the mass density per unit length.

The complex eigenvalue extraction solution sequence (Solution 28) of the MSC/NASTRAN finite element program was used to compute the free vibration frequencies and mode shapes for the beam. The Hess method (14) was selected for extracting the modes since this method is more efficient when all of the modes are desired. All of the modes were initially required for a complete verification of the difference matrix routines.

The simulated experimental model was made to differ from the F.E. model by adding a concentrated mass, damper, and spring to the beam. The location of these elements is shown in Fig. 1. The values used for the elements are listed in Table I as ΔM, ΔC, and ΔK. The mass, damping, and stiffness from the F.E. model at the same nodes and directions are also listed to give an indication of the relative magnitude of the differences. NASTRAN was again used for computing the complex frequencies and mode shapes of the experimental model.

Table II shows the comparison between the computed eigenvalues for the analytical model and the simulated experimental model for each of the four cases. All 16 of the modes were computed by NASTRAN. From Table II, a comparison can be made between the

complex valued eigenvalues. As expected, the real part of the analytical eigenvalues are zero since there is no damping present in the F.E. model, and the real part of the experimental eigenvalues are non-zero since damping is present. In general, the addition of the tip mass and the damper tends to lower the frequencies while the spring raises the frequencies. The modal damping is totally dependent on the concentrated damper.

The imaginary (frequency) part of the F.E. and experimental eigenvalues are plotted in Fig. 2 for case 1. If the eigenvalues matched exactly they would plot directly on the straight, 45° line. There is a small deviation from the straight line, but not enough to indicate any significant differences between the analytical and experimental models. Even if there were large deviations between the analytical and experimental eigenvalues, there would not be any way to use the results in Fig. 2 or Table II to relate the deviations to differences in physical mass, damping, or stiffness coefficients.

The real components of the first four mode shapes for the analytical model (case 1) are plotted in Fig. 3. Only the translational degrees of freedom are plotted. Even though the first frequency has the largest deviation (Fig. 2) the first mode shape matches up very closely. The opposite occurs for the second and third modes where the mode shapes deviate from each

other while the frequencies are very similar. As with the frequency plots, there is no way to relate the deviation from perfect correlation in mode shape plots to physical differences in mass, damping, or stiffness.

The Difference Matrix program was used to relate the differences between the experimental and analytical models in terms of differences in mass, damping, and stiffness. The computer program was verified using all four cases and various numbers of modes as input data. When all of the modes are included as input the only approximation in the procedure is from the Taylor series truncation. As previously discussed, in a real situation all the modes would not be available from tests. Plots of mass, damping, and stiffness difference matrices for case 1, using all 16 modes are shown in Fig. 4. The differences are plotted on a grid where each intersection of a grid line corresponds to a location in the matrix being plotted. For example, the mass difference shown in the figure corresponds to the (15, 15) location in the structure's mass matrix. In the figure the physical differences between the analytical and experimental models are clearly defined. The mass difference matrix indicates a mass difference at degree of freedom 15 which corresponds to the translational direction at the beam tip where the concentrated mass was added. The damping and stiffness errors at degree of freedom seven and one respectively, correspond to the

locations of the concentrated damper and spring. There were no other differences between the analytical and experimental models which is indicated by the flat areas in all three of the difference matrix plots. Even though the location of the difference is exact, there is some amount of disagreement between the actual magnitudes of the mass and stiffness, and the magnitudes computed by the error matrix program. The program computed a mass difference of 0.00011 while the actual concentrated mass was 0.0002. The spring magnitude was computed to be 3294, while the real spring was 5000. The magnitudes of the actual damper and the magnitude computed by the program were both 1.0. It is not surprising that the computed mass differences was so far off since the mass added to the experimental model was almost as great as the original mass in the analytical model. Since all of the modes were included in these calculations, the differences between the real values and the computed ones can be attributed to the higher order terms that are missing in the Taylor expansion. A procedure for improving the accuracy of the magnitudes will be discussed later in this section.

When less than all 16 modes are included in the calculations the results deteriorate. In Fig. 5 results are shown for the case where only one mode was included as input into the Difference Matrix program. The mass and damping difference plots do not

show anything but some distributed noise. The stiffness difference plot indicates a difference at the spring location, but the difference is of the wrong magnitude. (After examining the data, the sign of the difference was also found to be incorrect) Figure 6 shows difference plots where 10 modes are included as input. In this case the noise has virtually disappeared and the correct locations of the differences have shown up.

A compilation of results for all four test cases are shown in Figs. 7 to 9. In these figures the ratio of the computed to actual difference at the mass, damper, and spring location are plotted as a function of the number of modes used as input data into the Difference program. All four cases were run using 16, 8, 5, 3, 2, and 1 modes as input into the Difference program. From the mass difference plot (Fig. 7), it is seen that when the mass difference is large (case 1), the computed difference is only about half of the correct difference. When the mass difference was reduced (cases 2, 3 and 4) the computed difference was much closer to the correct difference. If the mass difference is as great or greater than the analytical mass, the location of the difference will be correct but the magnitude will not. From cases 2, to 4 it is also seen that the computed mass difference does not change with the level of the damping or stiffness differences.

Figure 8 shows the computed damping differences for the four cases. This plot shows that the differences are independent of the level of damping as well as independent of the magnitude of the mass and stiffness difference. Even when large amounts of damping are present in the structure the damping calculations are accurate (the damping level in case 2 was close to critical). It is encouraging to note that the accuracy is independent of the damping difference level, because in analytical modeling it is the damping values that are the most difficult to predict. Thus for a typical structure the difference procedure would work fairly well, since the mass and stiffness differences would ordinarily be small, and the magnitude of the damping difference would not matter.

Figure 9 shows the effects of the various difference ratios on the computed stiffness differences. Similar to the mass calculations, the accuracy of the difference is dependent upon its relative magnitude. When the stiffness difference is relatively large, the computed difference is inaccurate; when the difference is small, the computed value is much closer to the actual value. Again, the computed difference is independent of the level of the differences in the other parameters.

From any of the figures presented thus far it is apparent that when only a few modes are included the results are meaningless.

When less than eight modes are included the results are poor, and past eight modes the results are good and do not improve by including more than the first eight modes. To determine how the number of degrees of freedom used in the model effects the number of modes required for good results, a new model of the cantilever beam was constructed using 32 degree of freedom instead of 16.

The difference plots for this model were computed using the differences from case 3. The results are shown in Fig. 10. The difference matrices using 16 modes as input are shown in Fig. 11. From these results it is seen that while only 8 modes produced good results in the 16 degree of freedom model, at least 16 modes are needed in the 32 degree of freedom model.

Previously, it has been shown that the accuracy of the computed differences are dependent on the magnitude of the differences and the number of modes included in the calculations. In an attempt to improve the accuracy an iterative procedure was implemented (Fig. 12). In this procedure the differences computed by the Difference program are accumulated from all previous iterations and are then added to the mass, damping, and stiffness matrices for the analytical model. The updated analytical model is then used to compute a new set of differences for the next iteration.

The iterative procedure was tested using the differences from

test case 3 and the sixteen degree of freedom model. The results for three iterations are shown in Fig. 13. Without iterating, it was shown that when all sixteen modes are included in the calculations the results are very good. After iterating only twice, the results are exact. The same is also true when only eight modes are used. In general, when less than eight modes are used, the accuracy of the computed differences are not improved significantly by iterating. When only a few modes are included, the accuracy is not improved at all. The advantage of using the iteration procedure is that when an adequate number of modes are used the results will converge to the exact values regardless of the magnitude of the differences. The limitation of the iterative process is that it does not reduce the number of modes required for good results.

SAMPLE PROBLEM TWO: Simply Supported Beam

The second sample problem consists of a planar, simply supported beam. The finite element model of this problem is made up of nine node points and eight connecting beam elements (Fig. 14). All of the degrees of freedom are constrained, except for the y-rotations at nodes one to nine, and the z-translations at nodes two through eight. There are sixteen degrees of freedom for this problem. The same section properties that were used of for the first sample problem are also used here. The difference matrix

plots for this problem were generated using the iteration scheme shown in Fig. 12.

The "experimental" model was made to differ from the analytical model by adding three concentrated springs and seven dampers to the beam model. The locations and properties for these elements are shown in the figure. This sample problem differs from the first one in that the differences in the first problem were limited to a single mass, damper, and spring, while in this problem there are several springs and dampers at every node. Also, the level of damping is much less in this problem than in the previous one.

A comparison of the eigenvalues for the second sample problem is shown in Table III. From this comparison it is seen that the major differences between the analytical and experimental models are in the first frequency and the modal damping in the first seven modes. Beyond the seventh mode there are not any differences between the analytical and experimental eigenvalues. The first frequency is higher for the experimental model because of the additional stiffness from the three springs. The modal damping is different because the experimental model has the seven translational dampers while the analytical model does not have any damping. It is understandable that there is no modal damping in the higher modes for the experimental model since the higher

modes are dominated by rotations and the dampers only act in the translation direction.

The computed damping and stiffness difference matrices using the first mode only as input into the Difference program are shown in Fig. 15. From these plots it is impossible to identify any of the differences that actually exist between the analytical and experimental models. When only one mode was used for the first sample problem calculations the differences could not be identified either. When the number of modes was increased to four (Fig. 16) the correct differences were reasonably apparent in the difference plots. For the stiffness matrix plot, differences appear at degree of freedom 4, 6, and 8 which corresponds to the locations of the three springs that were added to the experimental model. In addition to the differences at these degrees of freedom, differences also appear at some of the other degrees of freedom. These differences do not actually exist in the models and would not appear if more modes were used as input. Many of these "extra" differences can be eliminated by examining the possible coupling that may exist in the analytical mode. For example, node two and six are not connected to each other so degrees of freedom 2 (z-translation, node two) and degree of freedom 10 (z-translation, node six) are uncoupled which allows for location (2,10) and (10,2) in the difference matrix to be set to zero. The same logic can be used to

eliminate some of the other unobtainable differences appearing in the plots.

In Fig. 17, the difference plots using four modes are recreated, except that the differences at uncoupled degrees of freedom are set to zero. In these plots the correct differences are even more evident although some differences continue to appear where there are not any true differences. There does not appear to be any way to eliminate these "extra" differences except by using more modes in the calculations. When the number of modes is increased to six (Fig. 18), both the computed stiffness and damping difference matrices are very accurate. In addition, no significant differences appear where they do not actually exist in the models. In Fig. 19, plots are shown where all sixteen modes are included in the computations, and as expected, the results are almost exact.

Conclusion

A general procedure for identifying and quantifying the differences between F.E. models and experimental data has been developed and demonstrated with simulated experimental data. The differences, which can be computed for linear, viscously damped components, are presented in terms of mass, damping, and stiffness coefficients. Since the differences are computed in

terms of mass, damping, and stiffness coefficients, possible modeling problems can be identified in the F.E. or analytical model.

From data generated for a damped cantilever beam and a damped simply supported beam, it was determined that the accuracy of the computed differences increases as the number of experimentally measured modes included in the calculations is increased. When the number of experimental modes is at least equal to the number of translational degrees of freedom both the location and magnitude of the differences can be computed very accurately. When the number of modes is less than this amount the location of the differences may be determined even though their magnitudes will be under estimated. When too few modes are available neither the location or the magnitudes of the differences can be identified.

In practice, it will be required to measure the experimental frequencies and mode shapes very accurately before the differences can be attributed to shortcomings in the analytical model. If the experimental data is not precise, the computed differences can still provide considerable insight into the possible locations of deficiences. The difference is that the deficiencies may be in the experiment and some judgement will be required to decide whether to modify the experiment or the analytical model.

References To Chapter II

1. Schaeffer, H.G.: A Review of the International Symposium on Structural Mechanics Software. Comput. Struct., vol. 8, no. 5, 1978, pp. 589-598.

2. Modal Analysis Verifies Statellite's Structural Math Model. Design News, vol. 41, no. 3, Feb. 4, 1985, pp. 86-90.

3. Cooley, J.W.; and Tukey, J.W.: An Algorithm for the Machine Calculation of Complex Fourier Series. Math. Comput., vol. 19, 1965, pp. 297-301.

4. Berman, A.; and Flannelly, W.G.: Theory of Incomplete Models of Dynamic Structures. AIAA J., vol. 9, no. 8, Aug. 1971, pp. 1481-1487.

5. Fuh, J.S.; Chen, S.Y.; and Berman, A.: System Identification of Analytical Models of Damped Structures. 25th Structures, Structural Dynamics and Materials Conference, Part. 2, AIAA, 1984, pp. 112-116.

6. Chen, J.C.; Peretti, L.F.; and Garba, J.A.: Spacecraft Structural System Identification by Modal Test. 25th Structures, Structural Dynamics, and Materials Conference, Part. 2, AIAA, 1984, pp. 478-489.

7. Hart, G.C.; and Yao, J.T.P.: System Identification in Structural Dynamics. ASCE J. Eng. Mech. Div., vol. 103, no. 6, Dec. 1977, pp. 1089-1104.

8. Dobbs, M.W.; Blakely, K.D.; and Gundy, W.E.: System Identification of Large-Scale Structures. SAE Paper 811050, Oct. 1981.

9. Blakely, K.D.; and Walton, W.B.: Selection of Measurement and Parameter Uncertainties for Finite Element Modal Revision. Proceedings of the 2nd International Modal Analysis Conference and Exhibit, Vol. 1, P.B. Juhl and D.J. Demichele, eds., Union College, Schenectady, NY, 1984, pp. 82-88.

10. Sidhu, J.: Reconiliation of Predicted and Measured Model Properties of Structures. Ph.D. Dissertation, Department of Mechanical Engineering, Imperial College of Science and Technology, London, 1983.

11. Meirovitch, L.: Analytical Methods in Vibrations. MacMillan, 1967.

12. Frazer, R.A.; Duncan, J.W.; and Collar, A.R.: Elemetnary Matrices and Some Applications to Dynamics and Differential Equations. Cambridge University Press, 1960.

13. Thomas, G.E., Jr.,: Calculus and Analytic Geometry. 4th ed., Addison-Wesley, 1972.

14. The NASTRAN Theoretical Manual. NASA SP-221(06), 1981.

TABLE I. - TEST CASES FOR SAMPLE PROBLEM ONE

Case	$\Delta M/M^a$	$\Delta C/C^b$	$\Delta k/k^c$
1	$\frac{2\times10^{-4}}{2.6\times10^{-4}}$	$\frac{1.0}{0}$	$\frac{5000}{78000}$
2	$\frac{5\times10^{-5}}{2.6\times10^{-4}}$	$\frac{1.8}{0}$	$\frac{2500}{78000}$
3	$\frac{5\times10^{-5}}{2.6\times10^{-4}}$	$\frac{1.0}{0}$	$\frac{2500}{78000}$
4	$\frac{5\times10^{-5}}{2.6\times10^{-4}}$	$\frac{1.0}{0}$	$\frac{25000}{78000}$

[a]Ratio of mass Δ to F.E. mass at node 9.
[b]Ratio of damping Δ to F.E. damping at node 5.
[c]Ratio of stiffness Δ to F.E. stiffness at node 2.

TABLE II. - COMPARISON OF ANALYTICAL AND "EXPERIMENTAL" EIGENVALUES FOR SAMPLE PROBLEM ONE

Mode	Analytical eigenvalue	Case 1	Case 2	Case 3	Case 4
		Experimental eigenvalue	Experimental eigenvalue	Experimental eigenvalue	Experimental eigenvalue
1	0 + 137i	-44.3 + 130i	-123 + 111i	-53 + 133i	-45 + 150i
2	0 + 840i	-247 + 761i	-438 + 581i	-245 + 782i	-258 + 874i
3	0 + 2 312i	-179 + 2 271i	-12 + 2 314i	-74 + 2 317i	-31 + 2 525i
4	0 + 4 447i	-203.9 + 4 381i	-378 + 4 359i	-21.4 + 4 425i	-183 + 4 794i
5	0 + 7 197i	-28.2 + 7 178i	-30 + 7 203i	-17 + 7 207i	-59 + 7 692i
6	0 + 10 427i	-195 + 10 428i	-360 + 10 387i	-202 + 10 430i	-158 + 10 972i
7	0 + 13 757i	-247 + 13 794i	-35 + 13 776i	-19.6 + 13 780i	-55 + 14 235i
8	0 + 16 371i	-197 + 16 369i	-359 + 16 304i	-199 + 16 359i	-168 + 16 572i
9	0 + 63 017i	0 + 62 922i	0 + 62 982i	0 + 62 982i	0 + 62 982i
10	0 + 75 727i	0 + 75 711i	0 + 75 721i	0 + 75 721i	0 + 75 721i
11	0 + 84 033i	-3 + 83 944i	-5 + 840191	-3 + 84 019i	-3 + 84 019i
12	0 + 94 026i	0 + 93 974i	0 + 94 007i	0 + 94 007i	0 + 94 007i
13	0 + 103 928i	-2 + 103 875i	-4 + 103 909i	-2 + 103 909i	-2 + 103 909i
14	0 + 112 599i	0 + 112 559i	0 + 112 584i	0 + 112 584i	0 + 112 584i
15	0 + 119 278i	0 + 119 256i	-1 + 119 270i	0 + 119 270i	0 + 119 270i
16	0 + 123 471i	0 + 123 466i	0 + 123 470i	0 + 123 469i	0 + 123 470i

TABLE III. - COMPARISON OF ANALYTICAL AND "EXPERIMENTAL" EIGENVALUES FOR SAMPLE PROBLEM TWO

Mode	Analytical eigenvalue	Experimental eigenvalue
1	0 + 386i	-48 + 488i
2	0 + 1 541i	-48 + 1 560i
3	0 + 3 455i	-48 + 3 466i
4	0 + 6 093i	-48 + 6 095i
5	0 + 9 349i	-47 + 9 352i
6	0 + 12 917i	-47 + 12 919i
7	0 + 16 031i	-48 + 16 033i
8	0 + 62 668i	0 + 62 668i
9	0 + 62 930i	0 + 62 930i
10	0 + 76 617i	0 + 76 617i
11	0 + 85 577i	0 + 85 577i
12	0 + 95 562i	0 + 95 562i
13	0 + 105 119i	0 + 105 119i
14	0 + 113 347i	0 + 113 347i
15	0 + 119 633i	0 + 119 633i
16	0 + 123 563i	0 + 123 563i

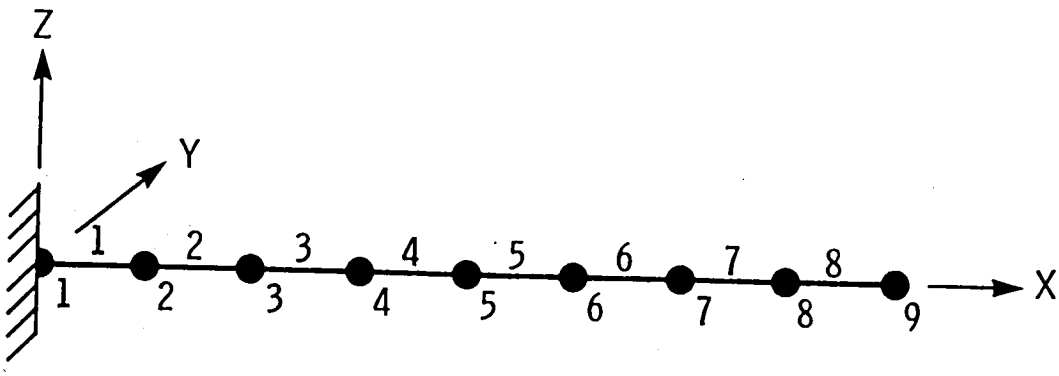

(a) Analytical model.

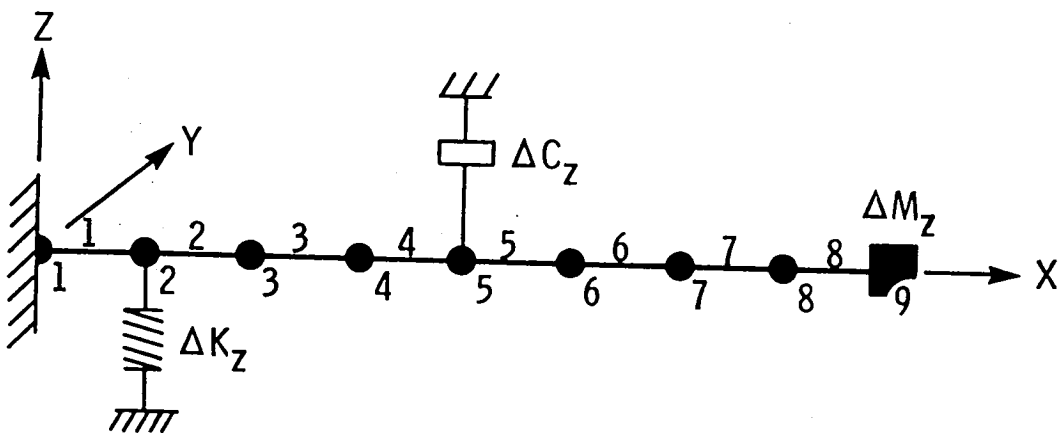

(b) "Experimental" model.

Figure 1. - Sample problem one.

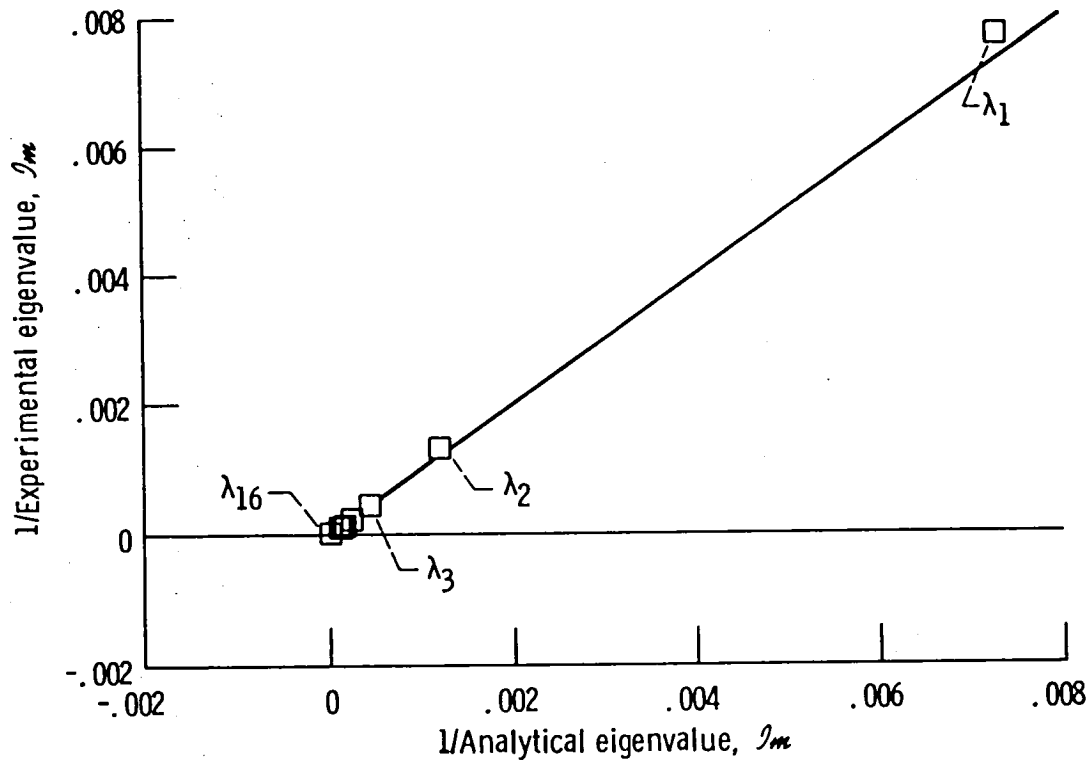

Figure 2. - Comparison of frequency data for sample problem one, case 1.

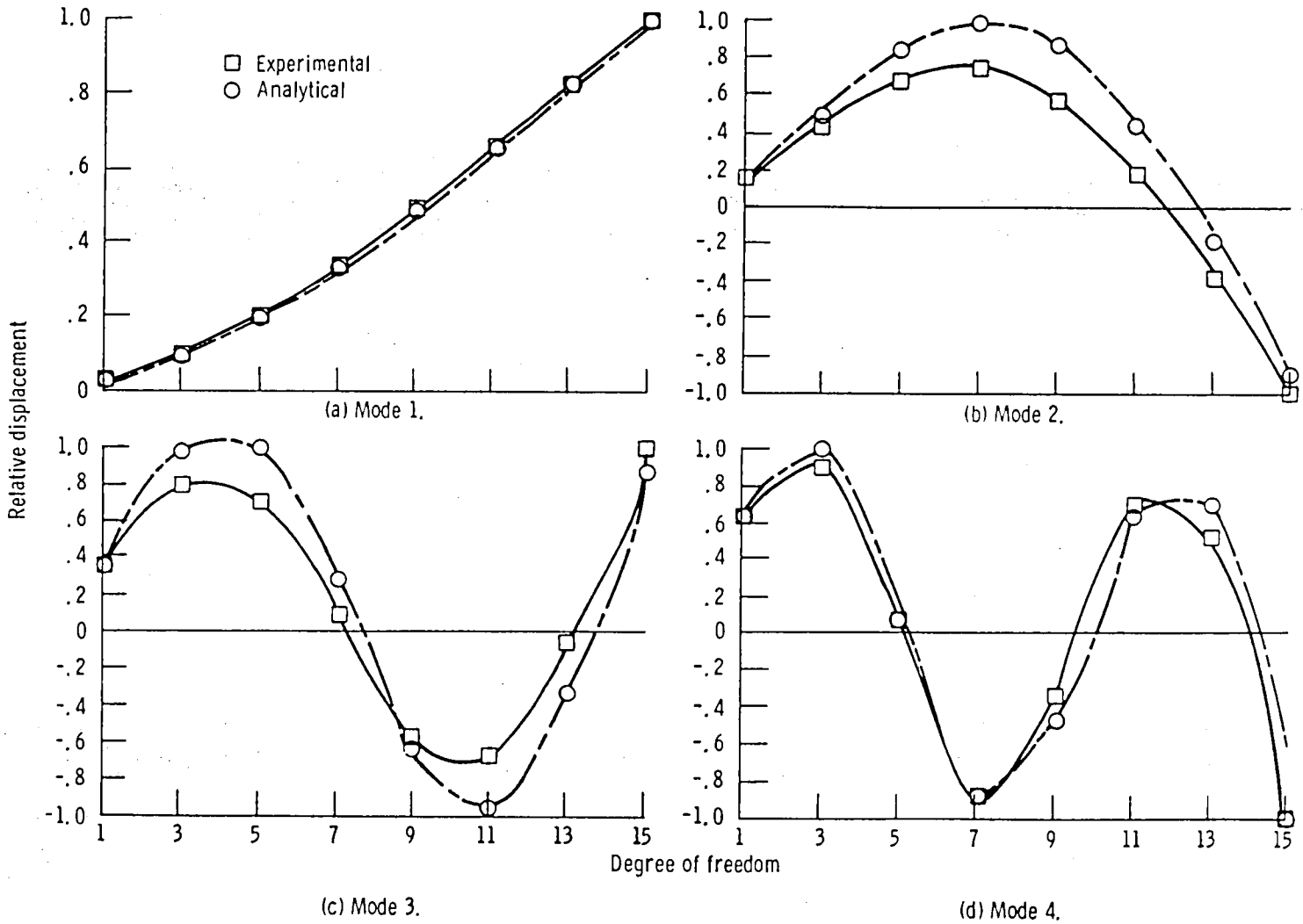

Figure 3. - Comparison of mode shapes for sample problem one, case 1.

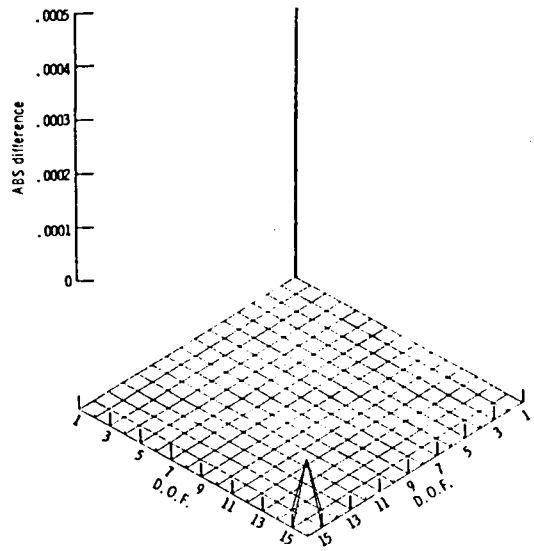

(a) Mass difference matrix.

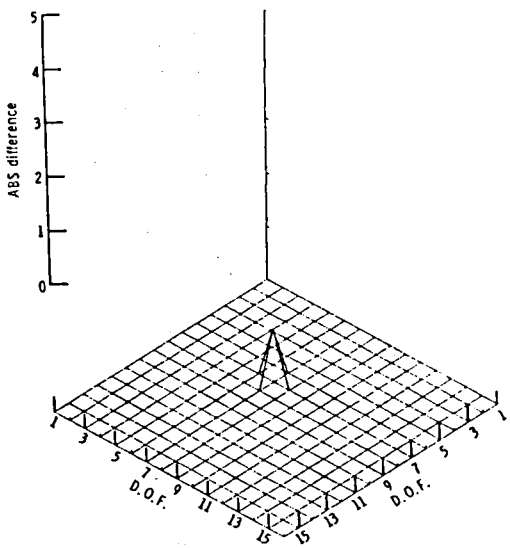

(b) Damping difference matrix.

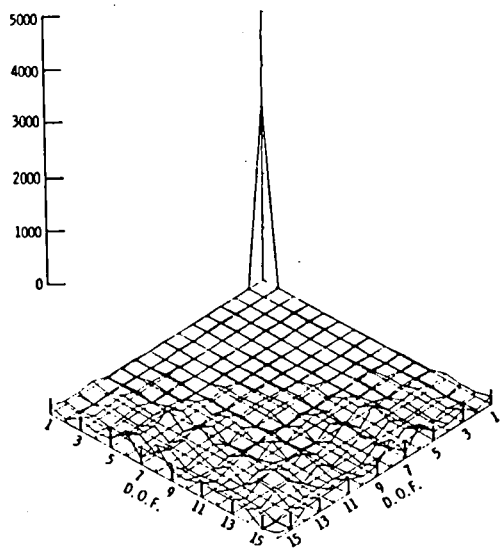

(c) Stiffness difference matrix.

Figure 4. - Computed differences for sample problem one, case 1, using 16 modes.

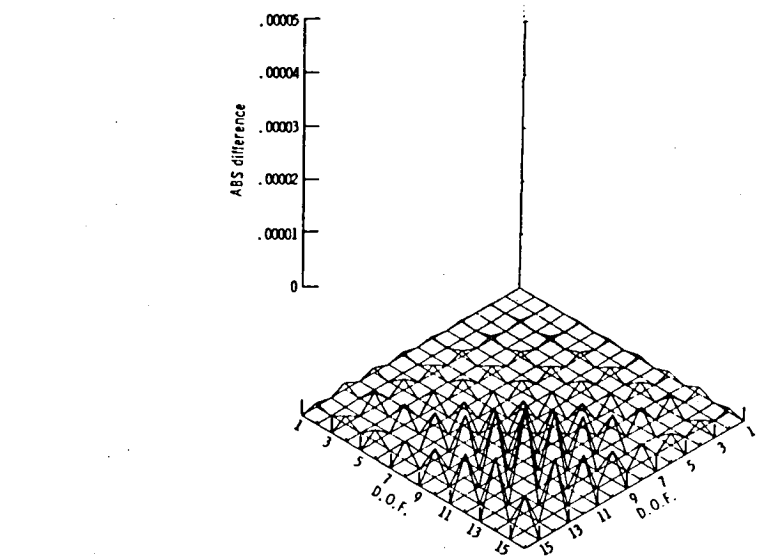

(a) Mass difference matrix.

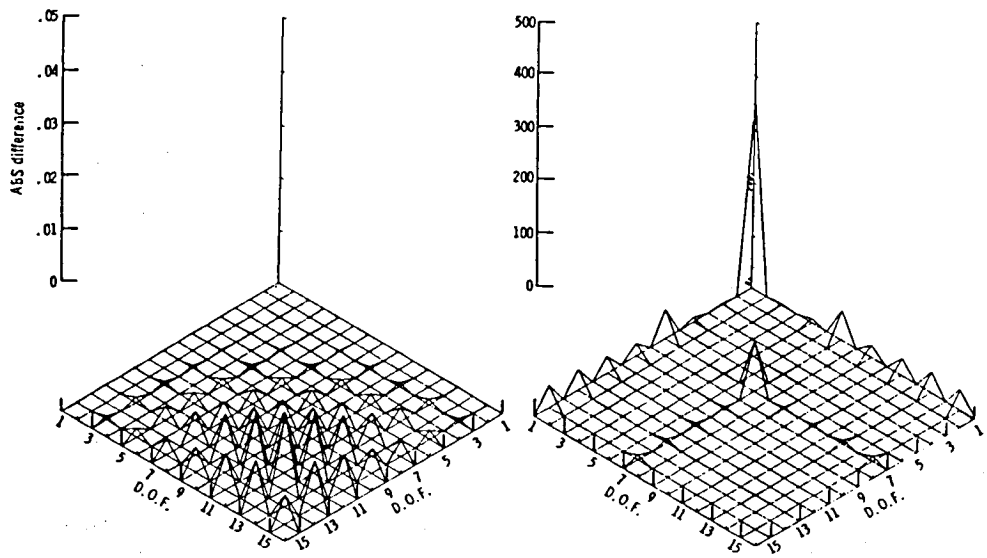

(b) Damping difference matrix.

(c) Stiffness difference matrix.

Figure 5. - Computed differences for sample problem one, case 1, using 1 mode.

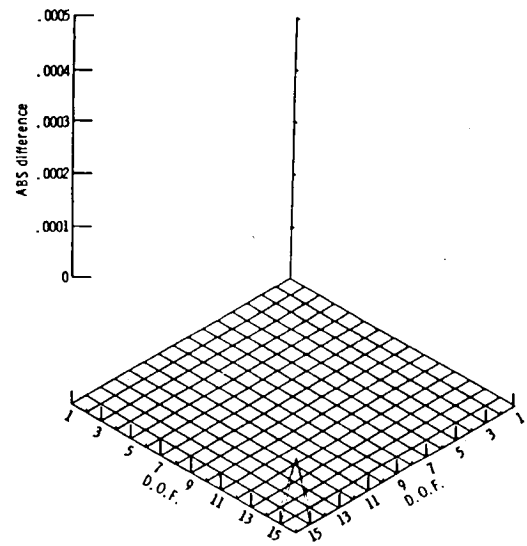

(a) Mass difference matrix.

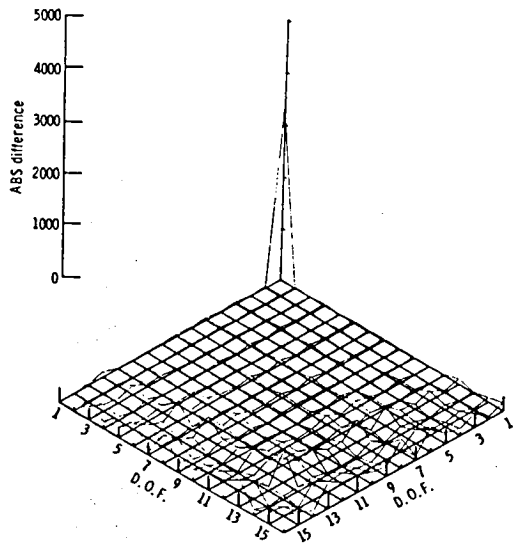

(b) Stiffness difference matrix.

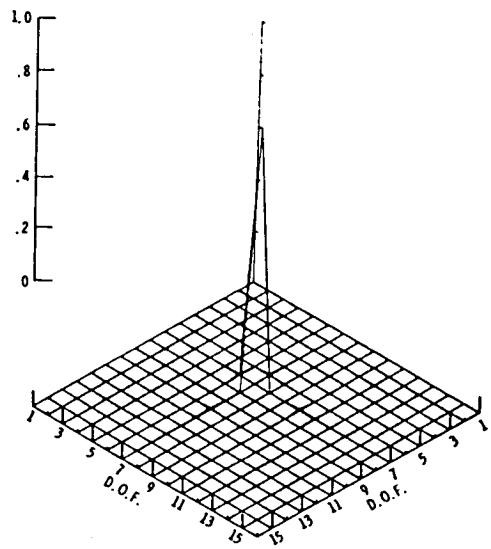

(c) Damping difference matrix.

Figure 6. - Computed differences for sample problem one, case 1, using 10 modes.

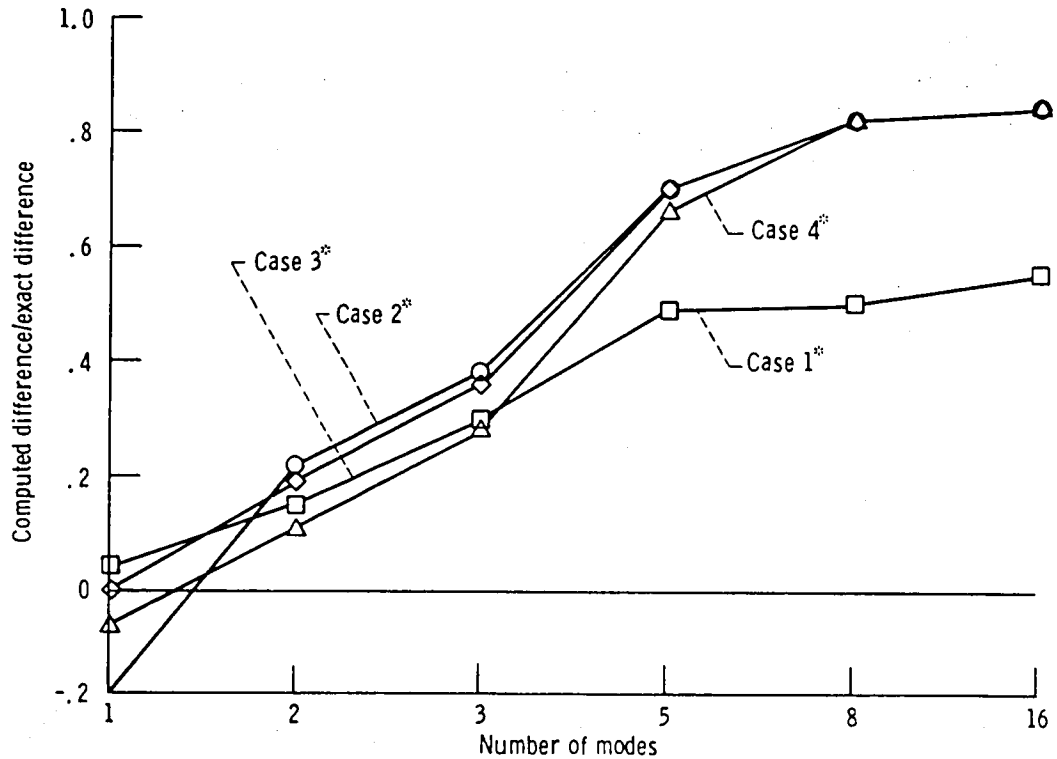

Figure 7. - Mass difference at concentrated mass location (sample problem one). (*See table I for case definition.)

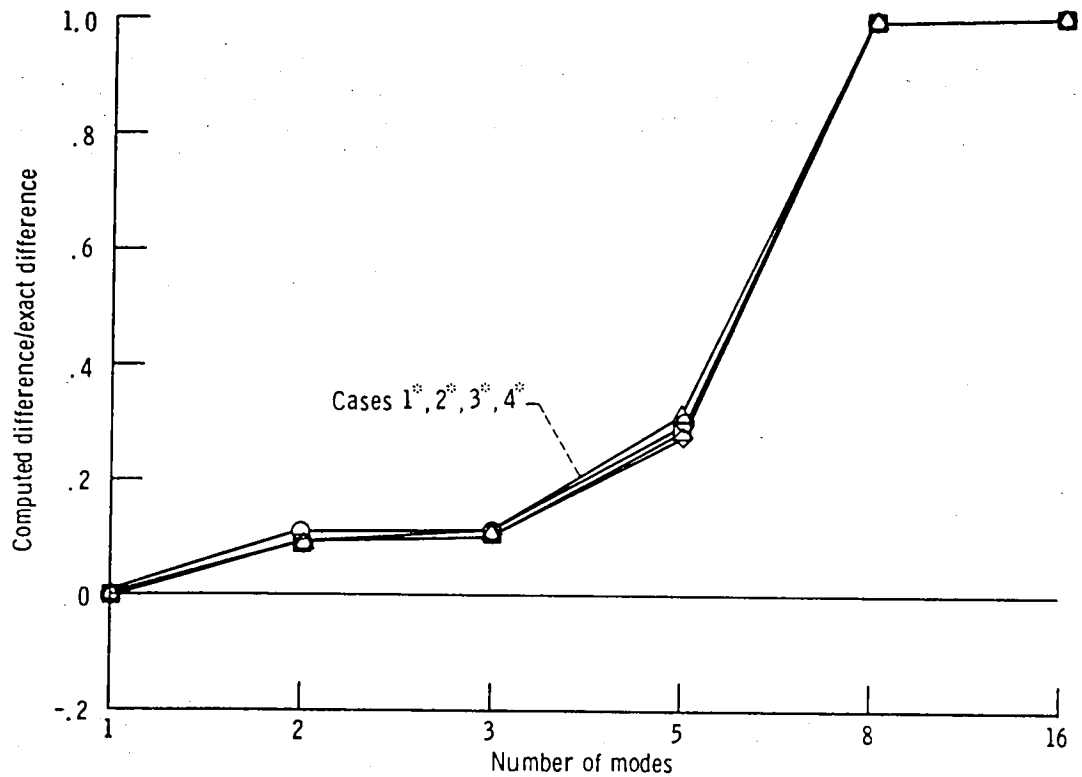

Figure 8. - Damping difference at concentrated damper location (sample problem one). (*See table I for case definition.)

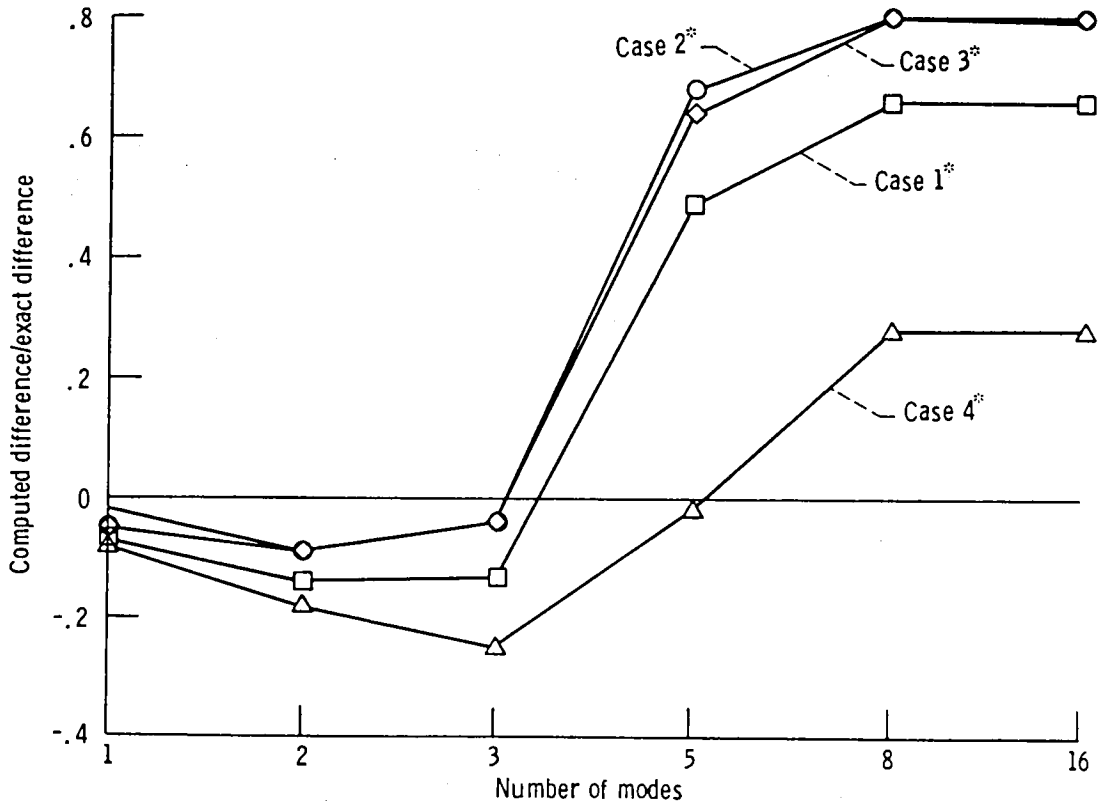

Figure 9. - Stiffness difference at concentrated spring location (sample problem one). (*See table I for case definition.)

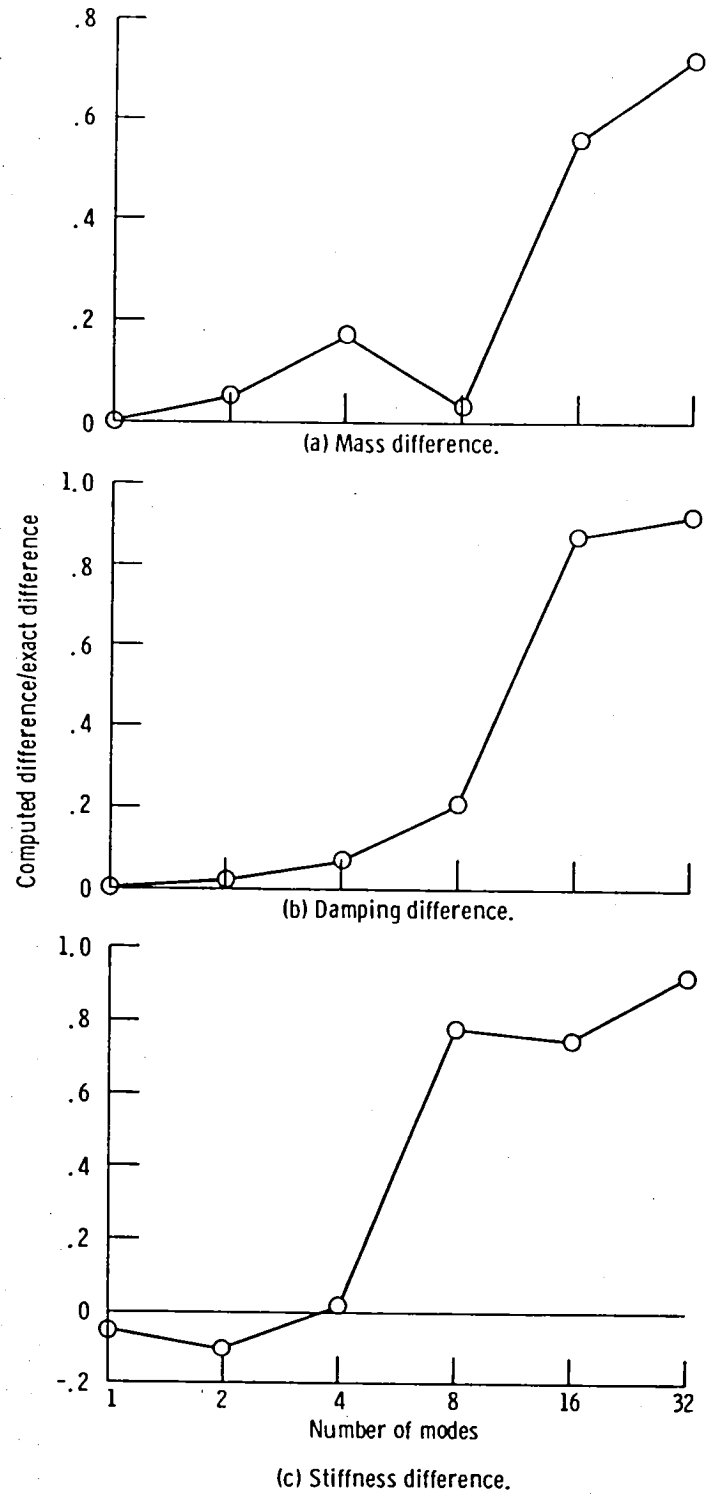

(a) Mass difference.

(b) Damping difference.

(c) Stiffness difference.

Figure 10. - Computed differences for 32 D.O.F. model.

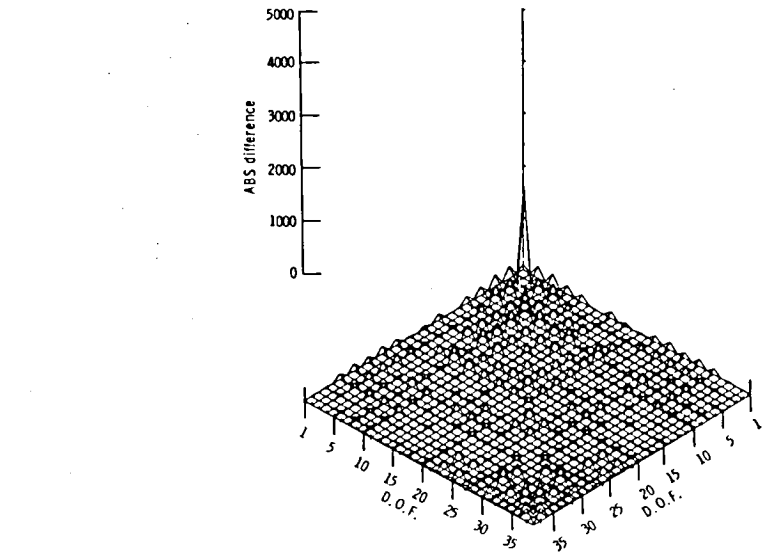

(a) Stiffness matrix difference.

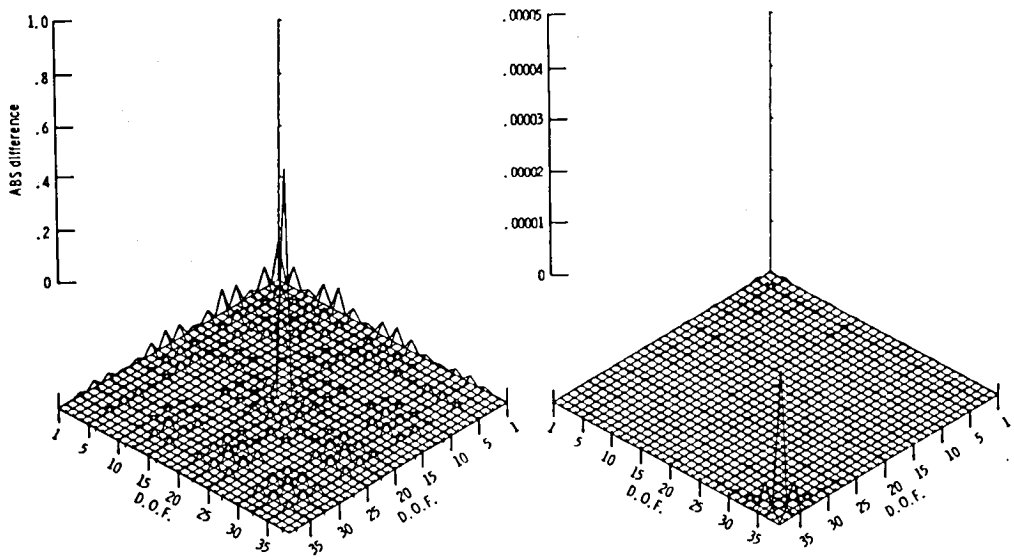

(b) Damping difference matrix.

(c) Mass difference matrix.

Figure 11. - Computed differences for 32 D.O.F. model, using 16 modes.

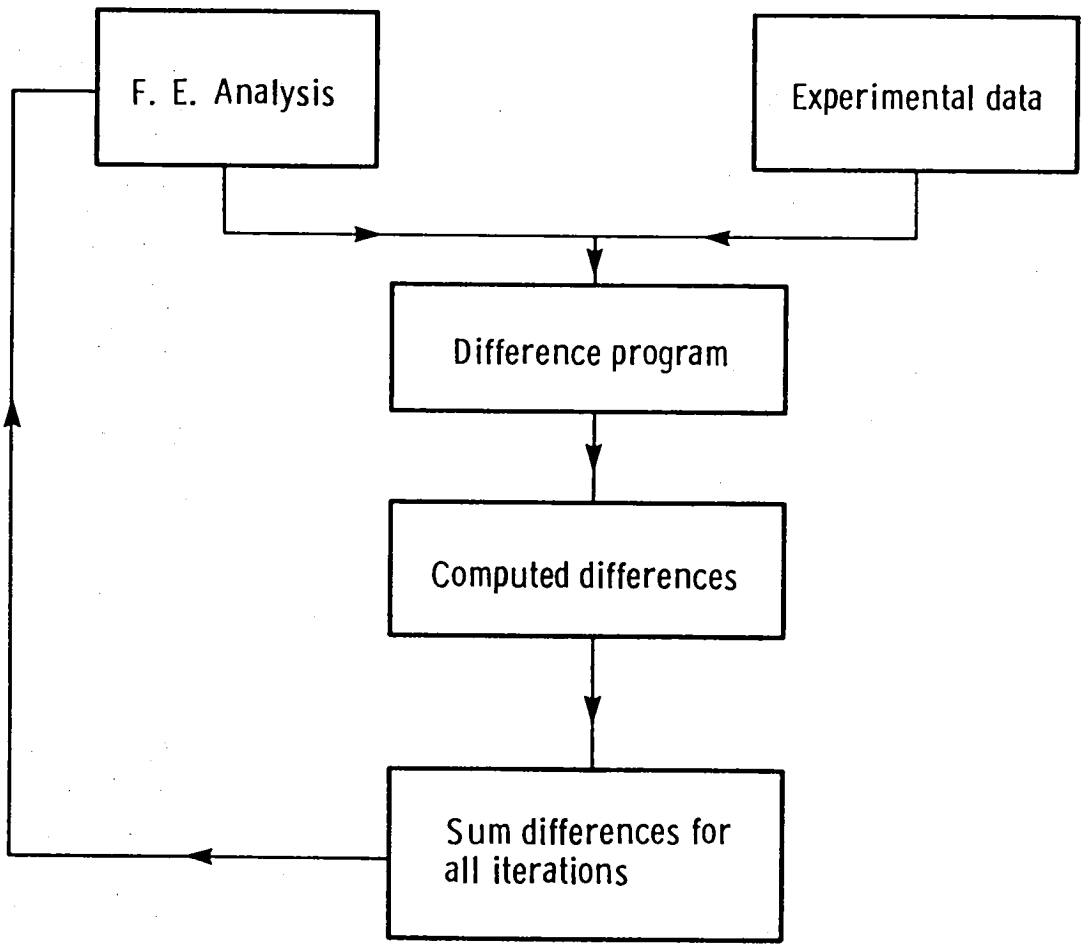

Figure 12. - Iteration scheme.

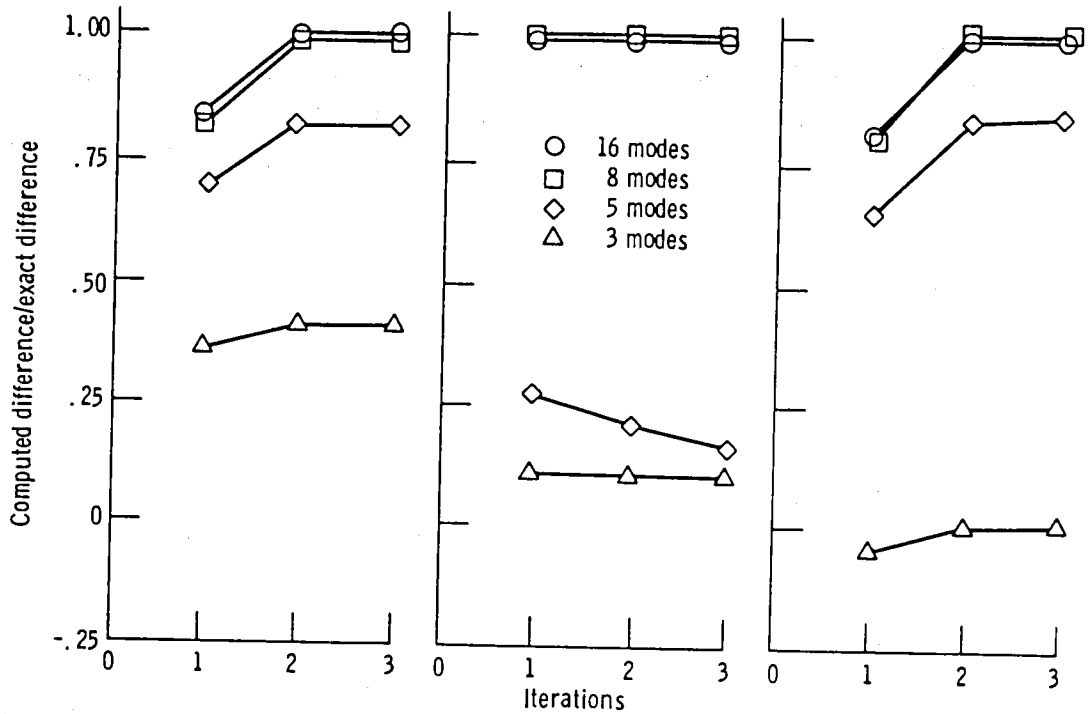

(a) Mass difference. (b) Damping difference. (c) Stiffness difference.

Figure 13. - Improvement in computed differences with iterations (sample problem one, case 3).

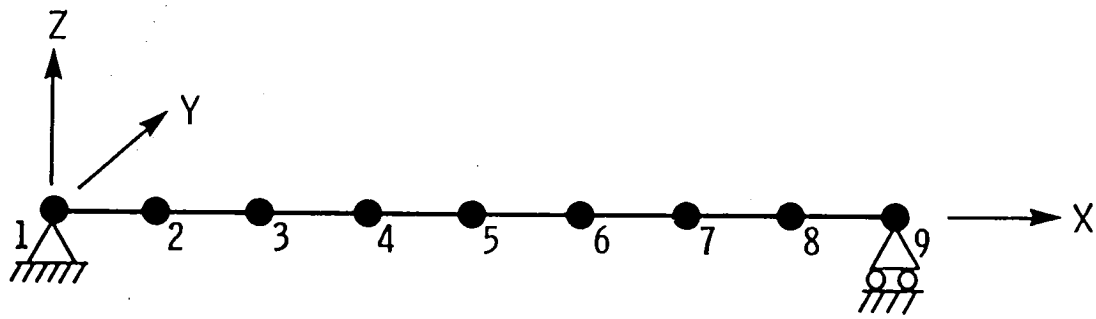

(a) Analytical model.

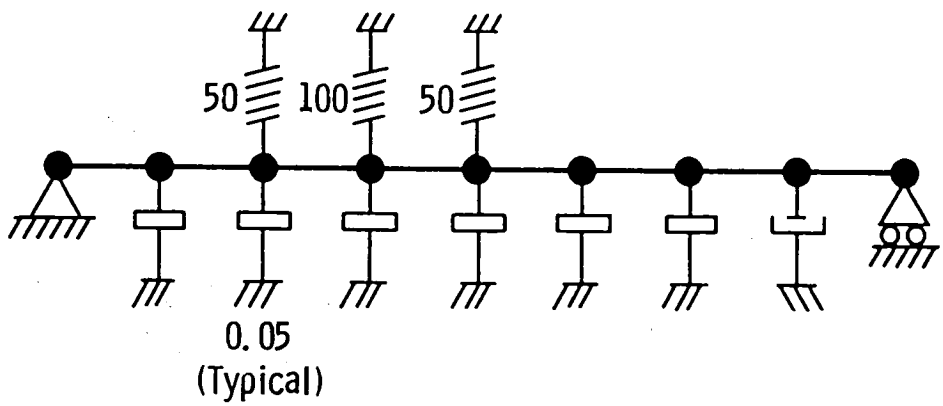

(b) "Experimental" model.

Figure 14. - Sample problem two.

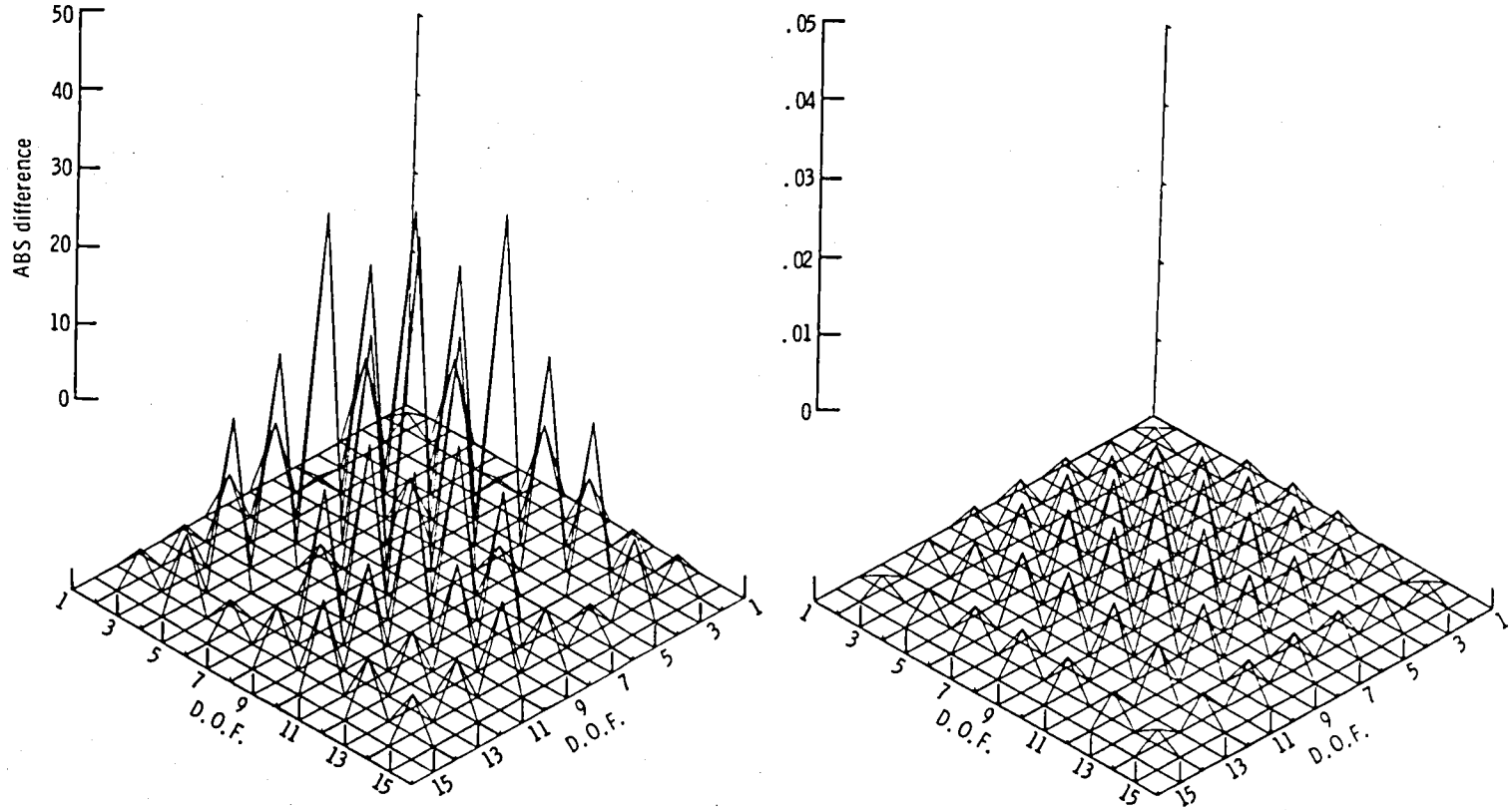

(a) Stiffness difference matrix.

(b) Damping difference matrix.

Figure 15. - Computed differences for sample problem two, using 1 mode.

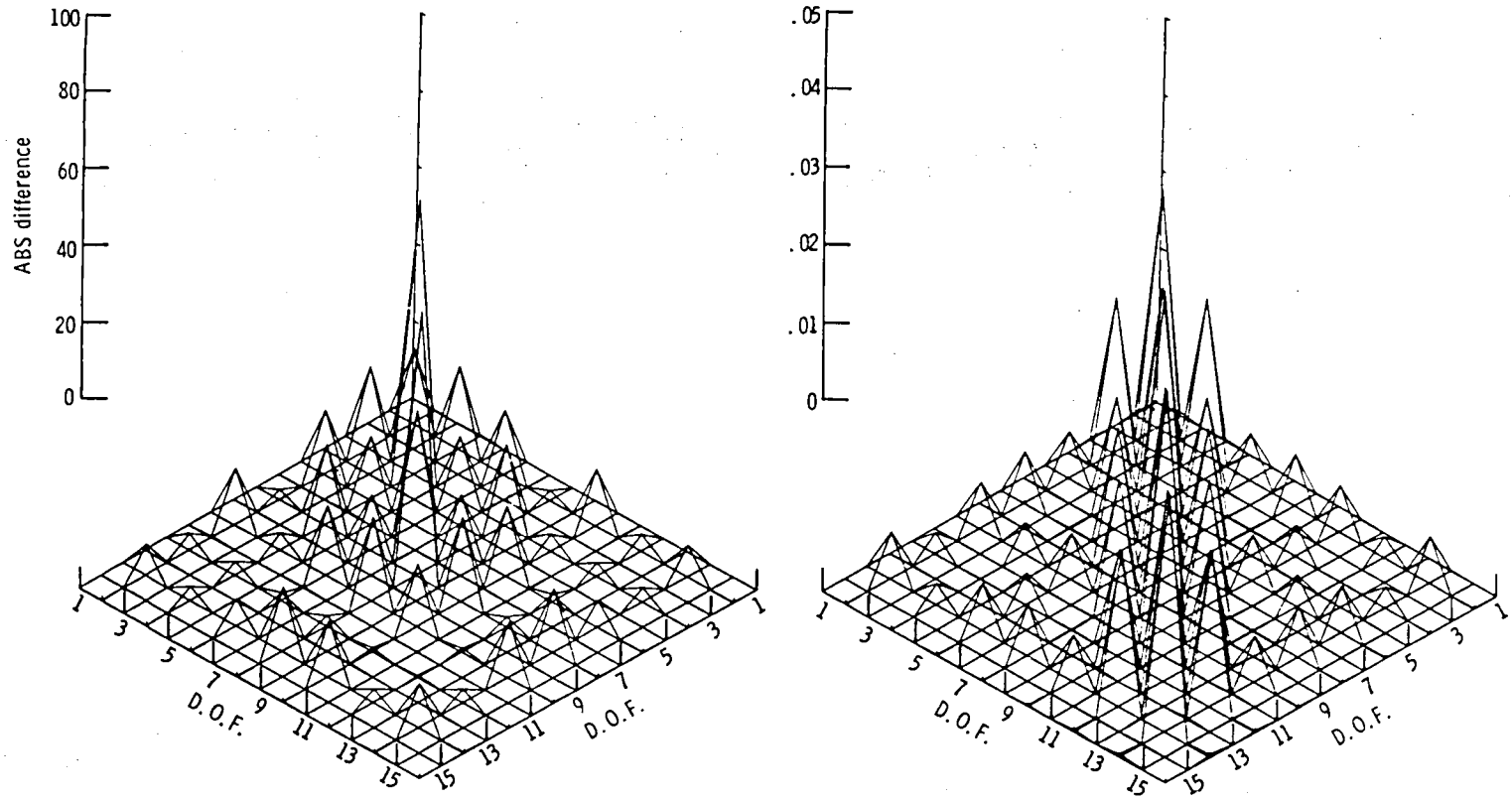

(a) Stiffness difference matrix.

(b) Damping difference matrix.

Figure 16. - Computed differences for sample problem two, using 4 modes.

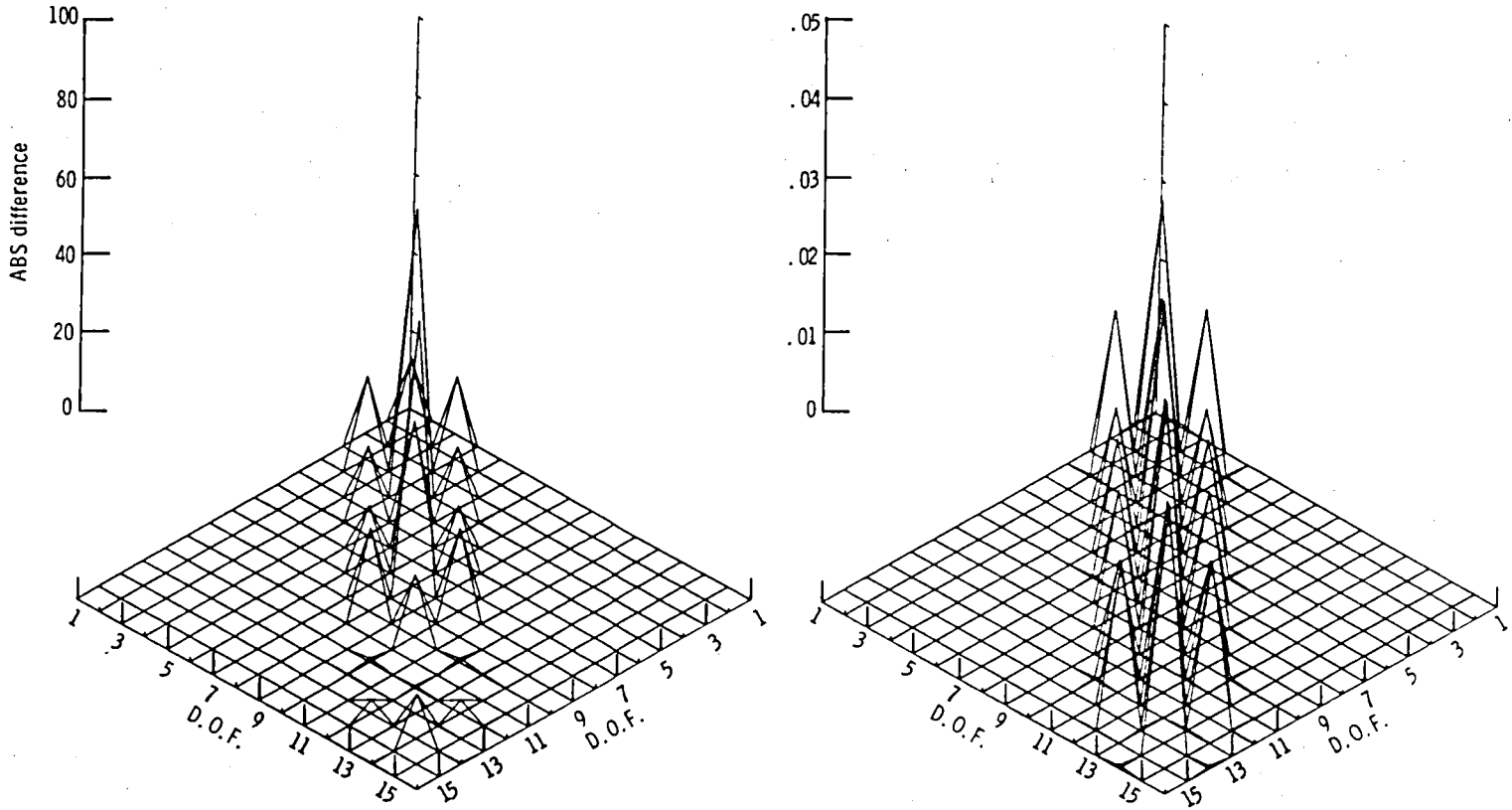

(a) Stiffness difference matrix.

(b) Damping difference matrix.

Figure 17. - Computed differences for sample problem two, using 4 modes and coupling constraints.

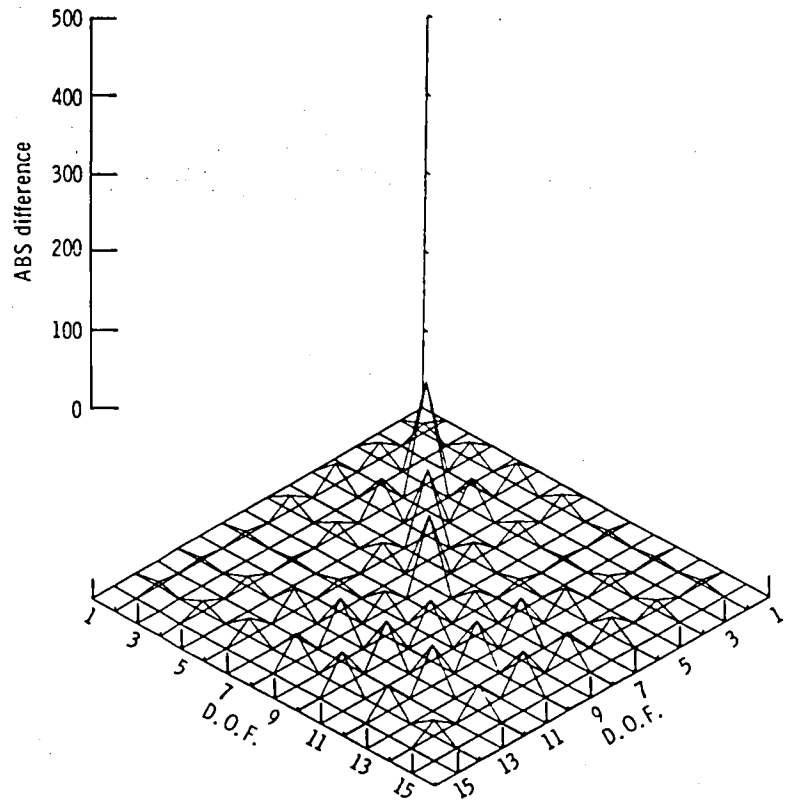

(a) Stiffness difference matrix.

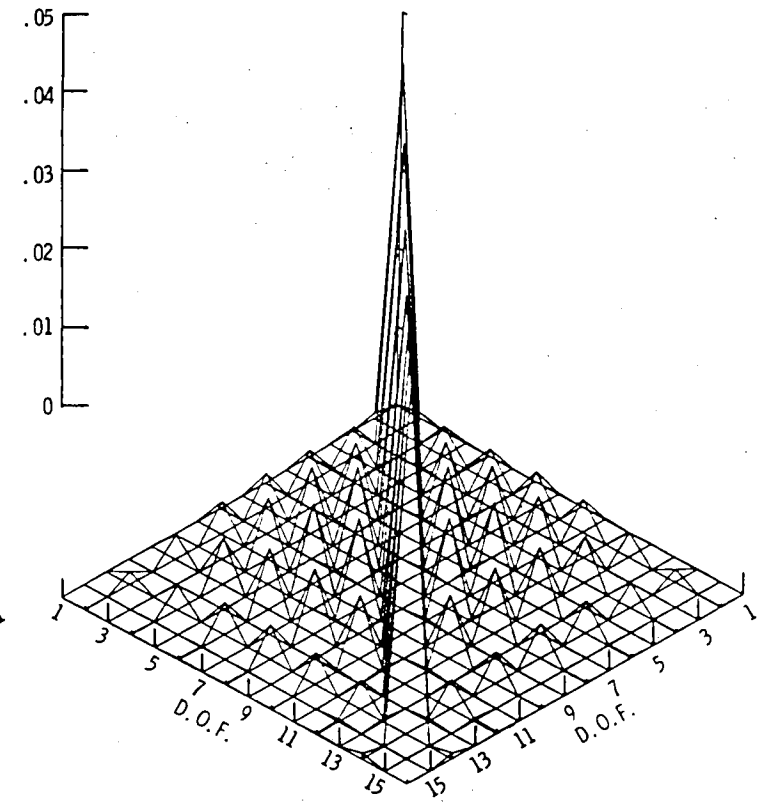

(b) Damping difference matrix.

Figure 18. - Computed differences for sample problem two, using 6 modes.

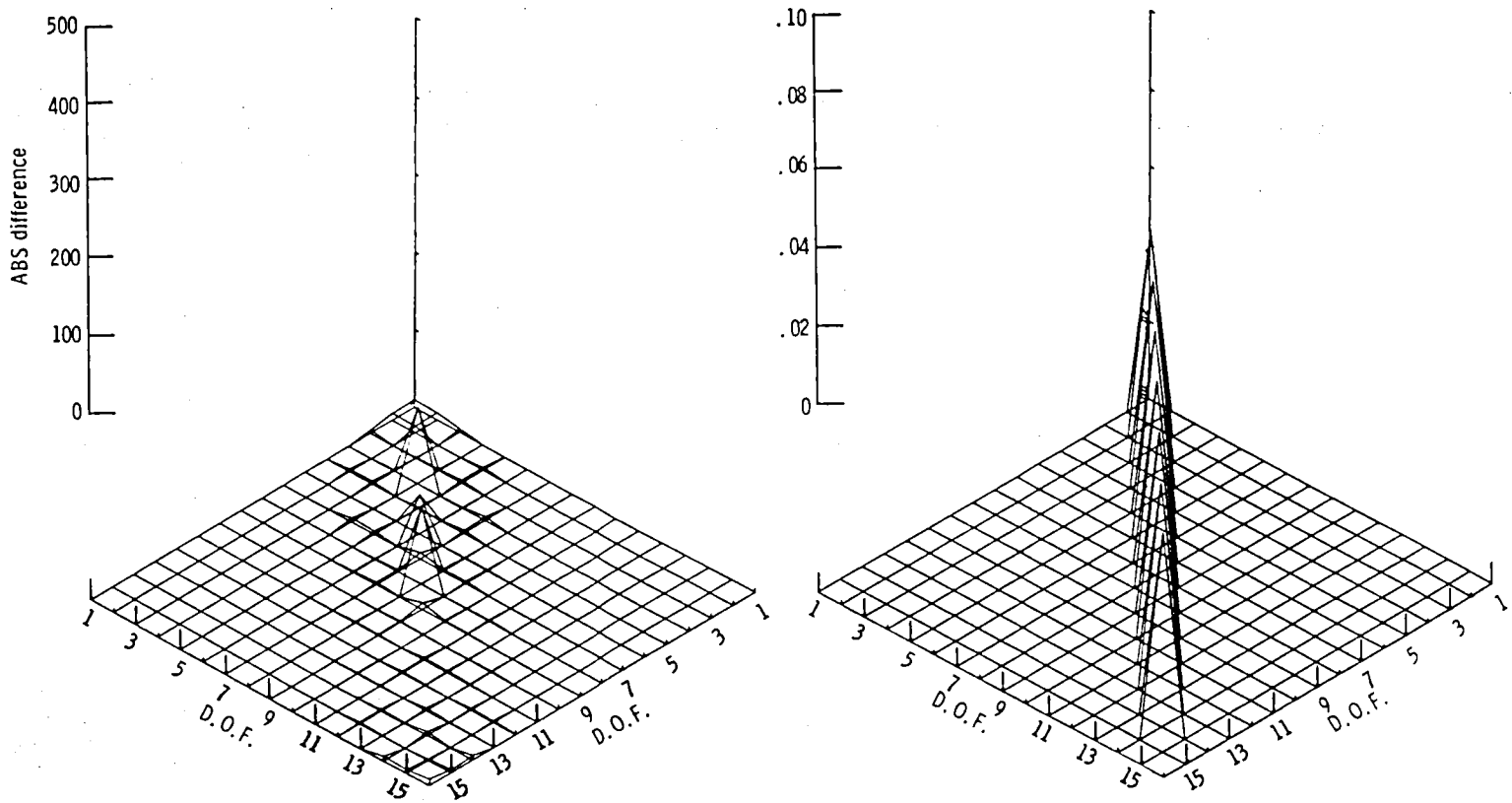

(a) Stiffness difference matrix.

(b) Damping difference matrix.

Figure 19. - Computed differences for sample problem two, using 16 modes.

CHAPTER III

IDENTIFICATION OF STRUCTURAL INTERFACE CHARACTERISTICS USING COMPONENT MODE SYNTHESIS

INTRODUCTION

The dynamic response of large structural systems is often analyzed using component mode synthesis (CMS) techniques. CMS is widely accepted for predicting coupled system response with increased modeling efficiency and flexibility over conventional methods. CMS techniques utilize a reduced set of component modes to characterize the overall system behavior. However, the inability to adequately model the connections between components has limited the application of CMS. Connections between structural components, and between components and ground are often mechanically complex and difficult to accurately model analytically. The modeling of these connections can profoundly influence predicted system behavior. This is because only the connections determine the boundary conditions which are imposed upon the system components. Thus, improved analytical models for connections are needed to extend the applicability of CMS and to improve system dynamic predictions.

Parameter identification (PID) techniques can be used to improve predicted response when experimental data are available. Modeling accuracy is improved with PID by reducing discrepancies between the measured characteristics of a physical system with those predicted by an analytical model of the system. Many techniques are available to carry out this process of parameter refinement. Most involve the determination of a set of structural parameters which optimally minimize differences between experiment and analytical prediction.

In this chapter, the combining of CMS and PID methods to improve the analytical modeling of the connections in a component mode synthesis model is explored. The approach involves modeling components with either finite elements or experimental modal data and then joining the components with physical connecting elements at their interface points. Interface connections in both the translational and rotational directions are addressed. Once the system model is derived, experimentally measured data is used with PID methods to improve the characterizations of the connections between components. Corrections in the connection properties are computed in terms of physical parameters. With this approach, the physical characteristics of the connections can be better understood, in addition to providing improved input for the CMS model.

The identification of connection characteristics is simplified by requiring individual components to be verified before they are incorporated into the coupled system model. This requirement will normally not present any difficulties, since component testing and verification has become a regular practice. With this requirement, the components are verified before they are used in the coupled system model. Any differences between the measured and predicted coupled system response can be solely attributed to inaccuracies of the estimated properties of the connections. Also, the quantity of test data that must be obtained from the coupled system is greatly reduced. This is particularly useful when it is impractical to obtain a complete set of vibration test data for a coupled structure. Examples, include large space structures, spacecraft systems, and turbomachinery.

Component Coupling Procedure

Numerous variations of the CMS method are currently available for the dynamic analysis of coupled structural systems (1,2,3). In the classical CMS approach, all of the system components are characterized in the modal domain using their respective modal parameters (frequencies and mode shapes). Coupling between components also is performed in the modal domain through use of modal constraints. These constraints are derived from displacement compatibility conditions existing at the component

interface locations. With the classical CMS approach, any components or connections that have been modeled in terms of physical coordinates (e.g., finite elements) must be transformed into the modal domain before they can be included in the coupled system equations of motion. The system equations, in terms of modal coordinates, are used to compute the system natural frequencies. The system mode shapes are computed by transforming the mode shapes obtained from the system equations back to physical coordinates.

Recent applications of the CMS method have shifted from the classical approach of utilizing only modal coordinates. Instead, techniques that use a mixture of both modal and physical coordinate systems have been implemented (3). There are several reasons for the shift to a "mixed" coordinate set. One reason is that a combination of component types can be incorporated into the coupled system equations without requiring all of the components to be in identical coordinate systems. This is particularly useful when some of the components have been modeled using F.E. methods and other component models have been derived from modal test data. In most of the currently used CMS methods boundary degrees of freedom of all of the components are expressed in terms of physical coordinates, and the internal degrees of freedom are expressed in either modal or physical coordinates. The inherent efficiency of the component representation is

retained. With physical boundary coordinates, components can be coupled utilizing classical direct stiffness assembly techniques as in conventional F.E. computer codes. Furthermore, nonlinear connecting elements can be used when boundary degrees of freedom are in physical coordinates. In the classical CMS approach, where modal coordinates are used, it is very difficult to incorporate nonlinearities into the coupled system model because of the difficulties associated with defining modal parameters for nonlinear elements.

In this chapter a simplified variation of the previously mentioned procedures for CMS is developed. The procedure is defined to be compatible with PID procedures which will be used subsequently for identifying the component interface characteristics. The modal components are first converted to "pseudo" finite elements to connect modal components to physical finite element components. The pseudo elements are then treated in the same manner as conventional finite elements, i.e., system property matrices are assembled through direct stiffness techniques.

Consider the system shown in Fig. 1. This system is comprised of two components which are coupled by a physical connecting component. The undamped, free vibration equation of motion for the uncoupled system is written in terms of physical coordinates as:

$$\begin{bmatrix} [M^I] & & \\ & [0] & \\ & & [M^{II}] \end{bmatrix} \begin{Bmatrix} \ddot{U}^I \\ \ddot{U}^C \\ \ddot{U}^{II} \end{Bmatrix} + \begin{bmatrix} [K^I] & & \\ & [K^C] & \\ & & [K^{II}] \end{bmatrix} \begin{Bmatrix} U^I \\ U^C \\ U^{II} \end{Bmatrix} = \{0\} \quad (1)$$

where [M] and [K] are the component system mass and stiffness matrices, and $\{\ddot{U}\}$ and {U} are the vectors of component nodal accelerations and displacements (the superscripts refer to the component identification). Equation (1) can further be partitioned by separating displacements internal to the components from those that are at the interfaces between components. When this is done Eq. (1) is written as:

$$\begin{bmatrix} \begin{bmatrix} M^I & & \\ & M^I_{bb} & \\ & & \begin{bmatrix} M^{II}_{bb} & \\ & M^{II} \end{bmatrix} \end{bmatrix} \begin{Bmatrix} \ddot{U}^I_i \\ \ddot{X}^I_b \\ \ddot{X}^{II}_b \\ \ddot{U}^{II}_i \end{Bmatrix} + \begin{bmatrix} \begin{bmatrix} 0 & \\ & C^c \end{bmatrix} & -C^c_{II\ I} \\ -C^{c\,T}_{II\ I} & \begin{bmatrix} C^c_{II} & \\ & 0 \end{bmatrix} \end{bmatrix} \begin{Bmatrix} \dot{U}^I_i \\ \dot{X}^I_b \\ \dot{X}^{II}_b \\ \dot{U}^{II}_i \end{Bmatrix} + \begin{bmatrix} \begin{bmatrix} K^I & -K^I_{Ib} \\ -K^{I\,T}_{Ib} & K^I_{bb} + K^c_I \end{bmatrix} & -K^c_{II\ I} \\ -K^{c\,T}_{II\ I} & \begin{bmatrix} K^{II}_{bb} + K^c_{II} & -K^{II}_{IIb} \\ -K^{II\,T}_{IIb} & K^{II} \end{bmatrix} \end{bmatrix} \begin{Bmatrix} U^I_i \\ X^I_b \\ X^{II}_b \\ U^{II}_i \end{Bmatrix} = \{0\} \quad (2)$$

The coupled system equation is obtained by applying the displacement compatibility conditions at the interface between the components and the connections. The displacements of the component and the connection must be equal at the interface therefore:

$$U^I_b = U^c_{Ib}$$

and

$$U^{II}_b = U^c_{IIb} \quad (3)$$

Using Eq. (3), the transformation matrix, [T], which relates the dependent and independent displacement sets is:

$$\begin{Bmatrix} U^I \\ U_b^I \\ U_{Ib}^c \\ U_{IIb}^c \\ U_b^{II} \\ U^{II} \end{Bmatrix} = \underbrace{\begin{bmatrix} 1 & 0 & 0 & 0 \\ 0 & 1 & 0 & 0 \\ 0 & 1 & 0 & 0 \\ 0 & 0 & 1 & 0 \\ 0 & 0 & 1 & 0 \\ 0 & 0 & 0 & 1 \end{bmatrix}}_{T} \begin{Bmatrix} U^I \\ U_b^I \\ U_b^{II} \\ U^{II} \end{Bmatrix} \tag{4}$$

From conservation of energy principles and the above transformation, the coupled equation of motion is found from:

$$[K]_{coupled} = [T]^T [K]_{uncoupled} [T]$$

and

$$[M]_{coupled} = [T]^T [M]_{uncoupled} [T] \tag{5}$$

Substituting the property matrices from Eq. (2) into Eq. (5) the coupled equation of motion is:

$$\begin{bmatrix} M^I & & & \\ & M_{bb}^I & & \\ & & M_{bb}^{II} & \\ & & & M^{II} \end{bmatrix} \begin{Bmatrix} \ddot{U}_l^I \\ \ddot{X}_b^I \\ \ddot{X}_b^{II} \\ \ddot{U}_l^{II} \end{Bmatrix} + \begin{bmatrix} 0 & & & \\ & C^c & -C_{II\ I}^c & \\ & -C_{II\ I}^{c\,T} & C_{II}^c & \\ & & & 0 \end{bmatrix} \begin{Bmatrix} \dot{U}_l^I \\ \dot{X}_b^I \\ \dot{X}_b^{II} \\ \dot{U}_l^{II} \end{Bmatrix} + \begin{bmatrix} K^I & -K_{Ib}^I & & \\ -K_{Ib}^{I\,T} & K_{bb}^I + K_I^c & -K_{II\ I}^c & \\ & -K_{II\ I}^{c\,T} & K_{bb}^{II} + K_{II}^c & -K_{IIb}^{II} \\ & & -K_{IIb}^{II\,T} & K^{II} \end{bmatrix} \begin{Bmatrix} U_l^I \\ X_b^I \\ X_b^{II} \\ U_l^{II} \end{Bmatrix} = \{0\} \tag{6}$$

The procedure outlined above can be used to couple any number of physical components into the system equations. As mentioned previously, when modal components are to be coupled into the system model they are converted to pseudo physical components and then are treated in the same manner as conventional physical components. The pseudo physical property matrices are obtained from orthogonality relationships between the property matrices and the modal parameters. When the component mode shapes are normalized so that the modal mass matrix equals the identity matrix, the modal and physical property matrices are related by:

$$[\phi]^T[M][\phi] = [I]$$

and

$$[\phi]^T[K][\phi] = [\tilde{w}^2] \qquad (7)$$

where [M] and [K] are the component physical mass and stiffness matrices, $[\tilde{w}^2]$ are the component frequencies, and $[\phi]$ is the matrix of component mode shapes.

When experimental modal data is used to characterize the component, the matrix $[\phi]$, containing the component mode shapes may be rectangular. If "m" mode shapes are measured, and the value of the mode shapes are recorded at "n" different physical locations on the component, then the mode shape matrix will be of order n x m. Normally, there will be more measurement locations available than there will be modes that can be measured. To

obtain a square modal matrix from experimental mode shape data, data at some measurement points can be neglected so that the number of points is equal to the number of modes. When data at measurement points is discarded no information is lost as far as the overall system response is concerned, so long as measurements at the component's interface points are retained. Once a square mode shape matrix is available, the pseudo physical property matrices are related to the modal data by:

$$[M_p] = [\phi^T]^{-1} \quad [\phi]^{-1}$$

and

$$[K_p] = [\phi^T]^{-1} [\omega^2] [\phi]^{-1} \tag{8}$$

where $[M_p]$ and [Kp] are the component pseudo mass and stiffness matrices. (The coefficients of the mass and stiffness matrices are in terms of physical coordinates corresponding to the location and direction where the mode shapes are measured).

The matrices computed in Eq. (8) are designated as pseudo matrices because their physical interpretation is unlike that of conventional mass and stiffness matrices. Because it is impractical to measure all of the component modes, the modal data will be incomplete (see (4)) and will not contain all the information required to produce the actual component mass and stiffness matrices. Therefore, although the mass and stiffness

matrices computed in Eq. (8) are in terms of physical rather than modal coordinates, the matrices will not necessarily represent the actual physical mass and stiffness characteristics of the component. The mass and stiffness matrices from Eq. (8) will reproduce the measured frequencies and mode shapes, and will be suitable for representing the component in the coupled system model.

Either the "free" or the "fixed" boundary component modes can be used for the component characterization. The "free" mode shapes are those modes that correspond to the component when it is in the unconstrained or free boundary condition. In many situations these modes are more conveniently obtained than the fixed boundary modes. This is particularly true when the modes are measured experimentally, because the component itself does not have to be physically constrained during the experimental testing. In practice, the free boundary condition often is approximated by suspending the component from flexible cords or by supporting it on soft springs.

The fixed modes are obtained by simultaneously constraining all of the component's boundary degrees of freedom while performing the modal testing. Analytically, the fixed modes are computed as easily as the free modes. Experimentally, they are more difficult to obtain, because all of the component's boundary degrees of

freedom must be fully constrained during the experiment. To attain this condition requires that elaborate fixtures be attached at the components boundary locations, and in practice, full constraint is never completely achieved. Another difficulty of using fixed boundary mode shapes is that an additional set of "static" deflection or constraint modes must be added to the set of fixed boundary modes. These modes are required so that the component will have flexibility at its boundary locations where it is connected to adjacent components.

Normally, the values of the experimental mode shapes are measured in the translational directions. It is not generally practical to measure the values of the mode shapes in the rotational directions because of limitations in available instrumentation. However, it is sometimes desirable to couple rotational degrees of freedom between components. If the values of the mode shapes are not measured in the rotational directions, the pseudo matrices will only have translational degrees of freedom and there will not be means of coupling the rotational connecting stiffnesses. To circumvent this difficulty, the rotational values of the mode shapes can be extrapolated from the translational values, either by curve fitting through the translational degrees of freedom and then computing the slope of the curve at the connection location, or by using an approximate F.E. model of the component (see (5)).

When the rotational values are extrapolated from a curve fit any existing rotational inertia effects will not be reflected in the values of the rotations. Neglecting the actual independent motion of the rotation implies that there is no rotational inertia and that the rotations are dependent on the translations. Because of this dependence, the combined translational/rotational mode shapes can not be used directly to compute the pseudo matrices without encountering numerical problems during the matrix inversions in Eq. (8). A solution to this difficulty is to initially use only the translational mode shapes to compute the pseudo matrices. Then, a transformation which is based on the dependence between the rotations and translations is used to transform the pseudo matrices from the translational coordinate system to a combined translational/rotational system.

The dependent rotational values of the mode shapes can be related to the independent translations by:

$$U_{\theta_j} = \sum_{i}^{n} a_i U_{\Delta i} \tag{9}$$

Where U_{θ_j} is the dependent rotation at j, $U_{\Delta i}$ are the translations at the independent measurement points, a_i are the coefficients relating the independent translations to the dependent rotations (determined from curve fit, etc.), and n is the number of independent measurement points.

The transformation from the mixed coordinate matrices to the entirely translational pseudo property matrices is:

$$\left\{U_\Delta\right\}_n = \begin{bmatrix} T' & 0 \\ 0 & I \end{bmatrix}_{nxn} \left\{\begin{matrix} U_\Theta \\ U_\Delta' \end{matrix}\right\}_n \tag{10}$$

where [T'] is the transformation matrix derived from the relationships in Eq. (9) and $\{u_\Delta\}'$ is a subset of $\{u_\Delta\}$. For each rotational degree of freedom that is added in $\{u_\Theta\}$, a translational degree of freedom is removed from $\{u_\Delta\}'$. The selection of the translational degrees of freedom that are removed is arbitrary, and since a translation is removed for each rotation that is added, both systems will contain the same number of degrees of freedom.

Using the original translational pseudo property matrices from Eq. (8), the transformation in Eq. (10), and principles of conservation of energy, the pseudo matrices are derived in the combined translational/rotational coordinate system by:

$$\begin{aligned} [K_p]_{U_\Delta' U_\Theta} &= \begin{bmatrix} T & 0 \\ 0 & I \end{bmatrix}^T \begin{bmatrix} K_p \end{bmatrix}_{U_\Delta} \begin{bmatrix} T & 0 \\ 0 & I \end{bmatrix} \\ [M_p]_{U_\Delta' U_\Theta} &= \begin{bmatrix} T & 0 \\ 0 & I \end{bmatrix}^T \begin{bmatrix} M_p \end{bmatrix}_{U_\Delta} \begin{bmatrix} T & 0 \\ 0 & I \end{bmatrix} \end{aligned} \tag{11}$$

Once the component pseudo matrices in Eq. (11) are computed, they can be inserted into the system equations of motion and coupled to adjacent components using the previously discussed procedures.

The final coupled system equations can be used to predict the overall system dynamic characteristics. The frequencies that are computed from this equation will correspond to the overall system resonances. The accuracy of the predicted frequencies will be dependent on the precision with which the connections between components have been modeled. It has been assumed that the component modal models have been verified and are accurate, and also, that the proper component modes have been included in the model to adequately predict system response (see sample problem one).

The mode shapes derived from the system equations will correspond to the physical degrees of freedom included in the system model. When the combined translational/rotational model is used some of the mode shape values will correspond to translational degrees of freedom and some to rotations. The accuracy of the mode shapes, like the frequencies, will be dependent on the adequacy of the component modal representations and the modeling of the connections.

Parameter Identification Procedure

Once the system equations of motion and their corresponding frequencies and mode shapes are computed, and the experimental system modes have been measured, PID can be used to find an improved set of connection parameters that better predict the measured experimental system data. For this study the Weighted Least Squares method for parameter estimation is used (6).

If $\{\bar{c}\}$ and $\{c\}$ are vectors containing the measured and computed system frequencies and mode shapes respectively, then the weighted squared difference between the predicted and measured characteristics is:

$$\{F\} = [W](\{\bar{c}\} - \{c\})^2 \tag{12}$$

where [W] is the weighting matrix and {F} is a vector of weighted squared differences. To find the set of connection parameters that minimizes the weighted squared differences, the derivative of {F} with respect to the connection parameters is set to zero. Noting that the predicted characteristics {c}, are a function of the connection parameters {r}, the derivative of {F} is written as:

$$\frac{\partial\{F\}}{\partial\{r\}} = [W](\{\bar{c}\} - \{c\}) \frac{\partial\{c\}}{\partial\{r\}} = \{0\} \tag{13}$$

Expanding {c} in a Taylor series and truncating higher order terms, {c} is approximated as:

$$\{c\} = \{c\}_{est} + \frac{\partial\{c\}}{\partial\{r\}} \{\Delta r\} \tag{14}$$

Where $\{\Delta r\}$ are the differences between the estimated and actual values for the connection parameters. Substituting Eq. (14) into Eq. (13) and letting $\partial\{c\}/\partial\{r\}=[S]$ leads to:

$$[W](\{\bar{c}\} - \{c\}_{est} - [S]\{\Delta r\})[S] = \{0\} \tag{15}$$

From Eq. (15) it is desired to solve for $\{\Delta r\}$ so that the actual connection parameters can be determined. Solving for $\{\Delta r\}$ can not be accomplished by simple inversions, however, because in general the number of measured and predicted characteristics will be greater than the number of connection parameters, rendering the matrix $[S]$ to be nonsquare. The vector $\{\Delta r\}$ can be solved for if Eq. (15) is first premultiplied by $[S]^T$. When this is done, $\{\Delta r\}$ is solved as:

$$\{\Delta r\} = \left([S]^T[W][S]\right)^{-1} [S]^T[W] \left(\{\bar{c}\} - \{c\}_{EST}\right) \tag{16}$$

An updated set of connection parameters is computed by:

$$\{r\} = \{r\}_{EST} + \{\Delta r\} \tag{17}$$

or by substituting from Eq. (16):

$$\{r\} = \{r\}_{EST} + \left([S]^T[W][S]\right)^{-1}[S]^T[W] \{\bar{c}\} - \{c\}_{EST} \tag{18}$$

Since $\{c\}$ is approximated by a truncated series, the improved connection parameters will be only an approximation to the final parameters. However, the final parameters can be obtained by iterating on Eq. (18).

A direct approach for computing the elements of the sensitivity matrix [S] is to perturb the analytical model with changes in the connection parameters, and then compute the resulting changes in the system characteristics. The elements are then computed by setting S_{ij} equal to the change in the C_i characteristic divided by the change in the r_j connection parameter. Alternative methods for computing these derivatives have been presented (see (7)) but for problems such as the example, with only a small number of connection parameters, the above method is adequate.

The selection of the system characteristics that are used in the estimation procedure is determined by data acquistion capability. Experimentally, it is generally easier to measure frequencies than mode shapes, so in many cases it may be practical to include more frequencies than modes shapes. Characteristics other than frequencies and mode shapes also can be utilized; in (8), it is suggested that kinetic energy may be a useful characteristic. Once the characteristics are chosen, the weight that is placed on each characteristic must be determined. If one characteristic is measured more accurately than another, then it can be weighted more heavily.

When the number of system characteristics is large, the size of the weighting and sensitivity matrices increases, and the matrix

in Eq. (18) may become ill conditioned for inversion (see (9)). The PID procedure only requires a minimum number of system characteristics to adequately identify the connection parameters since each component has already been verified. Therefore, the size of the matrices in Eq. (18) will be kept small and inversion problems will be minimized. Another problem may arise when the analytical model cannot be exactly made to fit the experimental data. When this is the situation the set of connection parameters that minimizes the differences, rather than eliminates them, must be used. The model may not be able to produce the desired measured system characteristics because of limitations in the component modal representation. Also, if the experimentally measured modes are not orthogonal, perfect agreement can never be achieved because the analytical model can only produce orthogonal mode shapes.

Sample Problem One: Coupled Beams

The following sample problem is offerred to demonstrate the component coupling and parameter identification procedures. To verify these procedures simulated experimental data generated from a F.E. model was used. The sample problem (Fig. 2) is comprised of two simply supported beams connected at their ends. For simplicity, both beam components were made identical. In actual applications the system can be partitioned into any set of

components that is desired. Each of the components in this problem are discretized into seven massless, planar beam elements. Concentrated translational masses are added between the elements at nodes 2 through 7 and 10 through 15. The components are connected by a rotational spring (K = 10.E5) at nodes eight and nine. A connection also is made to ground by a rotational spring (K = 10.E5) added to the second component at node 16.

The accuracy of the computed system frequencies as a function of the number of modes used for the component representations was evaluated with six, four, and two component modes (see Table I). Both the six and four component mode representations produced system frequencies that are in good agreement with the baseline F.E. solution. Although there are only six component modes in the F.E. solution, the six mode representation does not produce exact frequencies because the F.E. model has more than 6 degrees of freedom. The two mode representation allows for the first and third modal frequencies to be predicted satisfactorily but does not provide enough information for an accurate prediction of the second and fourth frequencies. At least two component modes are required so that there will be a rotational degree of freedom at each end of the component that is connected to ground (only one mode is needed for the other component). In every case the component mode solution produced frequencies that are higher than the baseline frequencies. This is understandable since the

component mode solution uses a truncated set of modes and therefore does not include all of the component's flexibility.

For the initial attempt at identifying the connection properties, only the simulated system frequencies from the F.E. model (Table II) were used in the parameter identification routines. It is preferable that the connection properties be identified without having to use system mode shapes because the mode shapes are considerably more difficult to experimentally measure than the frequencies. When either six or four component mode representations were used two possible solutions were found for the K_1 and K_2 connecting stiffnesses which satisfied the system frequency constraints (see Table II). The chosen solution was dependent on the initial starting estimates for K_1 and K_2. Although neither solution is equal to the actual connecting stiffnesses, the first one is reasonably close considering the limited number of system data used and the approximation of the component modal representation. When either of the solutions are input into the F.E. model they produce system frequencies that are very close to the exact frequencies. The first solution does produce a better set of system mode shapes. In an actual application, without more than system frequency information, it would be impossible to determine which of the two solutions is closer to the actual values of the connecting stiffnesses. Furthermore, since both the five and two system frequency cases

produced similar solutions there is no advantage to using more than two system frequencies. When two component modes are used a maximum of four system frequencies are available, therefore the five system frequency case cannot be analyzed. For the two component modes and two system frequency case, the solution failed to converge.

A subsequent attempt, using a combination of both system frequencies and mode shapes was made with the expectation that the identification of the connection properties would be improved. By adding the first mode shape as a constraint, along with the first five system frequencies, the second multiple solution was eliminated. When only one system frequency and one mode shape was used, the problem still converged to the first solution regardless of the initial estimates for the connecting stiffnesses. This combination of system data is ideal because, while it eliminates the multiple solution, it only requires a minimal amount of experimental data. Similar results were produced for both the six and four component mode representations, while the two mode representation continued to present difficulties.

Sample Problem Two: RSD Rig Verification

Once the component coupling and parameter identification algorithms were evaluated with simulated data (Sample Problem

One), it was decided to assess the procedures using actual experimental data. To accomplish this, the RSD (Rotating Structural Dynamics Rig) at NASA Lewis Research Center was selected. The RSD rig (Fig. 3) is designed to simulate engine structures to study active rotor control and system dynamics (component interaction) problems. The rig components, although considerably simpler than a real turbine engine's, were scaled such that they would simulate an actual engine's structural dynamics response characteristics.

The objective of the parameter identification was to determine the stiffnesses of the squirrel cage bearing support that connects each end of the rotor to the support frame. To accomplish this, the RSD rig was divided in two components; the rotor support frame, and the rotor. Each of these components was characterized and then verified experimentally, so that accurate component representations would be available for the coupled system model. In the system model the support frame was represented by an experimentally verified F.E. model while the rotor component was represented by experimental modal data. Since both components were experimentally verified, any differences that appeared between the predicted and measured system characteristics could be attributed to the uncertainties in the squirrel cage connections between components. This approach considerably simplified the verification task by reducing the quantity of modal data required from the coupled system.

The support frame finite element mesh is shown in Fig. 4. The frame is mounted on a relatively stiff base plate so grid points 35 through 39 are fully constrained. Grid points 19 and 20, where the rotor is attached, were allowed to freely displace. This free condition is representative of the conditions used during the modal tests and is also compatible with the requirements for the component coupling procedure. The grid points are connected with beam (bending and axial deformations) elements except for the diagonal elements at grid 35 which are modeled with rod (axial deformation only) elements. All of the elements are modeled with A36 steel properties. The frame F.E. model was analyzed with NASTRAN, to compute the component frequencies and mode shapes (Fig. 5). The frequencies were experimentally verified by using vibration data obtained from an HP 5423 Dynamic Analyzer. The rotor modal representation was obtained by measuring the rotor mode shapes in the free boundary condition. This condition was approximated by hanging the rotor from bungy cords. The component modal characteristics were generated from transfer function data obtained from the dynamic analyzer and impact testing. A total of six rotor modes were measured (see Fig. 6) including two rigid body and four elastic modes.

The support frame and rotor were coupled by combining the physical F.E. model of the frame with the modal representation of

the rotor. For simplicity the coupled system model was constrained to motion only in the vertical plane. This restriction allowed for a reduction in the required number of degrees of freedom in the system model and allowed for all of the system testing to be performed in one plane. The coupled system frequencies for the six mode rotor representation are plotted along with the measured frequencies in Fig. 7. The predicted frequencies were computed for different values of squirrel cage stiffness to determine the effect that the cages have on the system frequencies.

To generate these results it was assumed that both squirrel cages had identical stiffnesses. This was a rational assumption, since both cages are built to the same specifications. (Subsequent to this analysis the cage stiffness was measured as 5050 lb/in. using a static loading test.)

Only the first three computed system frequencies are shown because only three frequencies were measured. When all three frequencies are used the cage stiffness is identified as 5750 lb/in. This value is in good agreement with the measured stiffness (5050), considering that only three system frequencies were used for the parameter identification. In Fig. 7 it is shown that this amount of difference in cage stiffness does not have a significant effect on the system frequencies.

In addition to the six mode rotor representation, a four and two mode representation were used to determine the effect that the number of component modes has on the stiffness identification. The four mode representation identified the same cage stiffness as the six mode representation. The two mode representation identified the cage stiffness as about 2300 lb/in. or only 46 percent of the measured stiffness. It was expected that the two mode representation would be insufficient for identifying the cage stiffness because this representation is inadequate for accurately predicting the system modes. It is obvious that the two mode representation cannot produce very good results because only rigid body modes are included in the representation, and the system modes involve elastic bending in the rotor. Although rules of thumb are available for determining the required number of modes, additional work is required in this area.

Conclusion

From the two sample problems analyzed in this study it was determined that the stiffness characteristics of component connections can be identified using component mode synthesis and parameter identification procedures. Furthermore, the characteristics can be identified using experimentally obtained component modal representation and a minimal quantity of measured system modal data. In the first sample problem it was found that

multiple solutions are possible, but that they can be avoided when system mode shapes are included in the identification procedure. In the second problem it was found that the rotor for a rotor/support frame coupled system could be adequately represented by experimentally obtained modal data. It was also found that only three system frequencies had to be measured for the connection characteristics between the frame and rotor to be identified. From the results obtained thus far, it is determined that the quantity of data required for the component representations and for the connection characteristic identification is problem dependent. Therefore, each application must be treated on an individual basis.

References To Chapter III

1. Hurty, W.V.: Dynamic Analysis of Structural Systems by Component Mode Synthesis. JPL-TR-32-350, NASA CR-53057, 1964.
2. Craig, R.R., Jr.: Structural Dynamics. John Wiley and Sons, New York, 1981.
3. Martinez, D.R.; and Gregory, D.L.: A Comparison of Free Component Mode Synthesis Techniques Using MSC/NASTRAN. SAND 83-0025, 1984.
4. Berman, A.; and Flannelly, W.G.: Theory of Incomplete Models of Dynamic Structures. AIAA J., vol. 9, no. 8, Aug. 1971, pp. 1481-1487.
5. Berman, A.; and Nagy, E.J.: Improvement of a Large Dynamic Analytical Model Using Ground Vibration Test Data. 23rd Structures, Structural Dynamics and Materials Conference, Part 1, AIAA, New York, 1982, pp. 301-306.
6. Isenberg, J.: Progressing from Least Squares in Bayesian Estimation. ASME Paper 79-WA/DSC-16, Dec. 1979.
7. Collins, J.D., et al.: Statistical Identification of Structures. AIAA J., vol. 12, no. 2, Feb. 1974, pp. 185-190.

TABLE I. - COUPLED SYSTEM FREQUENCIES (SAMPLE PROBLEM ONE)

(CONNECTION STIFFNESS $K=10 \times 10^5$)

BASELINE FINITE ELEMENT SOLUTION	COMPONENT MODE SYNTHESIS SOLUTION		
	NUMBER OF COMPONENT MODES		
	6	4	2
1. 112 Hz	114 Hz (2%)	114 Hz (2%)	145 Hz (29%)
2. 165	177 (7%)	180 (9%)	197 (19%)
3. 421	425 (1%)	426 (1%)	431 (2%)
4. 496	523 (5%)	525 (6%)	561 (13%)
5. 927	932 (1%)	933 (1%)	---

TABLE II. - COMPUTED CONNECTION STIFFNESS

NUMBER OF SYSTEM FREQUENCIES	NUMBER OF COMPONENT MODES		
	6	4	2
5	$K_1=6.5\times10^5$, $K_2=7.4\times10^5$ and $K_1=3.7\times10^5$, $K_2=13.1\times10^5$	$K_1=6.3\times10^5$, $K_2=7.3\times10^5$ and $K_1=3.6\times10^5$, $K_2=12.5\times10^5$	(a)
2	$K_1=6.7\times10^5$, $K_2=7.4\times10^5$ and $K_1=3.7\times10^5$, $K_2=13.4\times10^5$	$K_1=4.1\times10^5$, $K_2=10.8\times10^5$ and $K_1=5.4\times10^5$, $K_2=8.1\times10^5$	(b)

[a]only four system frequencies available

[b]solution does not converge

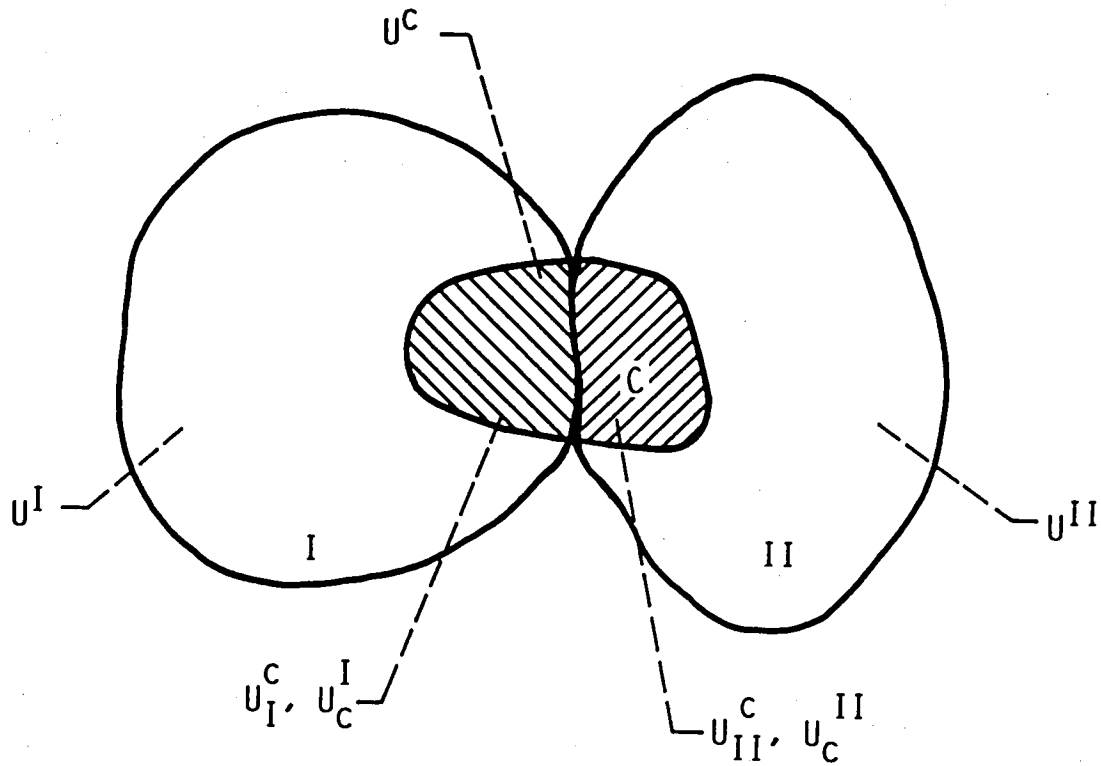

FIGURE 1.- THREE COMPONENT SYSTEM.

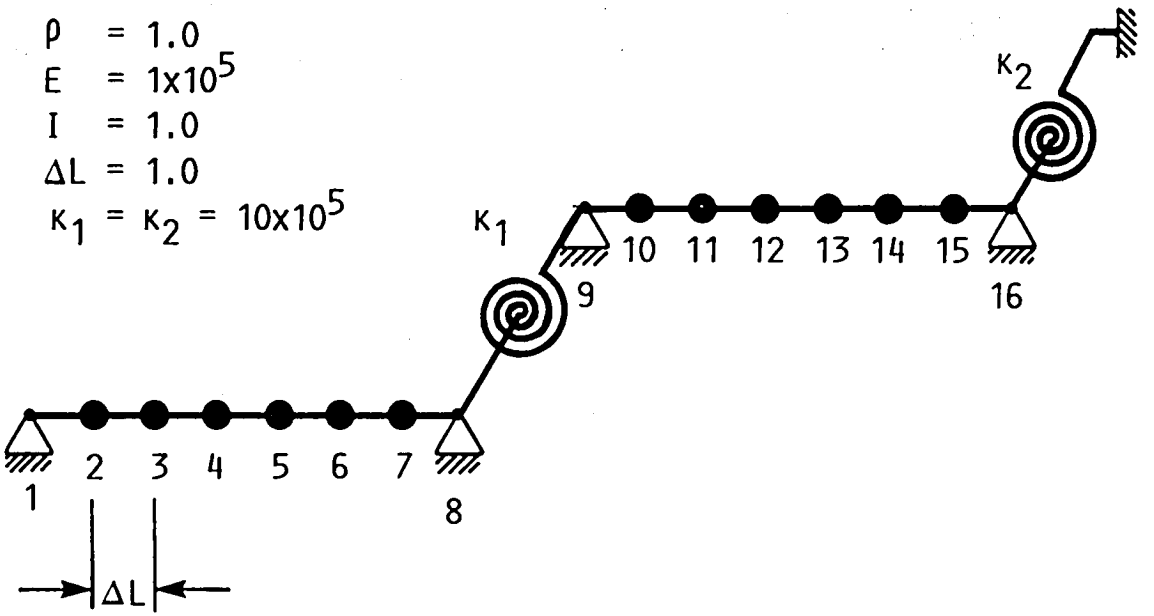

FIGURE 2.- COUPLED SYSTEM (SAMPLE PROBLEM ONE).

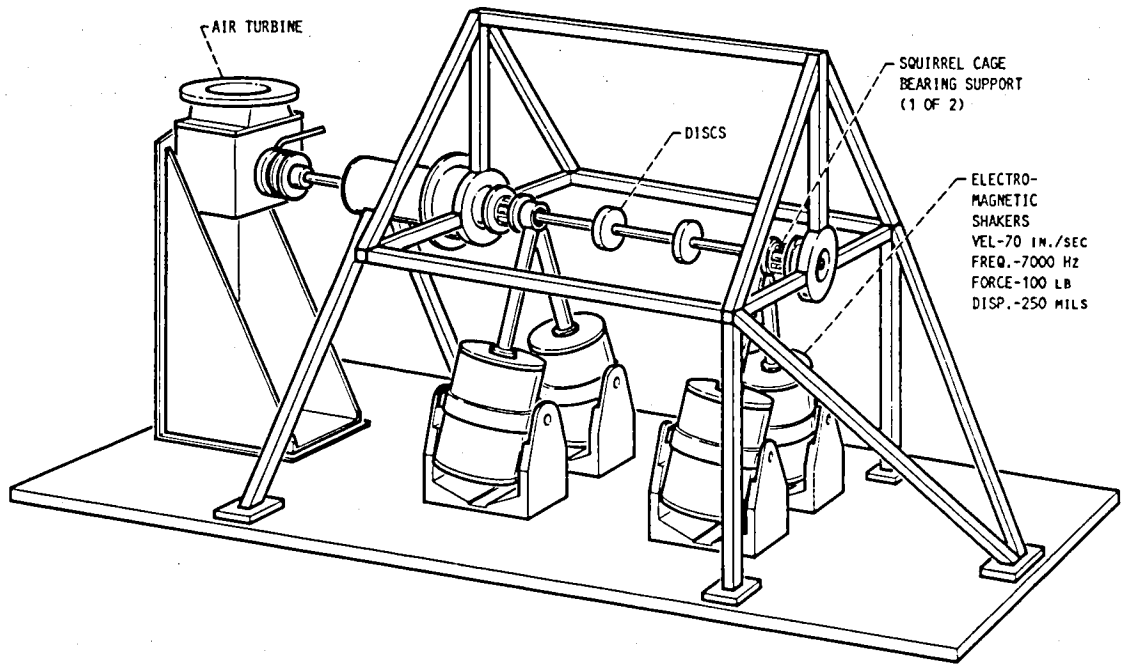

FIGURE 3.- ROTATING SYSTEM DYNAMICS RIG.

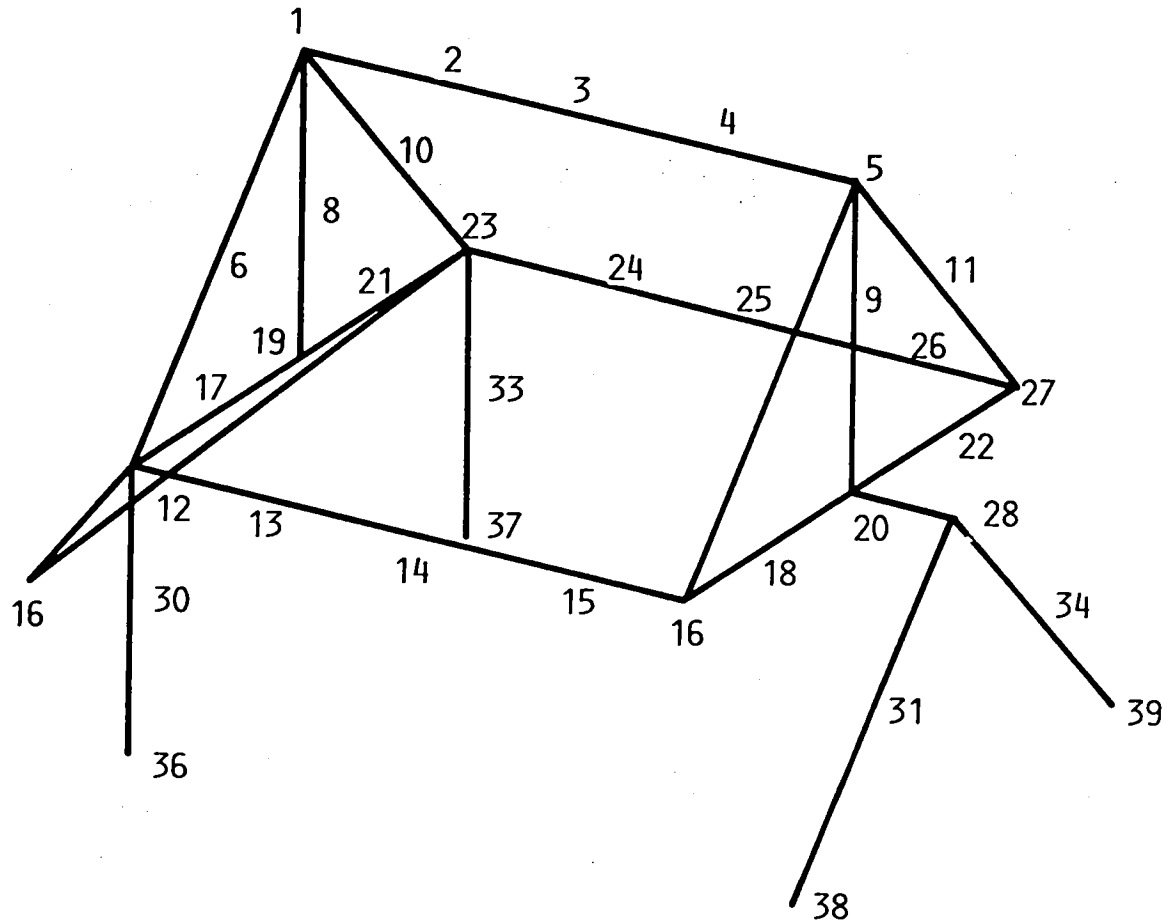

FIGURE 4.- SUPPORT FRAME F.E. MODEL.

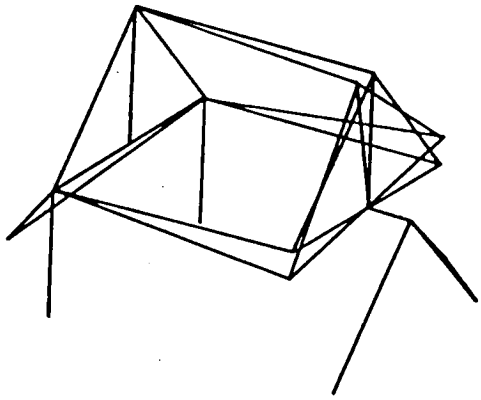

MODE 1: 35 Hz

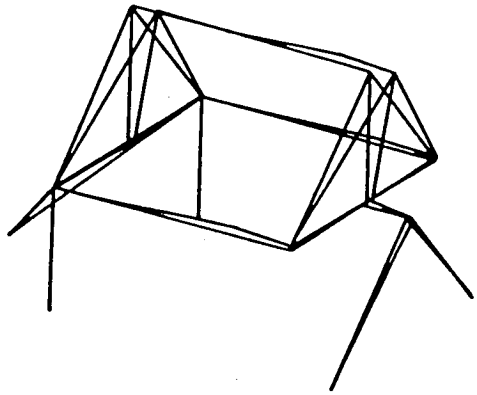

MODE 2: 41 Hz

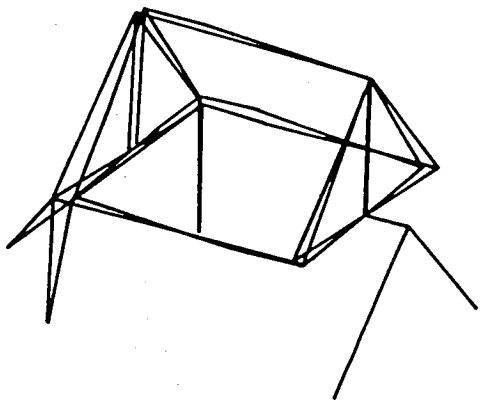

MODE 3: 61 Hz

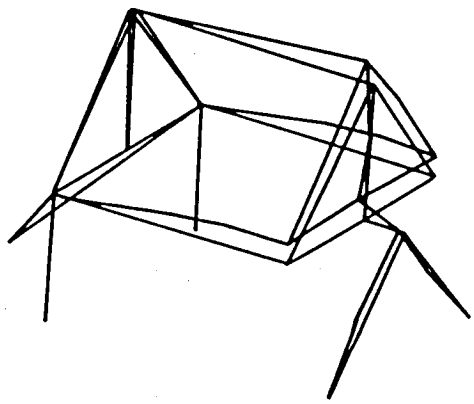

MODE 4: 72 Hz

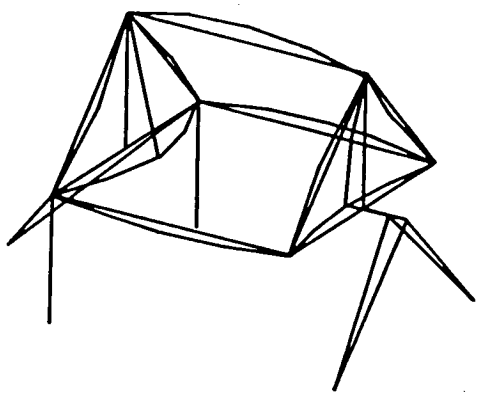

MODE 5: 80 Hz

FIGURE 5.- SUPPORT FRAME MODE SHAPES.

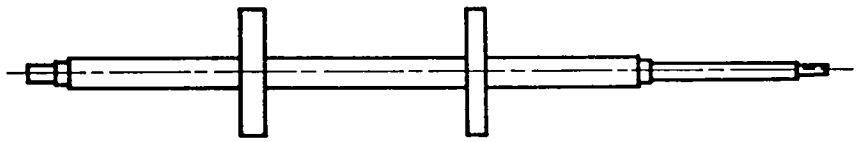

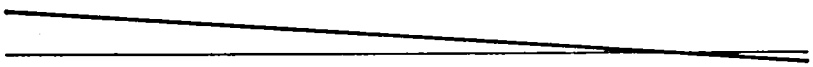

MODE 1: 0 Hz

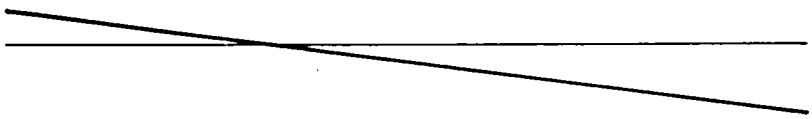

MODE 2: 0 Hz

MODE 3: 141 Hz

MODE 4: 304 Hz

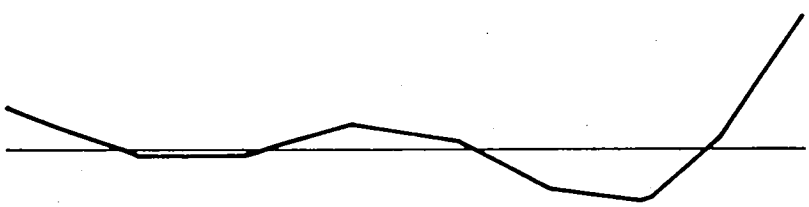

MODE 5: 609 Hz

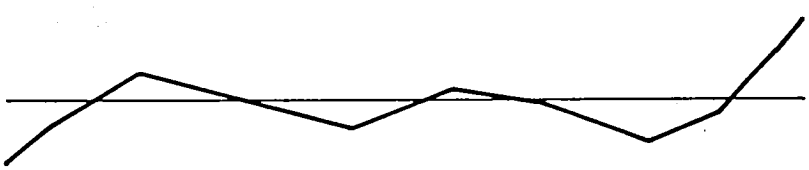

MODE 6: 897 Hz

FIGURE 6.- ROTOR MODE SHAPES.

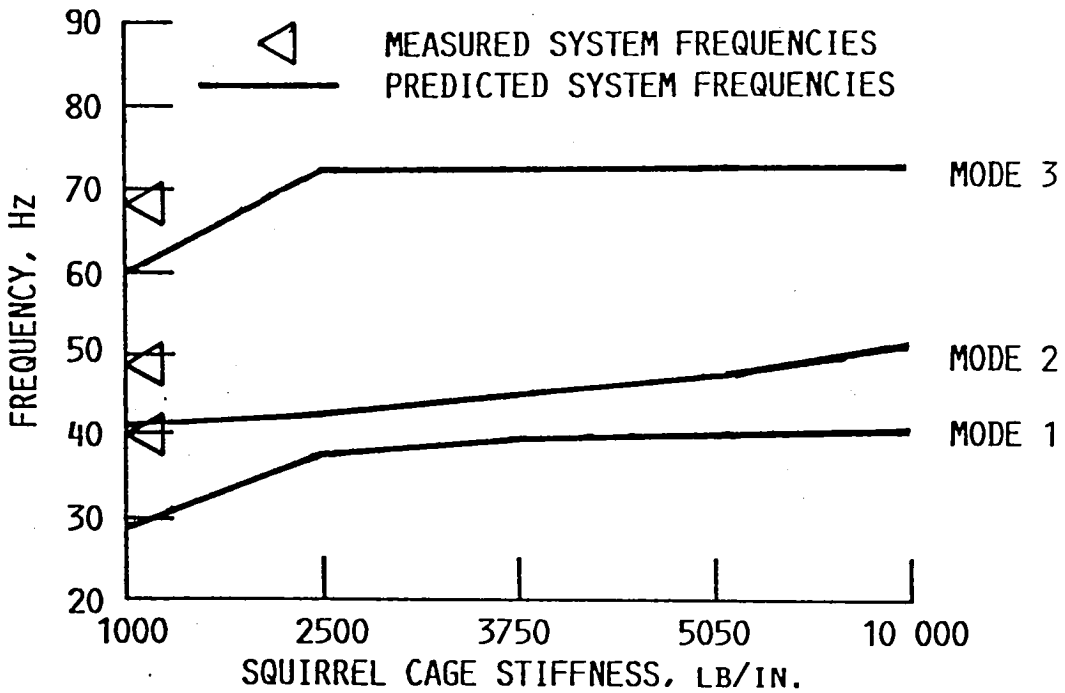

FIGURE 7.- COUPLED FRAME/ROTOR ANALYSIS (6 COMPONENT MODES).

CHAPTER IV

CHARACTERIZATION OF DAMPED STRUCTURAL CONNECTIONS FOR MULTI-COMPONENT SYSTEMS

Introduction

As discussed in the previous chapters, analytical models of structural systems normally do not normally possess characteristics which agree completely with those obtained from experiments. Although there are many possible explanations for the discrepancies, the major causes often can be attributed to inaccuracies in the data used to create the analytical model. Parameters such as material and dimensional properties, which are usually obtained from nominal design specifications, can differ considerably from the true values, thus causing the analytical model to be inaccurate. Structural properties such as damping and connection stiffnesses also are extremely difficult to predetermine, yet their influence on structural response predictions is profound.

For large structural systems it is common practice to utilize substructuring methods to create the analytical system model. These methods are used to construct the model by partitioning the structure into components, and then linking the individual components together with inter-component connections. The components frequently can be modeled with reasonable accuracy

whereas the connections are difficult, or in many situations impossible to analytically model. This is especially true when the connections contain significant amounts of damping.

The objective of the work in this chapter is to investigate the feasibility of determining the characteristics of viscously damped connections from test data obtained from the complete coupled system. It is desirable to be able to determine the connection stiffness and damping from tests performed on the complete system so that the difficulties associated with testing individual joints can be circumvented. The problem with testing individual joints is that often special test fixtures are required for mounting the joint. Also, conventional modal tests can not be performed on the joint because joints normally are very stiff, and thus require static and cyclic loading tests in determining stiffness and damping properties (1). Furthermore, although several joints may be nominally identical, their actual properties may vary enough to require that every joint be tested. When system tests are performed the difficulties associated with tests on individual joints are eliminated. Instead of special fixtures the system can be tested in its actual operating environment or hung from flexible suspenders. Conventional modal tests which are much simpler to perform than static or cyclic loading tests can generally be used because the system modes are in a suitable range. Also, the low frequency modal data contains information about the joints even though the joints themselves are relatively stiff.

Several previous studies have addressed the issue of identifying the stiffness of connections without considering damping. In Chapter III an attempt was made to identify the stiffness of connections by using a combination of a weighted least squares parameter identification and substructuring methods. This work showed that physical stiffness characteristics can be determined from experimentally obtained frequency data as long as sufficient test data are available. In Ref. 2 the stiffness characteristics of the connections between the Centaur G Prime Launch Vehicle and the shuttle orbiter were modified based on experimentally obtained modal data. The connections were altered so that a test-verified analytical model would be available for subsequent loads analysis. The modifications, based on engineering intuition and judgement were deemed satisfactory when the analytical and experimental frequency data were in agreement.

Previous studies that have addressed connection damping (1,3-7) have focused on identifying damping properties from tests on individual joints rather than from coupled system tests. In Ref. 1 a mix of analytical and experimental component models were combined to characterize the dynamics of a flexible spacecraft. For this study, joint stiffness and damping were ascertained before the joints were incorporated into the system model. Data obtained from cyclic loading tests indicated that the joint damping was primarily viscoelastic, although it was noted that

joints in actual space structures may exhibit nonlinearities and friction damping. Since the system modal properties computed from the experimentally derived joint models were in agreement with test results, there was no need to modify the joint characteristics by using the coupled system test data. In Ref. 3 damping and stiffness characteristics of a representative space truss joint were studied. In that work results from simplified joint models were compared to results obtained from a complex model which included dead bands, large deformations, and friction forces. It was concluded that simplified models based on linear springs and viscous dampers could represent the behavior of the more sophisticated joint model. No actual experimental data was used in that study. In Ref. 4 nonlinearities in a structural joint were identified by using an approach termed "force-state mapping". This approach involved simultaneously measuring the force on a joint along with its position and velocity. From the shape of the three dimensional surface generated by plotting force as a function of displacement and velocity the type and quantitative description of the joint mechanisms were identified.

In the present work a general procedure for component coupling is presented. This procedure accommodates components that have been modeled with either, finite elements or with modal data which has been obtained from analytical models or experiment. A parameter identification procedure based on the weighted least squares method

also is introduced. This procedure utilizes system test data to find an optimal set of stiffness and viscous damping connection properties. Finally, two example problems which use simulated experimental data are presented. For these problems both stiffness and damping connection properties are identified. A Monte-Carlo simulation is run to assess the effect of variance in the experimental data on the identified properties in the first problem. The effect of friction damping is evaluated in the second.

Component Coupling Procedure

The approach used for developing the coupled system equations of motion is extrapolated from the procedure of Ref. 8. In this approach component models are represented through the use of finite elements or with modal data. Component modal data may be obtained from experiment, or from a reduced finite element model. Once the component models are obtained, they are coupled at physical boundary degrees of freedom through physical connecting elements. In the present work both stiffness and viscous damping is accommodated in the connecting elements. Residual flexibility, which is discussed in Ref. 8 also is included.

Consider the system shown in Fig. 1. This system is comprised of two components which are coupled by a single connecting element.

The damped equation of motion for the uncoupled system is written as:

$$\begin{bmatrix} [M^I] & & \\ & [0] & \\ & & [M^{II}] \end{bmatrix} \begin{Bmatrix} \ddot{U}^I \\ \ddot{X}^C \\ \ddot{U}^{II} \end{Bmatrix} + \begin{bmatrix} [0] & & \\ & [C^C] & \\ & & [0] \end{bmatrix} \begin{Bmatrix} \dot{U}^I \\ \dot{X}^C \\ \dot{U}^{II} \end{Bmatrix} + \begin{bmatrix} [K^I] & & \\ & [K^C] & \\ & & [K^{II}] \end{bmatrix} \begin{Bmatrix} U^I \\ X^C \\ U^{II} \end{Bmatrix} = \{0\} \tag{1}$$

where [M], [C], and [K] are the system mass, damping, and stiffness matrices respectively, $\{\ddot{u}\}$, $\{\dot{u}\}$, and $\{u\}$ are the corresponding accelerations, velocities, and displacements in terms of physical and/or modal coordinates, and $\{\ddot{x}\}$, $\{\dot{x}\}$, and $\{x\}$ are the physical accelerations, velocities, and displacements at the connections. (Superscripts refer to component identifications.) Note that the connecting component is massless, and the other two components have no damping. For many systems it is reasonable to assume that the actual component damping is negligible, and that any significant damping is isolated in the connections.

Once partitioning between boundary and internal degrees of freedom has been completed, and displacement compatibility between components has been implemented, the coupled system equations of motion for the damped system may be derived as follows:

$$\begin{bmatrix} \begin{bmatrix} M^I & \\ & M^I_{bb} \end{bmatrix} & \\ & \begin{bmatrix} M^{II}_{bb} & \\ & M^{II} \end{bmatrix} \end{bmatrix} \begin{Bmatrix} \ddot{U}^I_I \\ \ddot{X}^I_b \\ \ddot{X}^{II}_b \\ \ddot{U}^{II}_I \end{Bmatrix} + \begin{bmatrix} \begin{bmatrix} 0 & \\ & C^c \end{bmatrix} & -C^c_{II\ I} \\ -C^{c\,T}_{II\ I} & \begin{bmatrix} C^c_{II} & \\ & 0 \end{bmatrix} \end{bmatrix} \begin{Bmatrix} \dot{U}^I_I \\ \dot{X}^I_b \\ \dot{X}^{II}_b \\ \dot{U}^{II}_I \end{Bmatrix} + \begin{bmatrix} \begin{bmatrix} K^I & -K^I_{Ib} \\ -K^{I\,T}_{Ib} & K^I_{bb} + K^c_I \end{bmatrix} & -K^c_{II\ I} \\ -K^{c\,T}_{II\ I} & \begin{bmatrix} K^{II}_{bb} + K^c_{II} & -K^{II}_{IIb} \\ -K^{II\,T}_{IIb} & K^{II} \end{bmatrix} \end{bmatrix} \begin{Bmatrix} U^I_I \\ X^I_b \\ X^{II}_b \\ U^{II}_I \end{Bmatrix} = \{0\} \tag{2}$$

where the component degrees of freedom $\{u\}$ are partitioned into internal $\{u_i\}$ and physical boundary $\{x_b\}$ degrees of freedom. For components modeled with finite elements, all of the degrees of freedom are physical. For modal components, the boundary degrees of freedom are physical while the internal, $\{u_i\}$, degrees of freedom are represented in terms of modal coordinates.

When modal data is used to characterize components, physical degrees of freedom at the component boundary must be derived from the modal data before the component can be input into Eq. (2). These degrees of freedom are obtained by transforming a subset of the modal coordinates into physical coordinates. The equation of motion for an undamped component in terms of physical coordinates, x, is:

$$[M]\{\ddot{X}\} + [K]\{X\} = \{0\} \tag{3}$$

The physical displacement x can be approximated by:

$$\{X\} = [\Phi_k]\{q_k\} + [G_b]\{q_b\} \tag{4}$$

where k is the number of measured or retained modes, q are generalized coordinates, and G_b is the residual flexibility matrix contains the flexibility which is not included in the component modal characterization. Normally, the component characterization is incomplete because the component model is constructed from a truncated set of component modes. The residual flexibility is used to supplement the truncated set of modes.

Analytically, the matrix G_b, containing the component residual flexibility is computed by summing all of the missing modal data (m + 1, N) at each of the boundary degrees of freedom, Beginning with:

$$[\Phi]^T[K][\Phi] = [\sim w^2 \sim] \tag{5}$$

Then solving for K:

$$[K] = [\Phi]^{T^{-1}} [\sim w^2 \sim][\Phi]^{-1} \tag{6}$$

The total component flexibility matrix is obtained by inverting K:

$$[F] = [K]^{-1} = [\phi][\sim w^2 \sim]^{-1}[\Phi]^T \tag{7}$$

In summation form:

$$F = \sum_{i=1}^{k} \frac{\phi_i \phi_i^T}{w_i^2} + \sum_{i=k+1}^{N} \frac{\phi_i \phi_i^T}{w_i^2} \tag{8}$$

where k is the number of kept modes and N is the total number of modes (For components modeled by F.E. N equals the total number of degrees of freedom whereas for actual components $N = \infty$). The term on the r.h.s. of Eq. (8) is termed the residual flexibility, G. From Eq. (8) it is evident that G is comprised of the "left-over" flexibility which is not included in the truncated set of modal data. Experimentally, the entries in the residual flexibility matrix are obtained by determining the differences between the curve fit and the experimentally measured frequency response functions (9).

The residual flexibility is implemented so that flexibility which is not contained in the truncated set of component modes is

included in the component model. The values of the residuals at the boundary degrees of freedom are required because they provide information necessary for accurate component coupling and for the creation of a precise system model. Only the diagonal terms in the matrix are used here because it was determined that the off-diagonal terms, which related the cross coupling between boundary degrees of freedom, have a negligible effect on the fidelity of the model (8).

Returning to Eq. (4) and partitioning {x} into internal, o, and boundary degrees of freedom:

$$\{X\} = \begin{Bmatrix} X_o \\ X_b \end{Bmatrix} = \underbrace{\begin{bmatrix} \phi_{ok} & 0 \\ \phi_{bk} & G^d_{bb} \end{bmatrix}}_{T} \begin{Bmatrix} q_k \\ q_b \end{Bmatrix} \tag{9}$$

where T is the transformation which relates the physical coordinates to the generalized coordinates. Pre- and post multiplying Eq. (3) by T (and knowing Φ and G are orthogonal):

$$[T]^T[M][T]\{\ddot{q}\} + [T]^T[K][T]\{q\} = \{0\} \tag{10}$$

which leads to the equation of motion:

$$\begin{bmatrix} M^* \end{bmatrix} \begin{Bmatrix} \ddot{q}_k \\ \ddot{q}_b \end{Bmatrix} + \begin{bmatrix} K^* \end{bmatrix} \begin{Bmatrix} q_k \\ q_b \end{Bmatrix} = \{0\} \tag{11}$$

$$\begin{bmatrix} M^* \end{bmatrix} = \begin{bmatrix} I_{kk} & 0 \\ 0 & 0 \end{bmatrix} \qquad \begin{bmatrix} K^* \end{bmatrix} = \begin{bmatrix} W^2_{kk} & 0 \\ 0 & G^d_{bb} \end{bmatrix}$$

where $[I_{kk}]$ is the identity matrix, $[w_{kk}^2]$ is the matrix of component frequencies, and $[G_{bb}^d]$ is the diagonal matrix of residual flexibilities, $\sum_{j=k+1}^{N} \frac{\phi_{jb}\phi_{jb}^T}{Wj^2}$ at the boundary, b degrees of freedom.

Using the transformation:

$$\begin{Bmatrix} X_i \\ X_b \end{Bmatrix} = \begin{bmatrix} \phi_{ik} & 0 \\ \phi_{bk} & G_{bb}^d \end{bmatrix} \begin{Bmatrix} q_k \\ q_b \end{Bmatrix} \tag{12a}$$

leads to:

$$\begin{Bmatrix} q_k \\ q_b \end{Bmatrix} = \begin{bmatrix} I & 0 \\ -G^{-1}\phi_{bk} & G^{-1} \end{bmatrix} \begin{Bmatrix} q_k \\ X_b \end{Bmatrix} \tag{12b}$$

Using the above transformation and Eq. 3, the component equations of motion in terms of modal and physical boundary coordinates are derived as:

$$\begin{bmatrix} I & \\ & 0 \end{bmatrix} \begin{Bmatrix} \ddot{q}_k \\ \ddot{X}_b \end{Bmatrix} + \begin{bmatrix} W_{kk}^2 + \phi_{bk}^T G^{-1} \phi_{bk} & -\phi_{bk}^T G^{-1} \\ -G^{-1}\phi_{bk} & G^{-1} \end{bmatrix} \begin{Bmatrix} q_k \\ X_b \end{Bmatrix} = \{0\} \tag{13}$$

After the component equations are transformed into the coordinate system used in Eq. (5), the component can then be incorporated into the system equations in the same manner as are the finite element components.

Once the system equations of motion are constructed, they can be used to predict the system frequencies and mode shapes. This modal

data is then used in conjunction with the experimentally measured modal parameters to identify the connection properties. Because the system is damped, the frequencies will be complex; the real part corresponding to the modal damping and the imaginary part to the modal frequency. The mode shapes also will be complex but for most damped systems (including the present research) the imaginary part can be disregarded.

Parameter Identification Procedure

Several methods are available for parameter identification (10). The methods which incorporate optimization strategies can be classified into three groups; least squares, weighted least squares, and Bayesian estimation. With the least squares method the set of parameters which minimizes the difference between the measured and predicted response is computed. The weighted least squares method is similar except that a "weight," corresponding to the relative confidence in the measured data, is incorporated. The Bayesian method permits specification of the randomness of the parameters that are being computed as well as the confidence in the measured data. Since in practice the randomness of the connection parameters may be difficult to quantify the Bayesian method normally is not useful. The weighted least squares method will be used in the present study because it is feasible and useful to quantify the confidence levels in the measured data.

Assuming that the component characterizations are accurate, and that an appropriate set of component modes has been used to represent the overall system response, a search can be initiated for a set of connection parameters which better predicts the system frequencies and mode shapes. The assumption that the component representation is accurate may require that experimental verification be performed on the component models before they are used in the system characterization. Although this approach may require additional effort in that verified component models are required, it greatly simplifies the parameter identification by limiting the location of possible inaccuracies to the connections. The requirement that an appropriate set of component modes be used normally can be met by including the lower modes, and by utilizing a number of degrees of freedom in the system model that is at least twice the number of modes of interest (a mode equates to 1 degree of freedom). This requirement is comparable to the modeling guidelines used for conventional finite elements. By including residual flexibilities, the requirement can be relaxed.

The parameter identification (PID) discussed in Chapter III is used here to find an improved set of connection parameters that better predict the measured system data. The difference between this work and the work in Chapter III is that in this work modal damping is included in the identification.

The improved set of connection parameters are computed iteratively from:

$$\{r\} = \{r\}_{EST} + ([S]^T[W][S])^{-1}[S]^T[W](\{\bar{c}\} - \{c\}_{EST}) \qquad (14)$$

where $\{r\}$ is the vector of improved connection parameters (physical stiffness and damping coefficients), $\{\bar{c}\}$ and $\{c\}_{EST}$ are the measured and computed system modal parameters, $[W]$ is a weighting matrix for the measured data, and $[S]$ is a sensitivity matrix containing the partial derivatives, $d\{c\}/d\{r\}$.

The vector of measurements, $\{\bar{c}\}$, can contain both complex frequency (frequency and damping), and/or mode shape data. For the mode shape data it is sensible to use a measure of the overall fit between the predicted and experimental mode shape instead of using values of the mode shapes at individual locations. A logical measure of the overall fit is the least squares difference between mode shape data points. The Mode Shape Correlation Coefficient (11) provides this kind of measure. The Mode Shape Correlation Coefficient is advantageous because it provides a quantitative measure of the fit between the entire analytical and experimental mode shape, and furthermore, it does not require the experimental and computed mode shapes to be normalized in the same manner.

The weighting matrix, $[W]$, is used for specifying the confidence levels as well as for scaling the system modal parameters. For example, to specify that the modal damping has equal importance to

the frequency, a larger weight may need to be placed on the damping parameter. This is due to the fact that the order of magnitude of modal damping is less than that of frequency. Also, a higher weight may be warranted for parameters that are more significant, or that have been measured with greater accuracy.

The sensitivity matrix, [S], although relatively laborious, is straightforward to compute. In the present study the sensitivity matrix is computed by perturbing the system with small changes in the connection parameters, {r}, and then recording the resulting changes in the system modal parameters, $\{c\}_{EST}$. A new sensitivity matrix is computed for each iteration of Eq. (14).

Sample Problem One: Coupled System

The first sample problem is presented to demonstrate the parameter identification procedures and to assess the feasibility of identifying physical connection properties from coupled system modal data. For this problem a finite element model was used to generate simulated experimental data. The model (Fig. 2) consists of three planar elastic beams connected at their ends with revolute (pinned) connections. Each connection is attached to ground by a linear, translational, spring, and viscous damper. The properties of the connections are varied by changing the value of 'm' and 'n' which are shown in the figure. Each of the beam components is

discretized into five beam elements with the beam mass lumped at the ends of the elements. The complex eigenvalue extraction capabilities (Sol 28) of MSC NASTRAN (12) were used to compute the simulated experimental frequencies, modal damping, and mode shapes for the coupled system. NASTRAN also was used for computing the free-free modes for the individual beam components. These modes are used for creating the modal components for the analytical model. Four modes, two rigid body and two elastic, were used for the component representations.

Figure 3 shows the effect that the grounded springs have on the system's undamped resonant frequencies. The results in this figure are generated from the experimental model. For $n = 0$, the first four modes resemble rigid body modes, reflecting the softness of the springs. As 'n' is increased the system becomes stiffer, the frequencies increase, and the system behaves more like a series of simply supported beams. For 'n' greater than eight, the grounded springs act as rigid supports. In the subsequent parameter identification, a range of 'n' values is investigated so that a performance assessment can be made for both very flexible, and relatively rigid, connections.

In Fig. 4, a comparison is made between resonant frequencies from the modal model (residual flexibilities not included) and those from the experimental model. Since four modes were used to

represent each component, and there are three components, the system modal model had twelve degrees of freedom. Based on this number of degrees of freedom it was expected that the first four or five modes could be predicted with reasonable accuracy. For low 'n' values there is very good agreement between the experimental and component mode models for the first five modes. This is expected since the component mode model is generated from free-free component modes. For low 'n', each component behaves as if it were freely supported. For larger 'n' values the system behaves like a series of simply supported beams, creating greater disagreement between the frequencies predicted by the experimental and modal models. This also is expected because the truncated component mode representation is better suited for predicting rigid body type motions, and has a more difficult time with the bending type behavior of the simply supported components. The mismatch for high 'n' values is still moderate, especially for the first three system resonant frequencies. Obviously, when more or less than four component modes are used the respective mismatch decreases and increases. In general, the modal model utilizing four component modes produced very reasonable results. When residual flexibility was included there almost was perfect agreement over the entire range of 'n' values.

In Fig. 5, the differences between the experimental and identified connection stiffnesses are plotted as a function of 'n' value. The

connection values were identified by minimizing the differences between the first seven system resonant frequencies. Mode shape data was not utilized. It was preferable not to have to use any mode shape data because shape data is considerably more difficult to measure experimentally than are frequencies. To initiate the parameter identification (Eq. (6)), initial estimates are required for the connection parameters. In creating the data shown in this figure, zero stiffness values were used for the initial estimates of the connection parameters. When the connection properties are better known, the initial estimates can be improved, and convergence is accelerated.

The strongest agreement between experiment and computed connection parameters is at 'n' = 4. This is in contrast to the highest frequency match (Fig. 4) which was at 'n' = 0. Even at 'n' = 0, where the difference is as large as thirty percent, the match is still fairly good considering the prevalent difficulties associated with determining connection properties. In many situations it is adequate merely to be able to determine the order of magnitude of the connection properties. For 'n' = 6, converged parameters could not be computed without including residual flexibilities, although the order of magnitude of the connection properties was determined correctly. With the inclusion of residuals, the connection stiffnesses were computed to within forty percent accuracy.

There are two reasons why disparities between the identified and experimental connection values may occur, even though the analytical model accurately predicts the system frequencies (e.g., at 'n' = 0,2,4). The first reason is that when the frequencies are relatively insensitive to the connection stiffnesses, a high degree of precision in the experimental data is required for accurate identification. In practice, this required degree of precision may not be attainable and only an order of magnitude estimate of the connection properties may be realized. The second explanation involves the existence of multiple solutions. For many systems, including the one presented in this paper, more than one set of connection properties exists which satisfies the objective of eliminating the differences between the measured and predicted modal parameters. When this is the case, the resulting set of connection properties is dependent on the initial estimates for the connections and on the step size used for computing the sensitivity matrix. Normally, the number of solutions can be minimized by utilizing additional frequencies and/or mode shapes in the identification. The number of possible solutions and the required quantity of experimental data can be determined beforehand by performing simulation studies with varying step sizes and initial estimates for the connection properties.

The data in Figs. 6(a) and (b) were created to assess the effect of damping on the identification of connection properties. For

these figures, the connection stiffnesses were held constant at 'n' = 4, and the damping was varied from 'm' = 0 to 1.4 (critical damping is near 'm' = 1.6). In Fig. 6(a) the flatness of the curves demonstrate the insensitivity of the stiffness computations to damping. Even for large damping, 'm' = 1.4, the connection stiffnesses are computed accurately. In Fig. 6(b) the effect of damping on the identified connection damping is displayed. Similar to the stiffness results, the identified damping also is fairly insensitive to the level of the damping. In general, when the level of damping is low, and hence frequency is unaffected by damping, there will not be any coupling between damping and stiffness, and the connection stiffness and damping properties may be identified independently.

A Monte Carlo simulation was used to assess the accuracy of the parameter identification for various degrees of experimental error. Normally, the level of experimental error in frequency is small, while the error in damping and mode shapes is relatively large. Based on this assumption, the coefficient of variation in the frequency measurements was set at 1 percent and the damping coefficient of variation was varied from 1 to 15 percent. For simplicity, mode shape data was not utilized. Simulated data was generated by making forty runs at 'n' = 4, 'm' = 1.2, and using a random number generator to select the experimental modal frequencies and damping (normal distributions were assumed). Plots

displaying the probability of achieving a precision level for the various degrees of measurement coefficient of variation are shown in Figs. 7(a) and (b). In these figures it is shown that as the coefficient of variation in the measured data increases, the probability of achieving a given level of precision decreases. For example, the probability of identifying the damping to within 20 percent of the actual damping is nearly 80 percent for a damping coefficient of variation of 1 percent, while it is less than 40 percent for a coefficient of variation of 15 percent. Obviously, as the required precision level is relaxed, the probability of reaching that level is increased.

From Fig. 7(b) it is evident that regardless of the damping coefficient of variation, the identified stiffness properties are reasonably precise. For example, the probability of attaining a 30 percent precision is very good (greater than 80 percent) for all three levels of damping coefficient of variation. These results were expected since for the mean damping used for the simulation ('m' = 1.2) the stiffness is fairly independent of damping. It should be noted that the results from the Monte Carlo simulation are problem dependent and can only be used for providing insight into the degree of accuracy that might be expected for other problems.

Sample Problem Two: Coupled System With Friction

The connections in many structural systems contain nonlinearities such as friction or gaps. For multi-degree of freedom systems it is virtually impossible to identify and characterize all of the complexities that may exist in connections. Often, a simplifying assumption is made that the connection damping can be adequately described by linear viscous dampers even though other types of damping exist in the connection. With this assumption the identification process and subsequent analysis are greatly simplified. In the second sample problem the effects of the viscous damping assumption are assessed by adding friction damping into the system. First, the effect of friction damping on the identified viscous damping connection properties is determined. Subsequently, a comparison is made between the actual response of the system with friction damping and the response of the identified system with the friction damping approximated by viscous damping.

The structure utilized for the second sample problem is identical to the first except that friction dampers have been added at each of the connection locations (Fig. 8). The friction dampers at each of the four connections were identical. The viscous dampers and grounded springs which were used in the first sample problem also were used here. The parameters for these elements (Fig. 2) were fixed at $m = 1$ and $n = 4$.

MSC/NASTRAN Solution 99 was used to compute the modal damping for the coupled system. The damping was computed by exciting the system and then allowing it to decay (Fig. 9). The rate of free decay then was used to compute an equivalent modal damping for each of the first seven modes at different levels of friction damping. To obtain the free decay response each mode was individually excited by applying a distributed sinusoidal load at the modal frequency with the same distribution as the mode shape. The magnitude of the sinusoidal load was set so that the resulting displacements were on the order of the system span/100. The excitation frequency and distribution was determined by assuming that the modal frequencies and mode shapes would be unchanged from the system without friction damping.

Equivalent viscous damping ratios were computed for four levels of friction damping. The friction ratio was defined as the ratio of the friction force at each of the four connection locations to the maximum value of the distributed sinusoidal excitation. Damping ratios were computed at friction ratios of $r = 0.0$, $r = 0.02$, $r = 0.10$, and $r = 0.50$. The resulting modal damping values are given in Table I. As expected, the equivalent modal damping increases with an increase in friction force. The damping ratios from this table next were used in the parameter identification to compute equivalent viscous dampers. The identified viscous dampers are given in Table II. Without friction damping, $r = 0.00$, the

identified dampers are very close in value to the actual dampers. When friction is present, the identified dampers do not appear to follow any pattern, but they do enable the predicted frequencies and modal damping to match the experimental data closely.

The performance of the identified models was assessed by comparing transient responses of the identified models to those from the experimental models at each of the four levels of friction damping. The models were excited by applying a step function input load at the center of the system. The effect of the step input is to excite all of the system modes, with a greater emphasis on the lower modes. The resulting system response, shown in Fig. 10, reaches a peak displacement just after the step load is applied and then decays while oscillating about a steady state displacement. The responses from the identified and experimental models were evaluated by comparing peak response, settling time, and RMS error (see Table III). At all four friction levels there was very little error in peak response (e.g., only 2 percent error at $r = 0.50$). The settling time error, which is defined as the error in time to reach 10 percent of the steady state displacement, increased considerably from the lower to higher levels of friction damping. For example, at $r = 0.50$ the time it took for the identified model to reach steady state displacement was twice that of the experimental model (122 percent error).

The Fourier transforms of the displacement responses were computed for $r = 0.10$ and $r = 0.50$ (Figs. 11(a) and (b)). To clarify these transforms, the steady state displacements were subtracted from the displacement responses. From the Fourier transforms it is seen that most of the discrepancy between the experimental and identified model responses can be attributed to the difference in contribution of the first mode. For both $r = 0.10$ and $r = 0.50$ transforms there is minimal difference, except for the first mode where the difference is extreme.

In Fig. 12, the amplitude and settling time errors are compared at three magnitudes of input load while the friction force was held constant at $r = 0.10$. Since the friction damping is amplitude dependent (inversely proportional to displacement and frequency), it was expected that the identified model would accurately match the experimental model response only at the same excitation levels and distributions as were used to compute the equivalent viscous damping ratios. Considering that the equivalent viscous dampers were derived by using sinusoidal excitation, and the responses in the figure are the result of a step input excitation, the identified model does a fairly reasonable job of predicting the experimental response for a broad range of excitation levels and distributions. As expected, the identified model over-estimates the system damping at high amplitudes. This is because the

equivalent viscous damping is inversely proportional to amplitude and therefore would have to be decreased for higher amplitude response.

Conclusion

A method for coupling multi-component systems, and for identifying connection stiffness and damping characteristics was developed and verified with simulated data. In the first sample problem component connection properties were determined for a three component planar beam model. From this analysis it was found that properties could be accurately identified for a broad range of connection stiffnesses and damping using relatively minimal measured data. The connection properties were identified using frequency data alone. Mode shape data was not required. By performing a Monte-Carlo simulation it was determined that connection damping and stiffness can be identified even in the presence of experimental error.

In the second sample problem equivalent viscous connection damping was identified for a model actually having friction and viscous damping. A comparison between the experimental and identified model showed that for particular ranges of input excitation the identified model could reliably predict peak response and settling time. However, at high levels of friction damping, the identified

model did not perform as well. Since many systems include connections with nonlinearities, it is important that unrealistic predictions concerning the in-service response of the system are not made. Instead, the extent of any nonlinearity should be determined by inspection of the measured data, and then the subsequent effect of any identified nonlinearity on system response should be explored.

References To Chapter IV

1. Soni, M.L.; and Agrawal, B.N.: Damping Snythesis for Flexible Space Structures Using Combined Experimental and Analytical Models. AIAA Paper 85-0779, Apr. 1985.

2. Chen, J., et al.: Modal Test/Analysis Correlation for Centaur G Prime Launch Vehicle. AIAA Paper 86-1002, May 1986.

3. Ferri, A.A.: Investigation of Damping From Nonlinear Sleeve Joints of Large Space Structures. Role of Damping in Vibration and Noise Control, L. Rogers and J.C. Simonis, eds.. ASME, 1987, pp. 187-195.

4. Crawley, E.F.; and Aubert, A.C.: Identification of Nonlinear Structural Elements by Force-State Mapping. AIAA J., vol. 24, no. 1, Jan. 1986, pp. 155-162.

5. Hertz, T.J.; and Crawley, E.F.: Damping in Space Structure Joints. AIAA Paper 84-1039, May 1984.

6. Bohlen, S.; and Gaul, L.: Vibrations of Structures Coupled by Nonlinear Transfer Behaviour of Joints; A Combined Computational and Experimental Approach. Proceedings of the 5th International Modal Analysis Conference, Union College, Schenectady, NY, 1987, pp. 86-91.

7. Hertz, T.J.; and Crawley, E.F.: Displacement Dependent Friction In Space Structural Joints. AIAA J., vol. 23, no. 12, Dec. 1985, pp. 1998-2000.

8. Martinez, D.R.; and Gregory, D.L.: A Comparison of Free Component Mode Snythesis Techniques Using MSC/NASTRAN. SAND-83-0025, June 1984.

9. Lamontia, M.A.: On the Determination and Use of Residual Flexibilities, Inertia Restraints, and Rigid-Body Modes. Proceedings of the First International Modal Analysis Conference and Exhibit, Union College, Schenectady, NY, 1982, pp. 153-159.

10. Isenberg, J.: Progressing From Least Squares to Bayesian Estimation. ASME Paper 79-WA/DSC-16, Dec. 1979.

11. Ewins, D.J.: Modal Testing: Theory and Practice. Research Studies Press, 1984.

12. MSC/NASTRAN Users Manual, MacNeil-Schwendler Corp., 1981.

TABLE I. - EQUIVALENT VISCOUS DAMPING RATIOS, ξ

Mode	r = 0	r = 0.02	r = 0.10	r = 0.50
94.9 Hz	0.024	0.031	0.048	0.082
119	.027	.035	.051	.100
145	.031	.032	.042	.080
208	.040	.036	.045	.110
307	.040	.041	.054	.100
408	.032	.035	.037	.080
484	.060	.063	.067	.140

TABLE II. - IDENTIFIED EQUIVALENT VISCOUS DAMPERS

	C_1	C_2	C_3	C_4
r = 0.00[a]	9.4	21	27	37
r = 0.02	20.6	7.7	23.3	43.6
r = 0.10	26.2	7.7	45.3	34.6
r = 0.50	25.1	52	54	53

[a]Actual values are $C_1 = 10$, $C_2 = 20$, $C_3 = 30$, and $C_4 = 40$.

TABLE III. - EVALUATION OF IDENTIFIED MODELS

	Peak amplitude (experimental)	Peak amplitude error, percent	Settling* time error, percent	RMS error
r = 0.00	0.755	0	0	0.00
r = 0.02	.754	2	13	.07
r = 0.10	.750	3	44	.11
r = 0.50	.731	2	122	.24

*Settling time = time to reach ±10 percent of steady state displacement.

U = PHYSICAL AND/OR MODAL DEGREES OF FREEDOM
X = PHYSICAL DEGREES OF FREEDOM

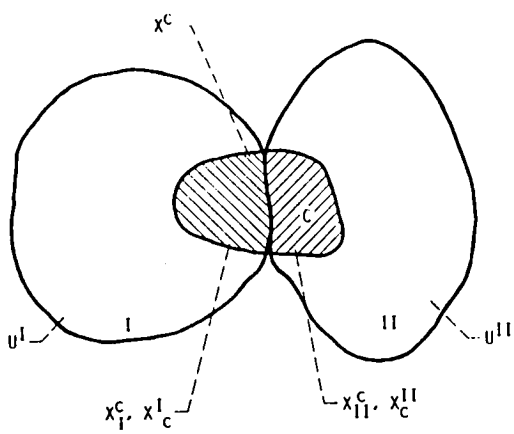

FIGURE 1. - THREE COMPONENT SYSTEM.

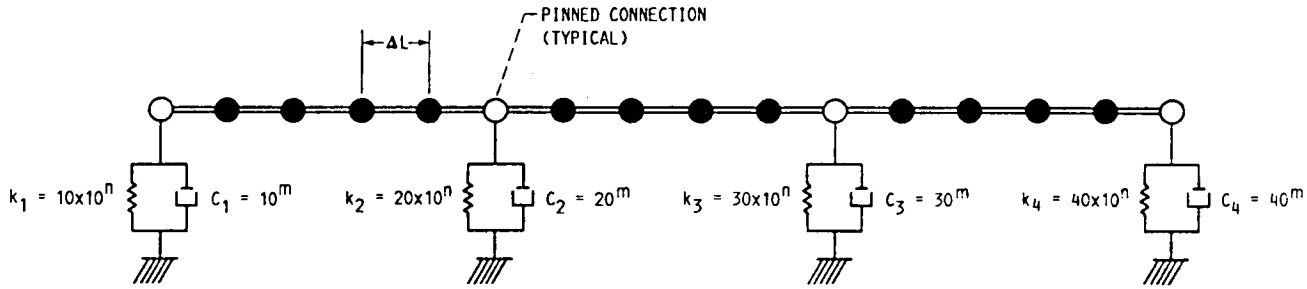

FIGURE 2. - THREE COMPONENT COUPLED SYSTEM ($EI = 10^5$, $\rho = 0.10$, $\Delta L = 1.0$).

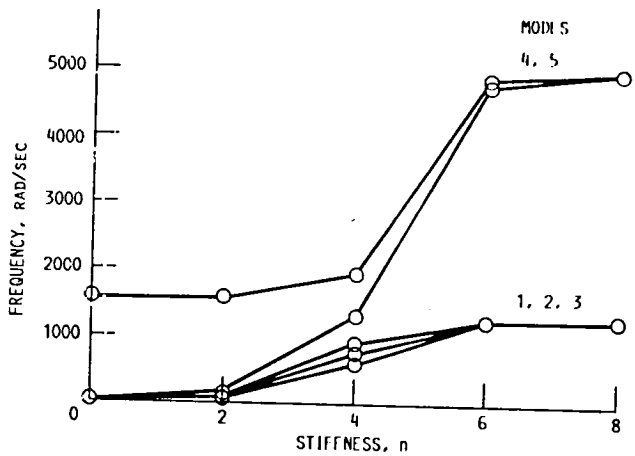

FIGURE 3. - MODAL FREQUENCIES FOR UNDAMPED EXPERIMENTAL MODEL.

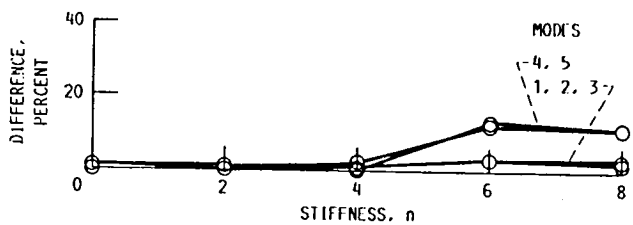

FIGURE 4. - FREQUENCY DIFFERENCE BETWEEN MODAL AND EXPERIMENTAL MODEL.

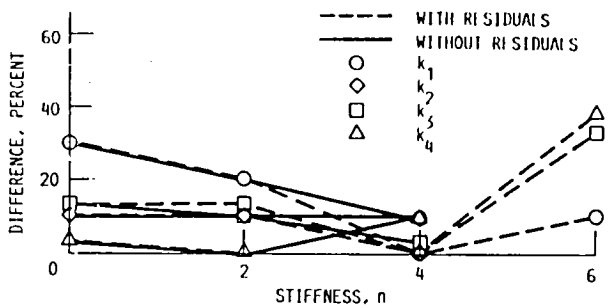

FIGURE 5. - DIFFERENCES BETWEEN IDENTIFIED AND EXPERIMENTAL CONNECTION STIFFNESSES (UNDAMPED).

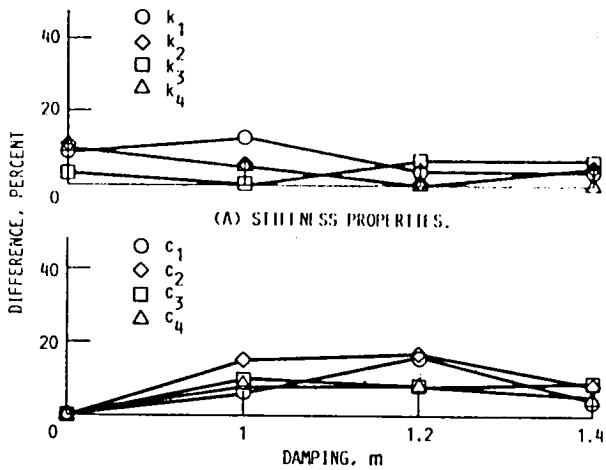

(B) DAMPING PROPERTIES.

FIGURE 6. - DIFFERENCES BETWEEN IDENTIFIED AND EXPERIMENTAL PROPERTIES.

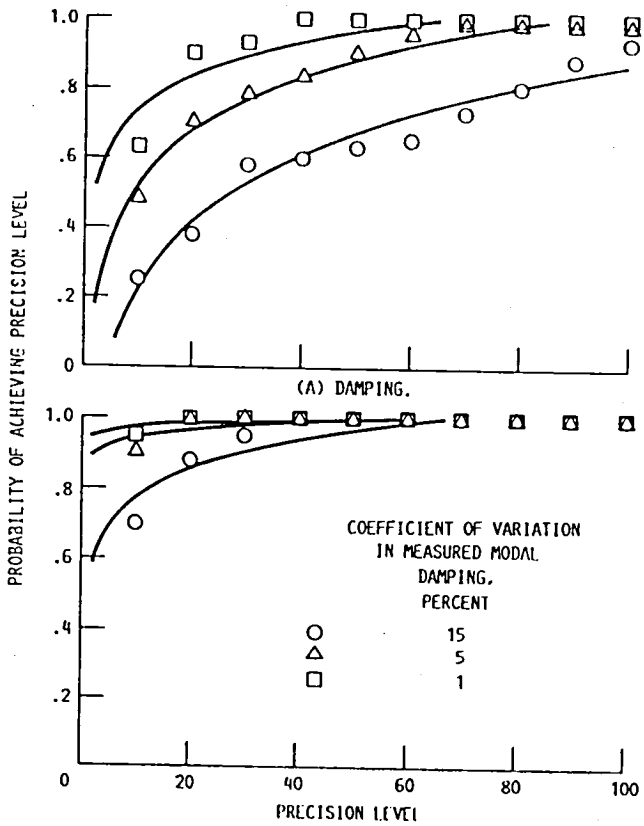

FIGURE 7. - PRECISION LEVEL, PERCENT DIFFERENCE BETWEEN IDENTIFIED AND ACTUAL PROPERTIES. (n = 4, m = 1.2, COEFFICIENT OF VARIATION IN MEASURED FREQUENCIES = 1%).

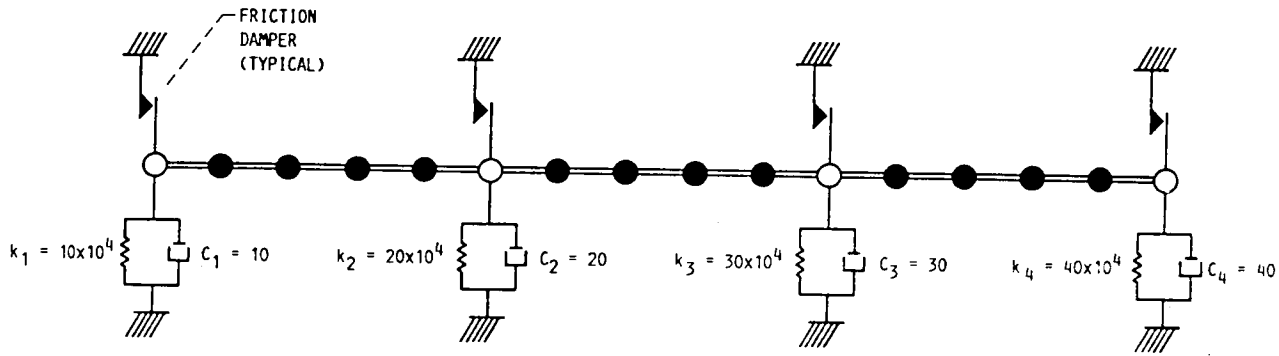

FIGURE 8. - THREE COMPONENT SYSTEM WITH FRICTION DAMPING.

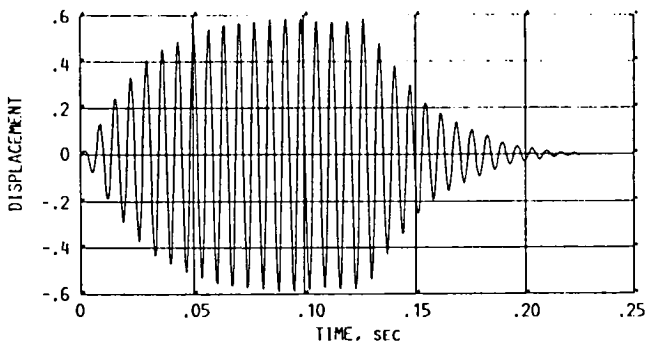

FIGURE 9. - TRANSIENT RESPONSE FOR MODE 3 AND FRICTION FORCE RATIO, r = 0.02.

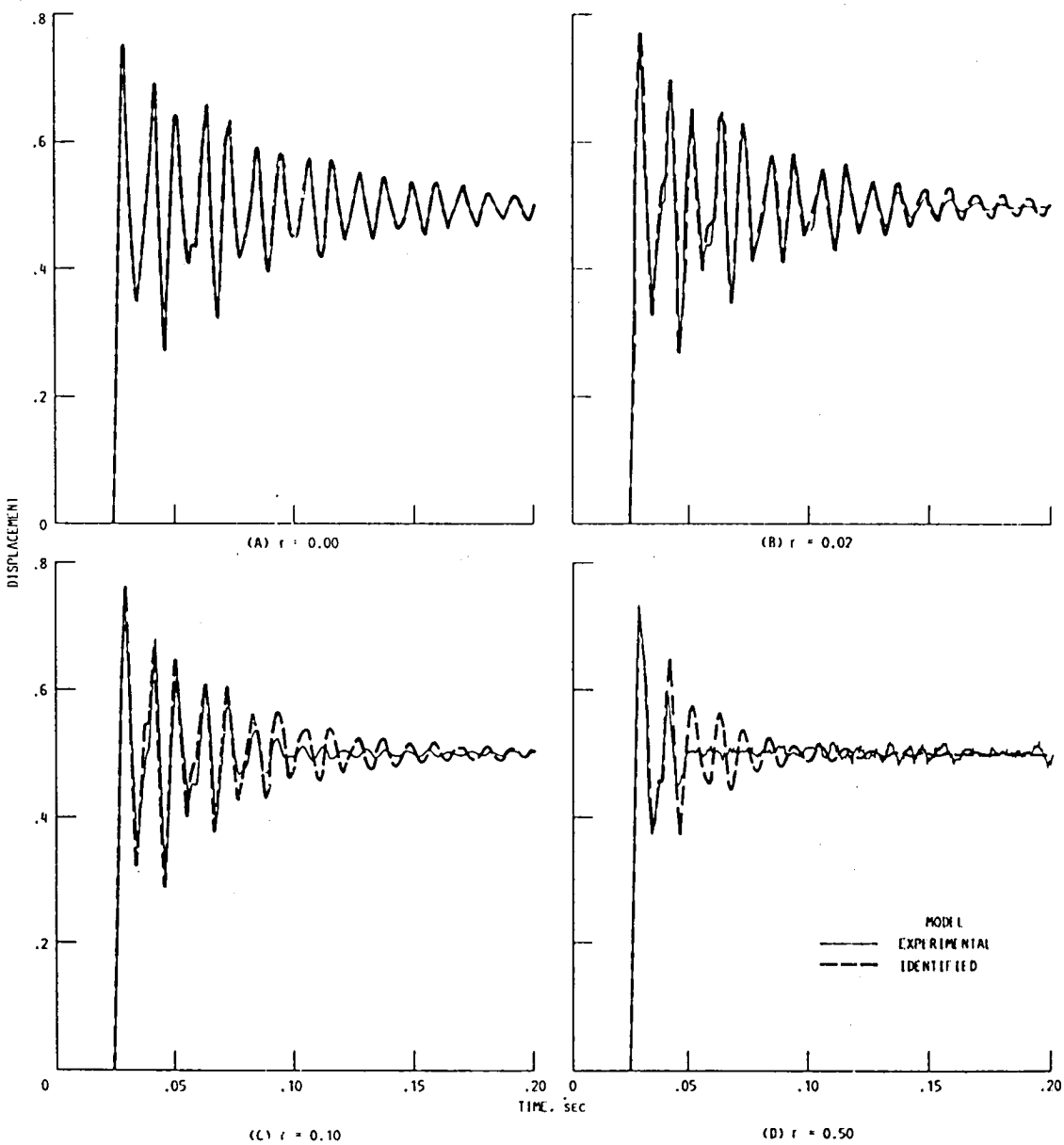

FIGURE 10. - COMPARISON BETWEEN EXPERIMENTAL AND IDENTIFIED MODELS' TRANSIENT RESPONSE.

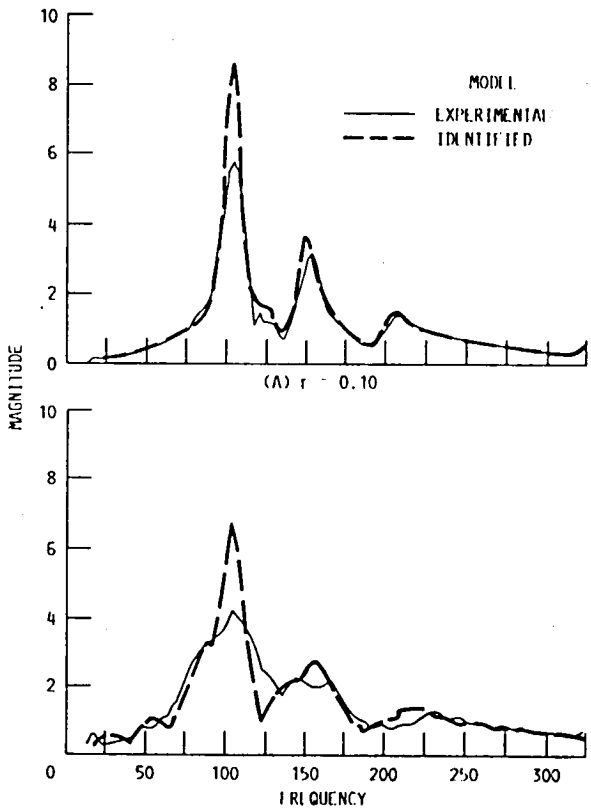

FIGURE 11. - FOURIER TRANSFORM OF DISPLACEMENT RESPONSE.

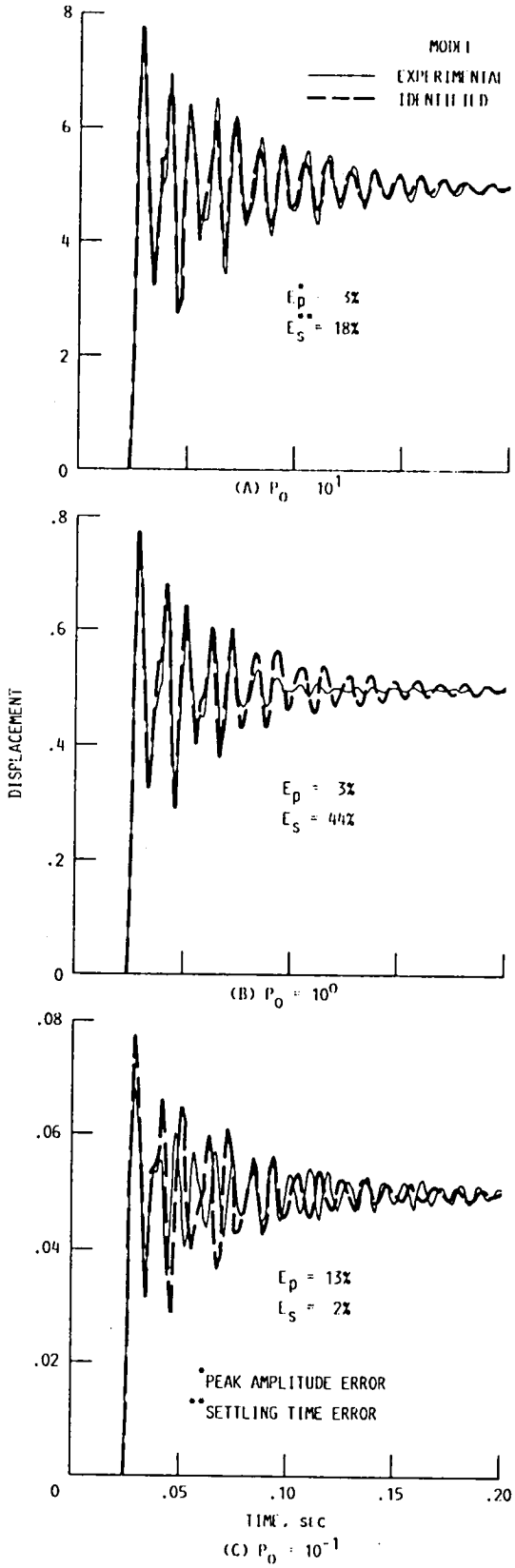

FIGURE 12. - STEP INPUT MAGNITUDE EFFECTS ON AMPLITUDE AND SETTLING TIME ERRORS, ζ = 0.10.

CHAPTER V

CONCLUSION AND RECOMMENDATIONS

In the present research methods for linking substructuring methods with Parameter Identification techniques are developed. It was demonstrated that the identification of structural dynamic systems can then be effectively performed by this combination of substructuring and Parameter Identification. With substructuring methods, component and connection properties can be identified independently. Independent identification of the structural properties was found to be advantageous because the identification problem is reduced to a collection of smaller order problems. For each of these problems the complexity of obtaining the experimental data, and the required quantity of data, is less than if the entire system were to be identified as a whole. Furthermore, the experimental data which is used to verify the component models also can be used to characterize the component in the system equations of motion.

In the present research it is shown that modal test data is effective for identifying both modeling problems in structural components, and for determining the stiffness and damping properties of inter-component connections. Identification methods which use modal, rather than time domain, test data are favorable for linear systems because the test apparatus for obtaining the modal data is readily available. Furthermore, the same test

equipment and post-processing software can be used for a wide range of structural dynamic systems. Modal testing also has advantages over time domain tests in that the modal data, which normally includes resonant frequencies and mode shapes, provides global system information which is useful for identifying overall, as well as specific, system characteristics (e.g., existence of rigid body modes, system flexibility).

The present research also demonstrates that the quality of the identified properties is dependent on both the quality and quantity of the experimental data. In general, parameter identification is improved when both the quality and quantity of experimental data are increased. In Chapter III it was found that several combinations of connection properties matched the initial test data, and it was not until additional experimental data was provided that the actual properties could be determined. For relatively simple systems, only a limited amount of test data may be required, while for larger, more complex systems, the required quantity of test data may become prohibitive. For most situations the quantity of test data required for an accurate identification can be predetermined by performing trail runs on approximate models. In Chapter IV the effect which the quality of test data has on the identified properties was assessed by using simulated data which contained experimental error. From these results it was found that the identified properties can be determined with reasonable accuracy, even in the presence of limited experimental error.

It also is shown in the present research that it is relatively easy to generate models which duplicate the test data, but that it can be difficult to generate physically accurate models. Therefore, an important issue to consider when evaluating the effectiveness of the identification is whether the resulting model is a better representation of the real system, or whether the model merely reproduces the available test data. The present research emphasizes this concern, whereas previous studies have stressed the formulation of models which merely match the test data.

A point of concern involves the identified model's capability to accurately predict in-service structural response. Since the fidelity of the identified model varies with the quantity and quality of the experimental data, methods for assessing the overall fidelity of the identified model are required. While the identified model maybe able to simulate situations that are similar to the test conditions, it may not be able to reliably simulate situations where the loading conditions or response levels differ from the test conditions. Statistical methods which ascertain the effects of uncertainty in the identified parameters could be useful in these circumstances.

Based on the system studied in Chapters III and IV it was found that connection properties normally can be determined by using only measured resonant frequencies. Mode shape data normally are

not required. This situation is favorable because mode shape data are more difficult to obtain experimentally, and when available, may be of questionable accuracy.

In Chapter IV the effects of nonlinearity were assessed for a friction damped system; it was found that small amounts of friction can be approximated with viscously damped models. Since many structural systems, particulary systems with complex connections (e.g., space structures), contain at least some amount of nonlinearity, it is important that general identification methods be developed which are capable of predicting both the type of nonlinearity and it's characteristic parameters. As presented in this research, several investigators have attempted to identify nonlinearities in individual structural connections, but none have confronted the problems associated with multicomponent/connected systems. Parameter Identification methods which use time domain based test data may be applicable for identifying structural systems containing nonlinearities but, clearly, additional work is required in this area.

APPENDIX A

Evaluation of Shepard's Method for Identifying Modeling Errors

Introduction

A limitation of the procedures developed in the previous chapters is that often both frequency and mode shape data is required for the identification of the component or connection structural properties. Since mode shape data is relatively difficult to obtain, and when it is available from tests it's accuracy is questionable, it is desirable to be able to identify the properties using frequency data alone. In this chapter a method proposed by Shepard (1) which is based on using discrepancies between measured and predicted frequencies for identifying modeling errors is evaluated.

Formulation Of Equations

Although the details of this method appear in (1) a summary of the procedure is outlined here for clarity. The objective of the derivation is to relate the differences between predicted and measured modal frequencies to discrepancies in mass and stiffness properties. The derivation begins by using Rayleigh's quotient to relate frequency to energy:

$$w_m^2 = \frac{V_m}{T_m} \qquad (1)$$

In this relation w is the modal frequency, and V and T are the total potential and kinetic energy for the mode. 'm' is the mode number. Taking the natural logarithmic of both sides of (1) and differentiating:

$$\left(\frac{dw}{w}\right)_m = \frac{1}{2} \sum_{i=1}^{n} \left(\frac{dv_i}{V} - \frac{dt_i}{T}\right)_m \qquad (2)$$

where dw is taken as the difference between the predicted and measured frequencies, and dv_i and dt_i are the differences between the predicted and actual potential and kinetic energies for each of the system elements. The summation is over all elements, n.

By assuming that the variation between predicted and actual mode shapes is small, the energy differentials can be related to stiffness and mass differentials, and Eq. (2) is rewritten as:

$$\left(\frac{dw}{w}\right)_m = \frac{1}{2} \sum_{i=1}^{n} \left(\frac{v_i}{V} \frac{dk_i}{k_i} - \frac{ti}{T} \frac{dm_i}{M_i}\right)_m \qquad (3)$$

where k_i and m_i are element stiffness and mass parameters. Equation (3) can further be simplified when the mass properties of the elements are known, or when massless connections are considered. When this is the situation dm_i is equal to zero and Eq. (3) can be written in matrix form as:

$$\begin{bmatrix} v_{1_1}/V_1 & v_{2_1}/V_1 & \cdots & v_{n_1}/V_1 \\ v_{1_2}/V_2 & & & \vdots \\ \vdots & & & \vdots \\ v_{1_m}/V_m & \cdots & & v_{n_m}/V_m \end{bmatrix} \begin{Bmatrix} dk_1/k_1 \\ \vdots \\ dk_n/k_n \end{Bmatrix} = \begin{Bmatrix} \frac{dw_1}{w_1} \\ \vdots \\ \frac{dw_m}{w_m} \end{Bmatrix} \quad (4)$$

The matrix on the l.h.s. is referred to by Shepard as the modal reference matrix. This is a square matrix containing the ratios of the element strain energy to the strain energy for the entire structural system for each mode. The ratios are obtained from the analytical model. By inverting the modal reference matrix, and then multiplying the frequency differences by the inverted matrix, the distribution of stiffness errors or differences, dk_i/k_i, is computed.

It is important to note that the modal reference matrix is square. This is because there is an equal number of measured modal frequencies as there are elements. This requirement imposes severe limitations on the procedure because in practice it is impossible to measure all of the modal frequencies and thus the system of equations will be incomplete and therefore unsolvable.

Results

Two alternative approaches that circumvent this limitation were investigated. The first approach involved substituting dv_i/v_i back into Eq. (4) for dk_i/k_i and then solving for discrepancies

in terms of differences in component strain energy instead of in terms of element stiffness. It was believed that by using this approach differences in the individual elements could still be identified but with only a limited amount of frequency data. The procedure for identifying the element differences entails dividing the structure into as many substructure components as there are measured frequencies. Next, strain energy discrepancies would be identified for each component using the modified Eq. (4). Then, based on the computed strain energy differences the structure would be partitioned into a different set of domains, a new set of differences would be computed, and the procedure would be repeated until the desired degree of precision in the locations of differences was determined. If desired, an element level of resolution could be obtained (see Fig. 1). Unfortunately, several attempts at implementing this approach were unsuccessful.

The second approach that was investigated for circumventing the rigid frequency requirements of Shepard's method was based on the assumption that the component mass and stiffness representations could be assumed to be accurate and the discrepancies were caused by differences in connections between components. If the component representations are accurate then $dk_j/k_j = 0.0$ for all of the elements in the components and the corresponding rows and columns of the modal reference matrix can be eliminated. By

reducing the size of the modal reference matrix the required quantity of measured frequencies is considerably reduced.

As a test case for the second approach the supported beam shown in Fig. 2 was studied. The objective was to identify the two connection properties, k_1 and k_2, using two measured frequencies. The identification of the connections was attempted using both a "rigid" and "flexible" beam model. The model stiffness was varied by changing it's modulus of elasticity. Except for differences in the connection stiffnesses the same model was used for both the reference and experimental beam. The connection properties for both models are given in Table I. Once the models were generated the strain energy from the reference model and the differences between the frequencies from the experimental and reference models were used in Eq. (4) to compute the differences in the connection stiffnesses.

For the rigid model ($EI = 10.0 \times 10^7$) there is little deformation and therefore negligible strain energy in the beam for the first two modes. Because there is no strain energy in the beam elements no information is lost by removing the rows and columns of the modal reference matrix corresponding to the beam elements. Actually, the rigid beam system is naturally reduced to a two degree of freedom system and the complete modal references matrix can be represented by a two by two matrix. As expected for this

system the identified difference, shown in Table I, are computed exactly. For the flexible model ($EI = 10.x10^3$) there is deformation and strain energy in the beam for the first two modes and some information is lost by eliminating the rows and columns of the modal reference matrix corresponding to the beam elements. Similarly to the rigid beam analysis, the connection stiffness properties were also computed correctly for this model.

The effect of experimental error was assessed for the rigid beam model by adding a two percent error to the experimental frequencies. When this error was included in the analysis the resulting connection stiffnesses were off by 4 percent. For systems with a larger number of connections the size of the modal reference matrix would increase and the effect of experimental error could be amplified even more. Fortunately, in practice, frequency data normally can be measured well within 2 percent accuracy.

Conclusion

From the analysis performed on the rigid and flexible beam models it is concluded that for systems where the component analytical models are accurate, the connection stiffness properties can be identified using Shepard's method. By applying this method to both a rigid and flexible beam model it was determined that the identification of the connection stiffness properties is independent of the component flexibility or equivalently, the

amount of component strain energy for the measured modes. The computation of the connection properties does require that the number of connections does not exceed the number of measured system frequencies.

References to Appendix

1. Shepard, G.D.: Spatial Distribution of Model Error Based on Analytical/Experimental Frequency Discrepancies. Proceedings of the 5th International Modal Analysis Conference, Union College, Schenectady, NY, 1987, pp. 1665-1668.

TABLE I - SYSTEM PROPERTIES FOR IDENTIFICATION OF CONNECTION DIFFERENCES

	"Rigid" Beam	"flexible" Beam
Reference Model Connection Stiffness	k_1=900.,k_2=1100.	k_1=900.,k_2=1100.
Reference Model Frequencies (Hz)	f_1=223.,f_2=354.	f_1=152.,f_2=335.
Experimental Model Connection Stiffness	k_1=850.,k_2=1250.	k_1=850.,k_2=1250.
Experimental Model Frequencies (Hz)	f_1=223.,f_2=365.	f_1=223.,f_2=365.
Actual Difference	k_1=50.,k_2=150.	k_1=50.,k_2=150.
Identified Difference	k_1=50.,k_2=150.	k_1=50.,k_2=150.

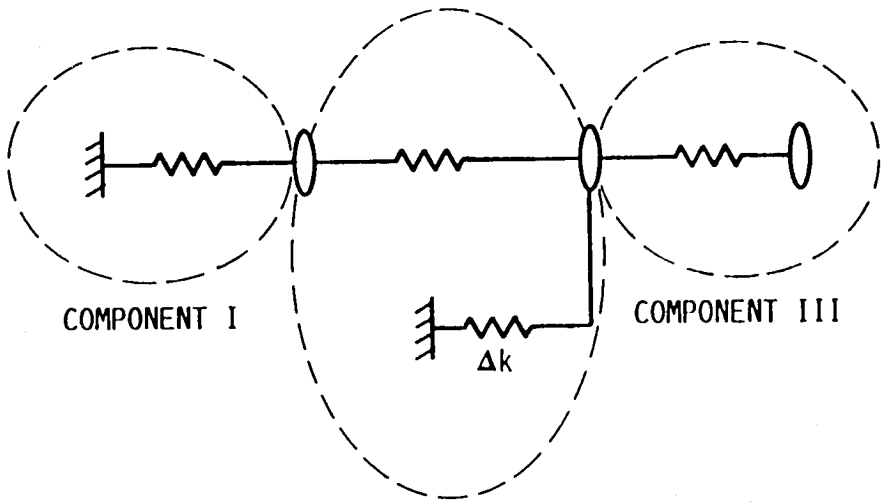

DIFFERENCE IDENTIFIED IN COMPONENT II

(A) INITIAL PARTITIONS.

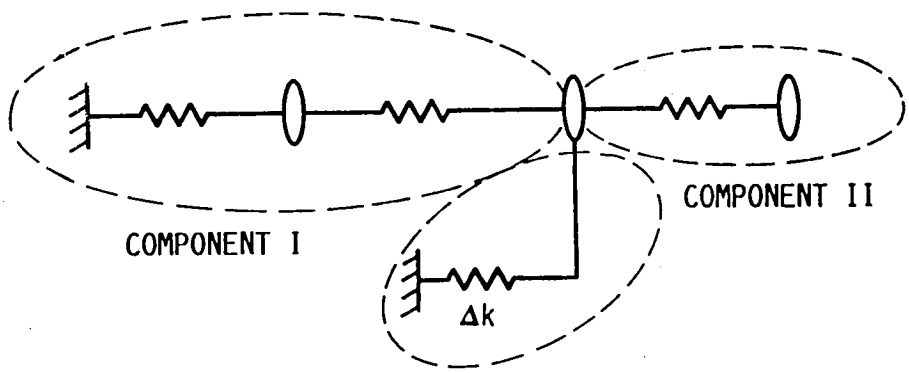

DIFFERENCE IDENTIFIED IN COMPONENT/ELEMENT III

(B) MODIFIED PARTITIONS.

FIGURE 1. - IDENTIFICATION OF ELEMENT STIFFNESS DISCREPANCY USING THREE SUBSTRUCTURES AND THREE MEASURED FREQUENCIES.

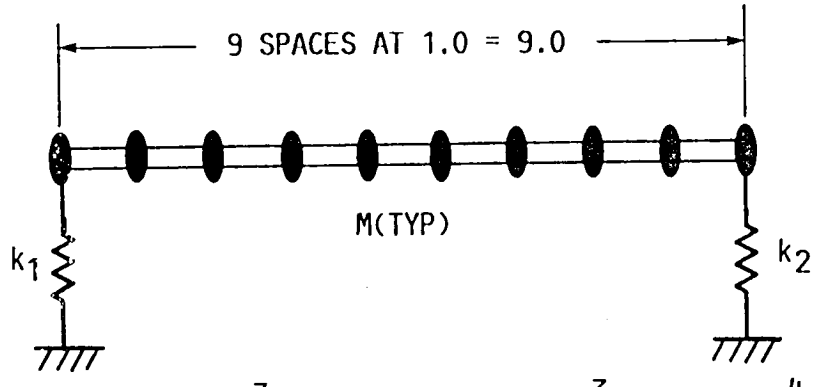

$EI_{RIGID} = 10x10^{7}$, $EI_{FLEXIBLE} = 10x10^{3}$, $M = 1x10^{-4}$

FIGURE 2. - IDENTIFICATION OF CONNECTION STIFFNESS FOR SIMPLE BEAM MODEL.

NASA
National Aeronautics and Space Administration

Report Documentation Page

1. Report No.	2. Government Accession No.	3. Recipient's Catalog No.
NASA TM-100812		

4. Title and Subtitle	5. Report Date
Parameter Identification Methods for Improving Structural Dynamic Models	June 1988
	6. Performing Organization Code
7. Author(s)	8. Performing Organization Report No.
Charles Lawrence	E-3994
	10. Work Unit No.
	505-63-1B
9. Performing Organization Name and Address	11. Contract or Grant No.
National Aeronautics and Space Administration Lewis Research Center Cleveland, Ohio 44135-3191	
	13. Type of Report and Period Covered
12. Sponsoring Agency Name and Address	Technical Memorandum
National Aeronautics and Space Administration Washington, D.C. 20546-0001	14. Sponsoring Agency Code

15. Supplementary Notes

This report was a thesis submitted in partial fulfillment of the requirements for the Degree of Doctor of Philosophy to Case Western Reserve University, Dept. of Civil Engineering, Cleveland, Ohio 44106 in May 1988.

16. Abstract

Recently, there has been an increased need to develop Parameter Identification methods for improving structural dynamic models. This need has arisen out of the inability of engineers to produce mathematical models which correlate with experimental data. The present research explores the efficiency of combining Component Mode Synthesis (substructuring) methods with Parameter Identification procedures in order to improve analytical modeling of structural components and their connections. Improvements are computed in terms of physical stiffness and damping parameters in order that the physical characteristics of the model can be better understood. Connections involving both viscous and friction damping are investigated. Substructuring methods are utilized to reduce the complexity of the identification problem. Component and inter-component structural connection properties are evaluated and identified independently, thus simplifying the identification problem. In the present research it was shown that modal test data is effective for identifying modeling problems associated with structural components, and for determining the stiffness and damping properties of inter-component connections. In general, Parameter Identification is improved when greater quantities of experimental data are available. The results of the present research demonstrate the relative ease of generating models which duplicate the experimental data. However, it is difficult to generate physically accurate models.

17. Key Words (Suggested by Author(s))	18. Distribution Statement
Parameter identification Structural dynamics	Unclassified - Unlimited Subject Category 39

19. Security Classif. (of this report)	20. Security Classif. (of this page)	21. No of pages	22. Price*
Unclassified	Unclassified	154	A08

NASA FORM 1626 OCT 86

*For sale by the National Technical Information Service, Springfield, Virginia 22161